DISCOVERING PLANT-SPECIFIC MECHANISMS UNDERLYING ENDOMEMBRANE-ACTIN INTERACTIONS AND METABOLIC SIGNALING

By

Pengfei Cao

A DISSERTATION

Submitted to
Michigan State University
in partial fulfillment of the requirements
for the degree of

Plant Biology—Doctor of Philosophy

2019

ABSTRACT

DISCOVERING PLANT-SPECIFIC MECHANISMS UNDERLYING ENDOMEMBRANE-ACTIN INTERACTIONS AND METABOLIC SIGNALING

By

Pengfei Cao

In eukaryotic cells, the endomembrane system compartments, including the endoplasmic reticulum, the vacuole and several other types of membrane-enclosed vesicles, are indispensable organelles and together exert essential cellular functions. In plant cells, the endomembranes interact extensively with the actin cytoskeleton, rather than the microtubules in mammalian cells, proposing significant questions of how the plant-specific endomembrane-actin interactions are established and regulated. My research identified the first ER-actin anchor protein in plant cells. Moreover, the research presented in this dissertation discovered that the abundance of certain cellular nutrients stimulates the metabolic signaling and subsequently triggers re-organization of the actin cytoskeleton and actin-associated endomembranes. A signaling transduction from metabolites and raw materials to manufacturing endomembrane compartments is arguably the first identified regulatory mechanism of such kind in all eukaryotes. Furthermore, additional data and considerations are expected to contribute further mechanistic understandings of the plant-specific endomembrane-actin interactions in a broad context of organelle morphogenesis, cellular functions and plant growth.

ACKNOWLEDGEMENTS

I want to say thank you to my parents for their unwavering support. They are not scientists, not ever being close to research. But nevertheless, they have the wisdom, and they keep teaching me and reminding me about the most important rules of conducting scientific research: it is normal that some experiments do not work; it is absolutely fine that most experiments do not work, and then I can simply step on an alternative career path.

I am grateful to have Dr. Federica Brandizzi as my PhD supervisor. In my eyes, she is a sincere and considerable mentor who urges the student to build a hardworking and rigorous attitude, broad knowledge, practiced skills, and everything essential for laying the foundation of a successful research career. I appreciate the help of the Brandizzi laboratory members, especially Luciana Renna, Gianni Stefano, Sangjin Kim, Starla Zemelis-Durfee, Yunting Pu and Yani Chen, for showing me the way of conducting research.

My PhD study was advised by a committee of Drs. Federica Brandizzi, Christoph Benning, Brad Day and Jianping Hu. I also had opportunities to collaborate with Dr. Robert Last. I was very fortunate to learn from these respected scientists, who guided me with suggestions on how to develop projects and, more importantly, tips of becoming a better young scientist.

When I was an undergraduate, Drs. Fei Yu and Xiayan Liu showed me the beauty of plant molecular and cellular biology. After I was further allured to embark on PhD study in this field, they continued to help and enlighten me with their wisdom of science and life. My six years in MSU was accompanied by many peer friends, especially Drs. Qiang Guo, Junwei Liu, Zhe Meng, Xiufang Xin, Jingyu Peng, Lina Yin, Mengran Fan, Anqi Xing, and Pengxiang Fan. As more patient and mature scientists, they inspired me with their values and visions for science.

This dissertation would not have been accomplished without the help of my undergrad assistants, especially Lucy Lu Liu, Nicole Szeluga and Yiming Zhao. In addition to their scientific contributions, I was greatly encouraged by their enthusiasm and genuine curiosity of science, and I feel fulfilled if the working experience with me ever helped their career development.

Here, I also would like to express my gratitude to Drs. Jonathan Walton, Jon Stoltzfus and Polly Hsu for granting me opportunities to teach undergraduate classes, which partially supported my research. Although the vague interest in teaching and interacting with undergrads was part of my motivation of pursuing a PhD, they helped me to explore the fun, the challenge, and the methodology of teaching.

TABLE OF CONTENTS

LIST OF TABLES

LIST OF FIGURES

CHAPTER 1. LITERATURE REVIEW: INTERACTIONS BETWEEN THE PLANT ENDOMEMBRANES AND THE CYTOSKELETON

Part of the work presented in this chapter has been submitted as part of an invited book chapter:

In book *Cytoskeleton: Diverse Roles in Plant's Life*. In book series *Plant Cell Monographs*.

ISSN 1861-1370. Springer. http://www.springer.com/series/7089

Pengfei Cao[1,2] and Federica Brandizzi[1,2,*]

[1] MSU-DOE Plant Research Lab, Michigan State University, East Lansing, MI 48824, USA.

[2] Department of Plant Biology, Michigan State University, East Lansing, MI 48824, USA.

*Corresponding author

1.1 INTRODUCTION

For most of the plant endomembrane compartments characterized to date, interactions with the cytoskeleton have been reported being necessary for their dynamic organization. Arguably, one of the best characterized organelles for interactions with the cytoskeleton is the endoplasmic reticulum (ER), the first organelle of the endomembrane system, which is responsible for the production of secretory proteins and lipids. As the most extensive organelle that spans throughout cytoplasm to connect other organelles from the nuclear envelope to the plasma membrane [1], the ER supports the dynamics and functions of most other organelles. In plant cells, the ER network forms thick membrane strands through tight interactions with F-actin bundles [2], providing a highway for rapid intracellular transport that bypasses a jammed cytoplasm and even the large central vacuole [3]. In the first section of this chapter, we focus on the roles of cytoskeleton system in ER morphogenesis, rearrangement of ER tubules and ER streaming, review recently identified plant proteins that are involved in ER-cytoskeleton interaction, and then provide ER-PM contact sites as an example of organelle-organelle interactions that rely on the cytoskeleton.

In most mature plant cells, the vacuole is the largest organelle that typically occupies more than 90% of the cell volume [4]. Pumping up the large-volume vacuoles provides turgor pressure to drive cell expansion and ultimately plant growth. Vacuoles are also the major storage compartment for proteins, sugars, along with many primary and secondary metabolites. Recent studies have revealed essential roles of the lytic vacuole in autophagy to degrade and recycle proteins, membrane lipids, and even organelles [5]. Since these vacuolar activities are essential for plant development, mutations that arrest vacuole biogenesis lead to embryo lethality [4]. Evidence suggests that the vacuolar membranes are associated with actin cytoskeleton, which is crucial for the morphology and biogenesis of plant vacuoles [6-10].

In addition to the ER and the vacuole, several other relatively smaller endomembrane compartments are connected with the plant cytoskeleton. In the plant cell secretory pathway, ER-produced cargoes are transported to the Golgi apparatus, which is disperse into mini stacks, closely associated with the ER and moves along actin. The *trans*-Golgi network (TGN) is the sorting station for secretion/exocytosis, endocytosis and vesicle transport to the vacuole. In plant cells, subpopulations of the TGN can be spatially independent from the Golgi apparatus. Their dynamics have been associated with both actin and microtubules [11, 12], and the underlying mechanisms will be discussed in this chapter. Additionally, autophagosomes are special transport vesicles that are formed in the autophagic response for degradation and recycling. An interplay between autophagosome and cytoskeleton system in mammalian and plant cells will be discussed.

In addition to reviewing various well-established and recently identified mechanisms of the endomembrane-cytoskeleton interactions in plant cells (Table 1.1), we bring up topics of great interest for the future research. First, the current understanding of the endomembrane-cytoskeleton interactions in plant cells is still limited in terms of both motor-driven dynamics and direct anchoring, which is also not well understood in yeast and mammalian cells. Furthermore, little is known about the signaling pathways beyond any of these direct interacting mechanisms that can integrate cytoskeleton remodeling and endomembrane dynamics to fulfill cellular and physiological functions. Brief summaries of potential regulatory mechanisms and plant specific activities related to the endomembrane-cytoskeleton interactions are included for a constructive discussion of this topic.

1.2 ER

1.2.1 Cytoskeleton system regulates distribution of ER tubules, sheets, and strands

A classical view of the ER network consists of sheet-like cisternae and tubules. Based mainly on models gathered in mammalian cells, formation of tubular ER is mainly dependent on transmembrane proteins with unique wedge-like topology, named reticulons and REEPs,that can bend the ER membrane and stabilize the curvature [13, 14]. Tubulated ER undergoes homotypic fusion through the action of the dynamin-like GTPase atlastins (ATLs) and a Rab GTPase, Rab10 [15, 16]. Additionally, Lunapark (Lnp) proteins stabilize the three-way junctions between ER tubules by interacting with reticulons, REEPs and ATLs [17, 18]. Studies in plant cells have functionally characterized Arabidopsis reticulons, Lnps and the ATL homolog RHD3 [19-28]. Four mechanisms may contribute to shaping ER sheets: 1) ER membrane-bound ribosomes may flatten and stabilize ER sheets; 2) transmembrane proteins with a large coiled-coil domain in ER lumen, such as CLIMP63 in mammalian cells, can self-interact and bring the opposite membranes together, serving as luminal spacers; 3) transmembrane proteins with a large coiled-coil domain in cytosol, for example p180 and kinectin in mammalian cells, can self-interact on the cytosolic side and stabilize the flat ER sheet; and 4) membrane-bending reticulon and REEP proteins curve the edges of ER sheet [29, 30].

Multiple lines of evidence suggest that the establishment of ER tubules and sheets is essentially determined by these membrane-shaping proteins. First, a tubular membrane network can be reconstituted in vitro simply with lipids and a small set of conserved membrane-shaping proteins [31, 32]. Secondly, overexpression or ablation of membrane-shaping proteins affects the ER sheet-tubule balance in plant cells [19-23, 25, 28]. Thirdly, mutant screens for regulators of ER morphology identified proteins localized to ER membrane and secretory pathway, but not the cytoskeleton

system [17, 20, 33]. Additionally, mathematical modeling of ER morphogenesis indicates that the influence of cytoskeletal forces seem to be limited to spatial distribution of ER membranes [34]. Collectively, this evidence prompted the hypothesis that the abundance of different membrane-shaping proteins and their interactions with membrane lipids form an ER network with sheets and tubules [34]. Nonetheless, the established ER tubules and sheets are distributed around the cell by cytoskeletal forces. The ER network in animal cells is mainly regulated by microtubules. When chemical intervention triggers depolymerization of microtubules, peripheral ER tubules retract to the central nuclear envelope and form collapsed ER sheets [35, 36]. In yeast cells, the integrity of actin cytoskeleton, rather than microtubules, is required for ER movement and its morphology [33, 37]. For plant cells, early studies using fluorescence and electron microscopies reported that ER membranes are frequently distributed in close proximity to actin cables [38-40]. Disruption of microtubules does not significantly alter the ER morphology, while treatment of actin depolymerizing drugs and genetic ablation of myosin motors both lead to collapsed ER with enlarged ER sheets and disappeared ER strands [2]. ER strands are a prominent feature of the plant ER, which is established by interactions between ER membranes and thick actin bundles [2, 40-44]. Disrupting thick actin bundles by latrunculin B treatment or knocking out class XI myosin genes lead to disappearance of ER strands and enlarged ER sheets [2, 44]. Another example is mutation of SYP73, an anchor of ER membrane to actin filament, which phenocopies disruption of the actin-myosin system [41]. By contrast, plant cells stimulated to form extreme actin bundling display thickened and elongated ER strands (Cao et al., unpublished data). Taken together, these studies suggest that the ER strands are an outcome of enhanced actin bundling and ER membrane-actin interactions.

The nature of ER sheets and ER strands in plant cells is still unclear. Recent studies of ER in cultured mammalian cells developed spatiotemporal analyses with super resolution microscopy,

which revealed that most peripheral ER structures classically identified as ER sheets are actually dense and dynamic matrices of ER tubules [45, 46]. Compared to cultured mammalian cells, commonly adopted plant cell types for ER study, such as tobacco leaf epidermal cells, Arabidopsis hypocotyl epidermal cells and expanding cotyledon epidermal cells generally display ER networks with a larger portion of sheets [2, 42, 47]. Meanwhile, these plant cell types are highly vacuolated so that the cytoplasmic content is pressured into a thin layer. Therefore, it is plausible, though lacking direct evidence so far, that in plant cells the ER sheets and ER strands are also dense matrices of tubules, and on the other hand, the formation of isolated ER tubules and thick ER strands in plant cells is largely dependent on the availability of cytoplasmic space sustained by cytoskeleton and other organelles.

1.2.2 Rearrangement of the tubular ER

In mature cells, such as expanded Arabidopsis cotyledon epidermal cells, the ER network generally does not experience dramatic alteration of morphology [42]; nevertheless, the entire ER network consistently undergoes fine rearrangement of ER tubules. Interestingly, despite the ER networks in mammalian cells and plant cells being primarily bound to two distinct types of cytoskeleton cables and motors, the ER tubules move with seemingly similar mechanisms. Studies in mammalian cells identified five scenarios of tubular ER initiation and elongation. In the three most common situations, the tubular ER is driven by strong association with the cytoskeleton system. The tip of an ER tubule can be pulled by kinesin or dynein motor sliding on a static microtubule, or alternatively form a Tip Attachment Complex (TAC) with the plus end of a microtubule that is being polymerized or depolymerized [29, 46, 48, 49]. In other cases, ER tubules can be pulled out by moving organelles, such as endosomes and lysosomes, or initiate *de novo* ER tubulation without any nearby microtubules or small organelles [46].

In plant cells, the actin cytoskeleton controls the organization and dynamics of ER network, including tubular ER movement. Studies showed that latrunculin B-induced depolymerization of actin filaments halts tubular ER generation [47, 50]. Furthermore, simultaneous imaging of ER tubules and actin bundles in plant cell extracts identified tubular ER elongation along the actin bundles, presumably driven by myosin [50]. However, compared to microtubules, actin filaments are thinner, more dynamic, and forming a densely packed network, which is challenging for high resolution imaging even in thin-layer cultured mammalian cells [46, 51]. It remains elusive whether in plant cells the ER tubule tip can bind to and be pulled by an end of polymerizing or depolymerizing actin filament, which would be resembling the tip binding between tubular ER and microtubule in mammalian cells. Advances of imaging techniques may also elucidate the mechanisms of microfilament-dependent ER reorganization in animal cells [52, 53], and unveil whether single actin filaments are involved in the *de novo* ER tubulation.

The microtubule cytoskeleton plays a minor role in ER dynamics. Recent studies closely monitored ER rearrangement in Arabidopsis hypocotyl epidermal cells and observed motor-driven ER tubule extension along microtubules, as well as ER subdomains that are statically anchored to crossing microtubules [54]. This work did not record ER tubule extension associated with microtubule growing plus end, suggesting the tip-attached TAC mechanism is not conserved in plant cells [54]. The mammalian TAC includes the microtubule plus end-binding protein EB1 and the ER transmembrane protein STIM1 [29]. AtEB1 exerts conserved functions of binding to microtubule plus end and regulating microtubule organization [55-57]. On the one hand, AtEB1 exhibits dual localization to microtubules and elusive endomembranes [56], and it is involved in modulation of endocytosis [57]. On the other hand, the functional homolog of STIM1 in plants has

not been identified yet. Taken together, these studies suggest that plant tubular ER rearrangement along microtubules mainly rely on microtubule motor proteins.

1.2.3 ER streaming

Imaging analyses of ER-retained fluorescent proteins report ER streaming as rapid bulk flow inside the ER lumen [2, 20, 42, 58]. Previous studies suggest that ER streaming is largely dependent on the integrity of ER strands. When the thick ER strands are abolished and the ER collapses due to depletion of myosin XI proteins or the ER membrane-actin anchoring protein SYP73, the maximal and average velocities of ER streaming are reduced [2, 41]. On the other hand, strikingly enhanced ER strands caused by a mutation of RHD3, the plant ATL homolog shaping ER tubules, also leads to significantly reduced ER streaming [20]. Therefore, both functional myosin XI motors and ER-cytoskeleton anchors are required for rapid ER streaming.

In plant cells, myosin XI proteins organize actin filaments and transport organelles on the actin tracks [59, 60]. A characterization of myosin XI members using live cell imaging and single and high-order mutants suggest that certain myosin XIs display ambiguous localizations and are involved in movement of multiple organelles [2, 61-65]. Myosin XI-K has been suggested to be associated ER membrane and it exerts a dominant role for moving ER network [2, 65]. However, it is still under debate whether the ER is the cargo and the cellular site of binding for myosin XI-K. Two lines of evidence are in conflict with this. First, manipulation of myosin proteins strongly affects the dynamics of other small organelles such as Golgi, peroxisomes, mitochondria, and endosomes [61, 62]. Besides, more than a dozen of plant myosin XI-binding proteins that have been identified so far are distributed to disperse punctae in the cytoplasm, rather than resembling a typical ER network [66-68]. Given that the ER is a complex organelle with distinct subdomains [40, 69], it is possible that the myosin XI-binding proteins are distributed only over specific ER subdomains. Considering the

extensive and strong association of the ER network with smaller organelles and endosomes in plant cells [70], it is also possible that myosin XIs drive small organelles and indirectly propel ER movement. Identification of new myosin adaptors and advance of imaging techniques may further our understanding of the relationship between ER movement and myosin motors.

1.2.4 Recently characterized plant proteins involved in ER-actin interactions

The NETWORKED (NET) superfamily proteins contain a N-terminal NET-actin-binding (NAB) domain and a coiled-coil domain that is responsible for protein-protein interactions and protein targeting to specific membrane structures [71]. Accordingly, three NET3 family members expressed in plant cells show filamentous distribution in colocalization with actin filaments and brighter foci that colocalize with distinct membranes. NET3A is accumulated around the nuclear membrane, whereas NET3B and NET3C are associated with the ER network. NET3C interacts with membrane-associated VAP27 in close proximity to the plasma membrane. Interestingly, VAP27 also interacts with microtubules [72, 73]. These results imply that NET3C and VAP27 define ER-PM contact sites that incorporate both F-actin and microtubule cytoskeletons. Compared with NET3C, NET3B appears to be more tightly associated the ER since overexpression of NET3B modulates the ER morphology in a manner reminiscent of SYP73-rearranged ER over the actin cables. Therefore, NET3B may function in anchoring ER network to the cytoplasmic F-actin. This feature is supported by the observation that overexpression of NET3B restricts ER membrane diffusion [74]. Further analyses are expected to reveal how the peripheral membrane protein NET3B is connected to the ER membrane and whether the NET3-proteins interact directly with actin.

SYP73 was identified in a search of ER localized proteins with both transmembrane domain and coiled-coil domain, which may anchor ER membrane to cytoskeleton as CLIMP63, p180 and kinetin function in mammalian cells [41]. However, the coiled-coil domain of SYP73 is cytosolic

and adjacent to an unconventional actin-binding domain, hence forming strong self-interactions that presumably strengthens actin binding rather than spacing or flattening the ER membrane [41]. As a consequence, overexpression of SYP73 leads to a rearrangement of ER network over actin cables [41], rather than augmenting ER sheets as it occurs for overexpression of CLIMP63 or p180 in mammalian cells [14].

Our current understanding of ER-associated actin-binding proteins may be still very limited. A study of cotton fibers identified GhCFE1A as a protein linking the ER membrane and actin cytoskeleton that functions in cotton fiber initiation and elongation [75]. Surprisingly, a recent study in mammalian cells revealed that Sec61β, a very commonly used marker of ER membrane in mammalian cells, binds microtubules and is able to remodel the network to overlay microtubules upon overexpression [76]. More proteins involved in ER-cytoskeleton interactions are expected to be identified with advances of organelle proteomics and methods studying protein-protein interactions [24, 77, 78].

1.2.5 Membrane-cytoskeleton interaction at the ER-PM contact site

The ER network spreads throughout the cytoplasm and interacts most other membrane-bound organelles to form inter-organelle contact sites. One type of contact sites that has gained recent attention in plant research is between the ER and the plasma membrane (PM). The ER-PM contact sites (EPCS) have been implicated in endomembrane dynamics, cytoskeleton organization, and intercellular communication as well as in functioning as a signaling platform to respond to biotic and abiotic stresses [79-81].

Several conserved protein families that bring ER and PM membranes together have been characterized in Arabidopsis, including extended-synaptotagmin family proteins (E-Syt, known as Syt1 in plants) and VAMP-associated proteins (VAP) [72, 73, 81-85]. VAP27 directly binds to

microtubules, and it also interacts with NET3C, a member of the plant specific membrane-associated actin-binding NET family [72].

In mammalian cells, both microtubules and actin cytoskeleton regulate the EPCS. A store-operated calcium entry (SOCE) complex is formed by plasma membrane-localized protein Orai1 and ER transmembrane protein STIM1, which can interact with the microtubule plus end-binding protein EB1 to regulate the calcium gating function of SOCE at the EPCS [86]. Recent studies reported an interplay between actin organization and the dynamics of EPCS [87, 88]. A major type of the EPCS is supported by ER-associated VAP protein interacting with ORP, which also binds to phospholipids on the PM [89]. A recent study in yeast identified an additional interaction between ORPs and myosin-I proteins [88]. Upon disruption of the EPCS, the local actin polymerization is impaired and the formation of endocytic vesicles is stalled [81, 88]. Interestingly, the actin cytoskeleton also transduces ER luminal signal to regulate the EPCS. Secretory proteins are produced in ER, and disturbance of proteostasis in the ER lumen triggers the unfolded protein response (UPR) that is detected by ER transmembrane sensors. A mammalian UPR sensor protein PERK interacts with an actin-binding protein, filamin A, to transduce the UPR signal to actin re-organization underneath the plasma membrane domain of EPCS [87]. Consistently, functional PERK is required for actin dynamics and EPCS formation [87]. Although plant homologs of PERK and filamin A have not been reported yet, the functional conservation of ER stress response mechanisms and F-actin side-binding proteins throughout eukaryotes suggests the existence of such interplay between the actin cytoskeleton and membranes at EPCS [90, 91].

1.3 VACUOLE

1.3.1 The vacuolar membrane is associated with the cytoskeleton

Earlier studies of the plant vacuole and the cytoskeleton suggested that these structures are associated, or at least, distributed in close proximity. Isolated and cultured cells, such as tobacco BY-2 cells and Arabidopsis protoplasts, were first utilized to visualize the vacuole membranes and the actin cytoskeleton [6-10]. Disruption of the actin cytoskeleton alters the vacuole morphology and the structures formed by the vacuolar membranes, most notably the transvacuolar strands (TVS). Upon microinjection of profilin, a potent actin monomer-binding protein that lead to F-actin depolymerization, TVS were deformed and cytoplasmic streaming stagnated [9]. This pioneering research, based mainly on bright field analyses, suggested that the actin cytoskeleton is involved in vacuole architecture, especially the TVS. The vacuolar structures can be easily visualized by GFP-tagged vacuole membrane-associated protein or FM4-64 and BCECF staining. Improved imaging in cultured cells revealed that the vacuole membranes form not only spherical structures, but also tubules, vesicles and other intricate configurations; moreover, the TVS appear to be composed of these minuscule yet complicated structures clustering along thick actin bundles [6, 7, 10, 92]. The TVS gradually disappear after application of actin polymerization inhibitors, while they are insensitive to microtubule-targeting chemicals [6, 8]. Furthermore, certain myosin inhibitors induce TVS collapse, while they have moderate or insignificant effects on the integrity of actin filaments [6, 10]. These lines of evidence suggest that the maintenance of TVS is dependent on actin filaments rather than microtubules, possibly via specific myosin motors and receptors. However, our current knowledge of TVS has been mostly acquired through genetic or chemical disruption of the cytoskeleton. How the TVS structures are established, what is their function, and whether they are dynamically regulated are still open questions. It is possible that the strands are essentially

cytoplasmic actin bundles wrapped by vacuole membranes that are maintained by strong membrane-cytoskeleton anchoring. In this scenario, the cytoskeleton-associated vacuolar membranes are possibly remains of smaller vacuoles after they undergo homotypic membrane fusion to form the large central vacuole. It is also possible that the TVS are induced-to-form structures that are regulated by cytoskeleton signaling.

1.3.2 Plant cytoskeleton controls vacuole morphogenesis

Whereas young meristematic cells generated either in embryonic or growing tissues contain multiple types of vacuoles, most mature plant cells contain one large central vacuole [93, 94]. Several studies in plant cells proposed the dynamic vacuole membrane fusion as the essence of vacuole biogenesis that is dependent on a remodeling of the actin cytoskeleton [95, 96]. In yeast cells, multiple vacuoles frequently undergo fusion and division in response to growth conditions and to exert their stress-related functions [97]. Vacuole membrane fusion is achieved by three stages: 1) priming of membrane lipid composition, 2) tethering regulated by Rab GTPase, and then 3) docking and fusion mediated by HOPS and SNAREs complexes [98]. Particularly, the homeostasis of phosphoinositides, an essential type of regulatory lipids for membrane fusion, also signals to the WAVE complex to regulate actin reorganization [99, 100]. In addition, yeast vacuole fusion requires Cdc42p and Rho1p, two Rho GTPases classically regulate actin remodeling through WAVE-Arp2/3 complexes [101-103]. During vacuole membrane fusion, Cdc42p is activated and, in turn, it stimulates actin polymerization to facilitate membrane-membrane docking before fusion [104-106]. Considering that both yeast and plant cells utilize actin rather than microtubules to mobilize organelles, and Rho of Plants (ROP) GTPases play conserved role of signaling to cytoskeleton remodeling [107], it is reasonable to hypothesize that the mechanism of actin-dependent vacuole

fusion is conserved in plant cells. This hypothesis is supported by studies in plant cells [95, 96] although the underlying mechanisms remain elusive.

Vacuolar occupancy of the cellular space during plant cell growth is determined by the number and size of vacuoles in a cell. Despite that providing turgor pressure to stimulate cell expansion has been recognized as a classic and critical function of the plant vacuole [108], the mechanisms regulating the vacuolar occupancy of cellular space and thereby controlling cell expansion are still poorly understood. Recently, two studies explored the interplay between vacuolar occupancy, the actin cytoskeleton, and the major plant growth hormone auxin [109, 110]. Vacuole dynamics, organization of actin cytoskeleton, and cell expansion were found to be individually affected by exogenously applied auxin in an auxin receptor-dependent manner [109, 110]. Furthermore, chemical interference and mutations of the action-myosin system were found to mitigate the vacuolar occupancy of the cellular space induced by auxin [110]. The downstream of auxin signaling is complex and multiple mechanisms may contribute to cell expansion; nevertheless, these studies provided significant evidence for vacuole-cytoskeleton interactions in response to developmental signals.

1.3.3 Actin-binding proteins associated with vacuole

Recent studies in searching actin-binding proteins yielded novel plant proteins that are involved in interactions between the vacuole and the actin cytoskeleton. As discussed above, the plant specific NET family consists of actin-binding proteins that are associated with various membranes. In Arabidopsis root epidermal cells, native promoter-driven expression of NET4A-GFP was found distributed on filamentous structures that are closely attached to the vacuolar membrane [71]. A study of vacuolar-type H^+-ATPase (V-ATPase) B subunits identified a conserved actin-binding domain and confirmed their actin binding ability and the effects on actin filament remodeling in vitro [111].

Despite of the vacuolar-type nomenclature, V-ATPase subunits are distributed throughout the secretory pathway and may not necessarily be contributing to the interaction between vacuolar membrane and actin cytoskeleton [111].

1.4 OTHER ENDOMEMBRANE COMPARTMENTS

1.4.1 Golgi

In mammalian cells, the Golgi stacks are linked in tandem to form a unique Golgi "ribbon" which is mostly distributed near the nucleus and the microtubule organizing center (MTOC). The positioning of the mammalian Golgi, as well as formation of Golgi "ribbon", are dependent on sophisticated interactions between Golgi matrix proteins and peripheral microtubules, microtubule-associated proteins, actin-binding proteins, and motor proteins [112].

In plants, the Golgi apparatus is composed of numerous mobile Golgi mini-stacks composed of several flattened membrane cisternae. The Golgi stacks are attached to the ER network and receive secretory cargo directly from the ER [43, 113, 114], independently of actin and microtubules [114]. The plant Golgi stacks also undergo long-range movement in a stop-and-go manner on the actin cables [43, 115]. Chemical disruption of F-actin, chemical inhibition of myosins or genetic ablation of Myosin XI genes causes reduced mobility of the Golgi [43, 62, 63, 114-116]. By contrast, treatment of microtubule-disrupting chemicals does not affect Golgi movement [114, 115].

Microtubules have not been considered required for long-range movement of the plant Golgi; however, examination of the diversified motor protein family in plants suggests that microtubule components are still involved in regulating Golgi dynamics. Arabidopsis and cotton homologs of Kinesin-13A localize to the Golgi [117, 118]. Since knocking out Kinesin-13A caused growth phenotypes and subtle aggregation of Golgi, it has been speculated that the kinesins may serve as temporal anchors between the Golgi and microtubules and regulate the Golgi positioning [117, 118].

Microscopy and quantitative analyses have provided evidence supporting a regulatory interplay between local actin organization and the stochastic Golgi movement. It has been reported that in epidermal cells of the root elongation zone, the Golgi stacks undergo fast movement with a velocity up to 7 μm s^{-1} in areas where thick and long actin bundles appear, while the Golgi stacks move more slowly and wiggly where F-actin is less bundled [119]. Another study using hypocotyl cells led to similar results showing a correlation between locally enhanced actin bundling and Golgi movement with higher velocity and less wiggle behavior [120]. Moreover, through the analyses of Golgi movement and actin organization, this study showed the potential of accurately predicting the movement pattern of overall Golgi stacks as well as the direction and velocity of specific Golgi movement [120]. The microscopy analyses facilitated by quantitative modeling [119, 120] suggest the intracellular organelle movement can be orchestrated by signaling to actin re-organization, and therefore is neither static nor completely stochastic.

1.4.2 TGN

Succeeding to the Golgi along the biosynthetic route, the *trans*-Golgi network (TGN) is an endomembrane compartment where the secretory pathway and the endocytic pathway converge. Owing to the presence of a cellulosic cell wall, the TGN in plant cells likely exerts non-conserved cargo sorting functions compared to animal cells. The plant TGN also exhibits unique dynamics and spatial distribution. In animal cells, the TGN is attached to the Golgi and collectively is transported along microtubules by microtubule-associated motors and anchoring proteins [121]. The plant TGN population is composed of a subgroup that associates with the Golgi (GA-TGN/early TGN) and a subgroup that is isolated from the Golgi (GI-TGN/late TGN) [12, 122]. In plant cells, chemical manipulation of the actin cytoskeleton and microscopic analyses suggested that the TGN is associated with and dependent on F-actin for transport [123, 124].

In this section, we will review recently identified proteins that directly connect the TGN to the cytoskeleton cables. For example, RISAP is a TGN-localized effector of RAC5 GTPase that can directly bind to F-actin and myosin XI, regulating membrane traffic and tip growth of tobacco pollen tubes [125]. RISAP contains a DUF593 domain that is shared by identified plant myosin adaptor proteins [68, 125]. Another TGN protein, HLB1, was recently identified in a forward screen for mutants whose primary root elongation is hypersensitive to latrunculin B [11]. Interacting with TGN-localized MIN7/BEN1 protein, HLB1 colocalizes with TGN markers and moves along F-actin cable, suggesting it functions in the intersection of post-Golgi trafficking and actin cytoskeleton [11]. The *hlb1* mutant exhibits broad but mostly mild defects in vesicular transport, including both exocytosis and endocytosis [11]. Meanwhile, in the *hlb1* mutant, the organization of F-actin is disrupted and displays less bundling in root epidermal cells and root hairs [11]. Therefore, HLB1 likely functionally connects the TGN to the actin cytoskeleton in a manner dependent on BEN1, although a direct interaction with of HLB1 and actin has not been demonstrated yet. If confirmed, the results would lend support to the earlier findings that the TGN dynamics depend on actin [123, 124]. A recent research identified a novel regulator of TGN dynamics, TGNap1, which is required for post-Golgi traffic to the cell surface and vacuole, microtubule-dependent biogenesis of a subpopulation of TGNs as well as efficient endocytosis [12]. Mechanistically, TGNap1 interacts with Rab6 and YIP4, two regulators of vesicular trafficking that bind on and off the TGN; TGNap1 also directly binds microtubules [12]. These results support the novel model whereby post-Golgi organelle traffic and biogenesis depend partially on microtubules. In this model, TGNap1 dynamically bridges the TGN to microtubules for biogenesis and traffic of a subpopulation of GI-TGNs [12]. Further characterization of TGN-associated proteins and their potential interactions with

cytoskeleton components are expected to provide comprehensive understanding of TGN dynamics and its crucial functions as the cargo sorting station.

1.4.3 Endosomes and endocytosis

Endosomes are small endomembrane compartments that internalize plasma membrane-associated proteins and carry cargo for recycling, degradation or sequestration. This process includes endosome biogenesis, transport and sorting, which are facilitated by the cytoskeleton. In animal cells, the biogenesis and intracellular movement of endosomes are mainly dependent on actin cytoskeleton and microtubules, respectively [126, 127]. On the plasma membrane, activation of WASH and Arp2/3 complexes initiates actin nucleation and polymerization to form a meshwork of actin filaments, which restricts a subdomain for endosome biogenesis [127]. Subsequently, the long-range intracellular traffic of endosomes is assumed by microtubules and associated motors. More than a dozen of kinesin and dynein motor proteins have specific client cargoes and largely identified adaptor proteins [126]. The cytoplasmic actin components are also frequently associated with endosomes and target membranes to control multiple aspects of the endosomes beyond biogenesis, including sorting and short-range transport of cargoes and subtle dynamics [126]. Interestingly, actin polymerization on the endosome surface initiates and stabilizes tubulation of membranes, and eventually leads to fission and myosin-driven transport. By contrast, studies of various endosomal cargoes in plant cells indicated that actin cytoskeleton is the primary driving force, though microtubules and microtubules-associated motors are also involved in endosomal transport [128-131].

A type of extensively investigated endosomal cargoes in plant cells are AUX1 and PIN auxin transporters, whose proper distribution on the plasma membrane of one side of the cell for directional auxin influx and efflux is crucial for the establishment of cell polarity as well as overall plant growth and development [132]. The transport and distribution of PIN1, PIN3 and AUX1 are all

primarily dependent on the integrity of F-actin, rather than microtubules [133-136]. Other evidence supports that microtubules contribute to the traffic of PIN-associated endosomes [128]. The microtubule-associated protein CLASP interacts with sorting nexin SNX1 and connects the endosomal membrane with microtubules [128]. Knockout mutants of *CLASP* show disrupted polar distribution of PIN2 as well as auxin-related plant growth phenotypes [128]. Furthermore, functional CLASP and integrity of microtubules prevent PIN2 from degradation [128]. Nevertheless, it should be noted that in animal cells the SNX proteins are a type of key regulators of endosome sorting and traffic, and several associations between specific SNX and kinesin/dynein proteins regulate the traffic of distinct endosomal cargoes [126]. Additional research also demonstrated the role of Arabidopsis SNXs in modulating the trafficking of the iron transporter IRT1 and vacuolar storage proteins [137-139], suggesting conserved functions of Arabidopsis SNXs for sorting and trafficking. Interestingly, a recent forward genetic screen for novel regulators of PIN3 cellular distribution identified a new mutant allele of ACTIN2, and reported that disruption of F-actin and microtubules confer distinct effects on PIN3 polarity and gravitropism [129]. Therefore, actin cytoskeleton and microtubules may be required for endosomal transport and assume diversified tasks.

Endocytosis facilitated by the actin cytoskeleton is critical for pathogen pattern recognition receptors (PRR) during plant immunity. Monitoring the mobilization of GFP-tagged FLAGELLIN SENSING2 (FLS2), a plasma membrane-localized receptor of bacterial flagellin (flg22), upon flg22 induction and chemical treatment revealed both critical but differential roles of F-actin and myosins [131]. Treatment with the myosin inhibitor 2,3-butanedione monoxime largely reduced the formation of FLS2-GFP-labelled endosomes by approximately 80% compared to the control [131]. By contrast, depolymerizing F-actin by latrunculin B treatment did not impede internalization of FLS2-GFP, but rather halted the FLS2-GFP-labelled endosomes from leaving the plasma

membrane [131]. Consistently, HopW1, a bacterial effector protein injected into the plant cell, disrupts F-actin and inhibits endocytosis [130]. These results are critical pieces of evidence supporting a broad model in which dynamic interactions between the cytoskeleton and membrane-bound organelles perceives pathogen invasion signals and coordinates downstream subcellular responses [140].

1.4.4 Other transport vesicles

The cellulose synthase complex (CSC) is an essential machinery for cell wall synthesis and biomass accumulation. It is well established that, at the plasma membrane, the CSC moves along the underlying cortical microtubule framework to synthesize and deposit cellulose microfibrils into the cell wall [141]. However, much less is known about the mechanisms of transporting the CSC from Golgi to plasma membrane. The plasma membrane loci where the CSCs are delivered are determined by the underlying cortical microtubules, though disruption of the actin cytoskeleton also affects distribution pattern of CSCs on the plasma membrane [142, 143]. Recent research provided further mechanistic insights into the delivery of the CSC to the plasma membrane by the synergistic exocyst complex and microtubules [144]. It has been shown that fusion between the exocyst complex and the target membrane relies on an interaction between CSI1, a microtubule-binding protein that tethers the CSC to the cortical microtubules [145], and PTL1, a plant protein bearing a domain, the MUN domain, which functions in exocytosis in animal cells [144, 146]. Thus, this final delivery step most likely employs mostly the conserved exocytosis machinery as well as plant specific regulators.

Questions remain about the driving force of CSC transport from Golgi and recycling from the plasma membrane. Arabidopsis Kinesin-4/FRA1 is required for deposition of cellulose on the cell wall [147]. FRA1 displays bona fide kinesin activity and mediates vesicular transport along cortical

microtubules [148]. However, another work demonstrated that Kinesin-4/FRA1 is involved in secretion of cell wall components but is not required for traffic of the CSC to the plasma membrane [149]. Therefore, it is possible that certain plant motor proteins exert diversified or nonexclusive functions that are still not fully appreciated. The possibility exists that a different cytoskeleton motor system carries the CSC-carriers from TGN to the plasma membrane. Last but not least, the rather isolated positioning of GI-TGN from Golgi may allow the TGN to be distributed in close proximity of the target site of plasma membrane, thus not requiring cytoskeleton cable to transport the CSC [141]. Another example of cytoskeletal force-driven vesicular transport is SHORT-ROOT (SHR), a signaling protein that regulates cell division and differentiation in root [150]. Type-14 kinesin KinG directly interacts with SIEL, a protein that tethers SHR on the endosome, and is required for the intercellular movement of SHR [150].

These reviewed studies of various cytoskeleton components and specific cargoes demonstrate the necessity of dissecting the client specificity of myosin, dynein and kinesin motors as well as characterizing their adaptor proteins in plant cells. It is important to consider also the findings that the plant cytoskeleton may indirectly contribute to organelle transport. For example, as detailed earlier, the ER network interacts with the actin cytoskeleton via characterized stable anchors and potential adaptor-attached myosins [69]. Recent work illustrated that the plant ER is in close association with endosomes and that disruption of ER architecture and streaming largely affects the mobility and endocytic function of endosomes [70]. These results support the possibility of an alternative scenario of endosome transport in plant cells in which endosomes are mobilized by the actin cytoskeleton through tethering to the ER network.

1.4.5 Autophagosome

Autophagosomes are small endomembrane-bound compartments formed during autophagy, a conserved degradation and recycling pathway that is usually upregulated upon stress. In mammalian cells, the autophagosome moves on microtubules to reach the lysosome, while the actin cytoskeleton is also required for formation and traffic of autophagosomes [151, 152]. The association of autophagosomes with microtubules involves mammalian the LC3 (microtubule-associated protein 1 light chain 3, homologs of yeast ATG8) family proteins and FYCO1 adaptor [153].

In plants, it has been shown that integrity of the microtubules is required for the induction of autophagosomes [154]. The Arabidopsis homologs of ATG8 similarly interact with microtubules [155]. An autophagy cargo receptor Joka2 colocalizes with cytoskeleton components in plant cells, which is similar to its mammalian homolog NBR1 [156]. Additionally, a recent study showed that NAP1, as well as other components of the actin-regulating SCAR/WAVE complex and Arp2/3 complex, are required for stress-induced autophagic responses [157]. This evidence suggests that the formation of the autophagic structures requires both stable cytoskeletal tracks and reorganization of the actin cytoskeleton.

1.5 ACKNOWLEDGEMENTS

We thank Dr. Sang-Jin Kim for helpful discussion. This work was primarily supported by NSF MCB1714561 and AgBioResearch to FB. We acknowledge infrastructure support by the Chemical Sciences, Geosciences and Biosciences Division, Office of BES, Office of Science, US DOE DE-FG02-91ER20021).

APPENDIX

Endomembrane Compartments	Protein/Interacting Partners	Notes	References
Endoplasmic reticulum (ER)	Myosin XIk, XI1, XI2	Required for ER streaming and maintenance of ER morphology	[1]
	SYP73	ER membrane-associated actin-binding protein	[2]
	NET3B	ER membrane-associated actin-binding protein	[3]
	GhCFE1A	ER membrane-associated actin-binding protein in cotton fiber	[4]
Golgi	Myosin XIk, XI1, XI2	Required for Golgi movement	[5-8]
	Kinesin-13A	Localized to Golgi and may contribute to Golgi positioning	[9, 10]
ER-PM contact site (EPCS)	NET3C and VAP27	Form a complex with interactions between NET3C and VAP27, NET3C and F-actin, VAP27 and microtubules	[11]
trans-Golgi network (TGN)	RISAP	ROP effector, associated with myosin and F-actin	[12]
	BEN1 and HLB1	HLB1 interacts with TGN-localized BEN1 on actin cytoskeleton	[13]
	TGNap1	Binds to microtubules and interacts with TGN-localized Rab6 and YIP4	[14]
Vacuole	NET4A	Associated with the tonoplast in root epidermal cells	[15]
Plasma membrane (PM)	NET1A	Associated with PM and accumulate at the plasmodesmata	[15]
	NET2A	Associated with PM in the shank of pollen tube	[15]
Endosomes and vesicles	CLASP and SNX1	Connects microtubules and endosomes that transport PM-localized proteins	[16]
	HopW1	A bacterial effector protein that disrupts F-actin and inhibits endocytosis in plant cells	[17]
	CSI1 and PTL1	Connects microtubules and delivers CSC-tethered vesicle to the PM	[18, 19]
	Kinesin-4/FRA1	Involved in secretion of cell wall components	[20, 21]
	KinG and SIEL	SIEL connects KinG to vesicles that transport SHR	[22]
Autophagosome	ATG8	Associated with microtubules	[23]
	NAP	Components of SCAR/WAVE complex and Arp2/3 complex are required for formation of autophagosomes	[24]

Table 1.1 Plant proteins that are involved in endomembrane-cytoskeleton interactions.

REFERENCES

REFERENCES

1. Valm, A.M. *et al.* Applying systems-level spectral imaging and analysis to reveal the organelle interactome. *Nature* **546**, 162–167 (2017).

2. Ueda, H. *et al.* Myosin-dependent endoplasmic reticulum motility and F-actin organization in plant cells. *Proc. Natl. Acad. Sci. U.S.A.* **107**, 6894-6899 (2010).

3. Stefano, G., Hawes, C. & Brandizzi, F. ER - the key to the highway. *Current Opinion in Plant Biology* **22**, 30-38 (2014).

4. Zhang, C., Hicks, G.R. & Raikhel, N.V. Plant vacuole morphology and vacuolar trafficking. *Front Plant Sci* **5** (2014).

5. Yang, X.C. & Bassham, D.C. New insight into the mechanism and function of autophagy in plant cells, Vol. 320. (ed. K.W. Jeon) 1-40 (Academic Press, 2015).

6. Sheahan, M.B., Rose, R.J. & McCurdy, D.W. Actin-filament-dependent remodeling of the vacuole in cultured mesophyll protoplasts. *Protoplasma* **230**, 141-152 (2007).

7. Kutsuna, N., Kumagai, F., Sato, M.H. & Hasezawa, S. Three-dimensional reconstruction of tubular structure of vacuolar membrane throughout mitosis in living tobacco cells. *Plant Cell Physiol.* **44**, 1045-1054 (2003).

8. Higaki, T., Kutsuna, N., Okubo, E., Sano, T. & Hasezawa, S. Actin microfilaments regulate vacuolar structures and dynamics: dual observation of actin microfilaments and vacuolar membrane in living tobacco BY-2 cells. *Plant Cell Physiol.* **47**, 839-852 (2006).

9. Staiger, C.J. *et al.* Microinjected profilin affects cytoplasmic streaming in plant cells by rapidly depolymerizing actin microfilaments. *Curr. Biol.* **4**, 215-219 (1994).

10. Hoffmann, A. & Nebenführ, A. Dynamic rearrangements of transvacuolar strands in BY-2 cells imply a role of myosin in remodeling the plant actin cytoskeleton. *Protoplasma* **224**, 201-210 (2004).

11. Sparks, J.A. *et al.* HLB1 is a tetratricopeptide repeat domain-containing protein that operates at the intersection of the exocytic and endocytic pathways at the TGN/EE in Arabidopsis. *Plant Cell* **28**, 746-769 (2016).

12. Renna, L. *et al.* TGNap1 is required for microtubule-dependent homeostasis of a subpopulation of the plant trans-Golgi network. *Nature Communications* **9**, 5313 (2018).

13. Voeltz, G.K., Prinz, W.A., Shibata, Y., Rist, J.M. & Rapoport, T.A. A class of membrane proteins shaping the tubular endoplasmic reticulum. *Cell* **124**, 573-586 (2006).

14. Shibata, Y. *et al.* Mechanisms determining the morphology of the peripheral ER. *Cell* **143**, 774-788 (2010).

15. Hu, J.J. *et al.* A Class of Dynamin-like GTPases Involved in the Generation of the Tubular ER Network. *Cell* **138**, 549-561 (2009).

16. English, A.R. & Voeltz, G.K. Rab10 GTPase regulates ER dynamics and morphology. *Nat. Cell Biol.* **15**, 169-178 (2013).

17. Chen, S.L., Novick, P. & Ferro-Novick, S. ER network formation requires a balance of the dynamin-like GTPase Sey1p and the Lunapark family member Lnp1p. *Nat. Cell Biol.* **14**, 707-716 (2012).

18. Zhou, X. *et al.* Reciprocal regulation between lunapark and atlastin facilitates ER three-way junction formation. *Protein & Cell*, 1-16 (2018).

19. Sparkes, I. *et al.* Five Arabidopsis reticulon isoforms share endoplasmic reticulum location, topology, and membrane-shaping properties. *Plant Cell* **22**, 1333-1343 (2010).

20. Stefano, G., Renna, L., Moss, T., Mcnew, J.A. & Brandizzi, F. In Arabidopsis, the spatial and dynamic organization of the endoplasmic reticulum and Golgi apparatus is influenced by the integrity of the C-terminal domain of RHD3, a non-essential GTPase. *Plant J.* **69**, 957-966 (2012).

21. Chen, J., Stefano, G., Brandizzi, F. & Zheng, H.Q. Arabidopsis RHD3 mediates the generation of the tubular ER network and is required for Golgi distribution and motility in plant cells. *J. Cell Sci.* **124**, 2241-2252 (2011).

22. Kriechbaumer, V. *et al.* Arabidopsis Lunapark proteins are involved in ER cisternae formation. *New Phytol.* **219**, 990-1004 (2018).

23. Tolley, N. *et al.* Overexpression of a plant reticulon remodels the lumen of the cortical endoplasmic reticulum but does not perturb protein transport. *Traffic* **9**, 94-102 (2008).

24. Kriechbaumer, V. *et al.* Reticulomics: protein-protein interaction studies with two plasmodesmata-localized reticulon family proteins identify binding partners enriched at plasmodesmata, endoplasmic reticulum, and the plasma membrane. *Plant Physiol.* **169**, 1933-1945 (2015).

25. Ueda, H. *et al.* Endoplasmic reticulum (ER) membrane proteins (LUNAPARKs) are required for proper configuration of the cortical ER network in plant cells. *Plant Cell Physiol.* **59**, 1931-1941 (2018).

26. Breeze, E. *et al.* A C-terminal amphipathic helix is necessary for the in vivo tubule-shaping function of a plant reticulon. *Proc. Natl. Acad. Sci. U.S.A.* **113**, 10902-10907 (2016).

27. Lee, H. *et al.* An Arabidopsis reticulon and the atlastin homologue RHD3-like2 act together in shaping the tubular endoplasmic reticulum. *New Phytol.* **197**, 481-489 (2013).

28. Zhang, M. *et al.* ROOT HAIR DEFECTIVE3 family of dynamin-like GTPases mediates homotypic endoplasmic reticulum fusion and is essential for Arabidopsis development. *Plant Physiol.* **163**, 713-720 (2013).

29. Westrate, L.M., Lee, J.E., Prinz, W.A. & Voeltz, G.K. Form follows function: the importance of endoplasmic reticulum shape. *Annu. Rev. Biochem.* **84**, 791-811 (2015).

30. Shibata, Y., Hu, J.J., Kozlov, M.M. & Rapoport, T.A. Mechanisms shaping the membranes of cellular organelles. *Annu. Rev. Cell. Dev. Biol.* **25**, 329-354 (2009).

31. Powers, R.E., Wang, S.Y., Liu, T.Y. & Rapoport, T.A. Reconstitution of the tubular endoplasmic reticulum network with purified components. *Nature* **543**, 257-+ (2017).

32. Wang, S., Tukachinsky, H., Romano, F.B. & Rapoport, T.A. Cooperation of the ER-shaping proteins atlastin, lunapark, and reticulons to generate a tubular membrane network. *eLife* **5**, e18605 (2016).

33. Prinz, W.A. *et al.* Mutants affecting the structure of the cortical endoplasmic reticulum in Saccharomyces cerevisiae. *Journal of Cell Biology* **150**, 461-474 (2000).

34. Shemesh, T. *et al.* A model for the generation and interconversion of ER morphologies. *Proc. Natl. Acad. Sci. U.S.A.* **111**, E5243-E5251 (2014).

35. Terasaki, M., Chen, L.B. & Fujiwara, K. Microtubules and the endoplasmic-reticulum are highly interdependent structures. *J. Cell Biol.* **103**, 1557-1568 (1986).

36. Shibata, Y. *et al.* The reticulon and DP1/Yop1p proteins form immobile oligomers in the tubular endoplasmic reticulum. *J. Biol. Chem.* **283**, 18892-18904 (2008).

37. Fehrenbacher, K.L., Davis, D., Wu, M., Boldogh, I. & Pon, L.A. Endoplasmic reticulum dynamics, inheritance, and cytoskeletal interactions in budding yeast. *Mol. Biol. Cell* **13**, 854-865 (2002).

38. Quader, H., Hofmann, A. & Schnepf, E. Reorganization of the endoplasmic reticulum in epidermal cells of onion bulb scales after cold stress - involvement of cytoskeletal elements. *Planta* **177**, 273-280 (1989).

39. Quader, H. Formation and disintegration of cisternae of the endoplasmic reticulum visualized in live cells by conventional fluorescence and confocal laser scanning microscopy: Evidence for the involvement of calcium and the cytoskeleton. *Protoplasma* **155**, 166-175 (1990).

40. Staehelin, L.A. The plant ER: a dynamic organelle composed of a large number of discrete functional domains. *Plant J.* **11**, 1151-1165 (1997).

41. Cao, P., Renna, L., Stefano, G. & Brandizzi, F. SYP73 anchors the ER to the actin cytoskeleton for maintenance of ER integrity and streaming in Arabidopsis. *Curr. Biol.* **26**, 3245-3254 (2016).

42. Stefano, G., Renna, L. & Brandizzi, F. The endoplasmic reticulum exerts control over organelle streaming during cell expansion. *J. Cell Sci.* **127**, 947-953 (2014).

43. Boevink, P. *et al.* Stacks on tracks: the plant Golgi apparatus traffics on an actin/ER network. *Plant J.* **15**, 441-447 (1998).

44. Peremyslov, V.V., Prokhnevsky, A.I. & Dolja, V.V. Class XI myosins are required for development, cell expansion, and F-actin organization in Arabidopsis. *Plant Cell* **22**, 1883-1897 (2010).

45. Nixon-Abell, J. *et al.* Increased spatiotemporal resolution reveals highly dynamic dense tubular matrices in the peripheral ER. *Science* **354**, aaf3928 (2016).

46. Guo, Y.T. *et al.* Visualizing Intracellular Organelle and Cytoskeletal Interactions at Nanoscale Resolution on Millisecond Timescales. *Cell* **175**, 1430-1442 (2018).

47. Sparkes, I., Runions, J., Hawes, C. & Griffing, L. Movement and remodeling of the endoplasmic reticulum in nondividing cells of tobacco leaves. *Plant Cell* **21**, 3937-3949 (2009).

48. Bola, B. & Allan, V. How and why does the endoplasmic reticulum move? *Biochem. Soc. Trans.* **37**, 961-965 (2009).

49. Waterman-Storer, C.M. & Salmon, E.D. Endoplasmic reticulum membrane tubules are distributed by microtubules in living cells using three distinct mechanisms. *Curr. Biol.* **8**, 798-806 (1998).

50. Yokota, E. *et al.* Myosin XI-dependent formation of tubular structures from endoplasmic reticulum isolated from tobacco cultured BY-2 cells. *Plant Physiol.* **156**, 129-143 (2011).

51. Pollard, T.D. & Goldman, R.D. Overview of the cytoskeleton from an evolutionary perspective. *Cold Spring Harb. Perspect. Biol.* **10** (2018).

52. Joensuu, M. *et al.* ER sheet persistence is coupled to myosin 1c-regulated dynamic actin filament arrays. *Mol. Biol. Cell* **25**, 1111-1126 (2014).

53. Poteryaev, D., Squirrell, J.M., Campbell, J.M., White, J.G. & Spang, A. Involvement of the actin cytoskeleton and homotypic membrane fusion in ER dynamics in Caenorhabditis elegans. *Mol. Biol. Cell* **16**, 2139-2153 (2005).

54. Hamada, T., Ueda, H., Kawase, T. & Hara-Nishimura, I. Microtubules contribute to tubule elongation and anchoring of endoplasmic reticulum, resulting in high network complexity in Arabidopsis. *Plant Physiol.* **166**, 1869-U1042 (2014).

55. Molines, A.T. *et al.* EB1 contributes to microtubule bundling and organization, along with root growth, in Arabidopsis thaliana. *Biology Open* **7**, bio030510 (2018).

56. Mathur, J., Mathur, N., Kernebeck, B., Srinivas, B.P. & Hulskamp, M. A novel localization pattern for an EB1-like protein links microtubule dynamics to endomembrane organization. *Curr. Biol.* **13**, 1991-1997 (2003).

57. Dhonukshe, P., Mathur, J., Hulskamp, M. & Gadella, T.W.J. Microtubule plus-ends reveal essential links between intracellular polarization and localized modulation of endocytosis during division-plane establishment in plant cells. *BMC Biol.* **3**, 11 (2005).

58. Boevink, P., SantaCruz, S., Oparka, K.J. & Hawes, C. Virus-mediated delivery of the green fluorescent protein to the endoplasmic reticulum of tobacco cells. *Mol. Biol. Cell* **7**, 426-426 (1996).

59. Nebenfuhr, A. & Dixit, R. Kinesins and myosins: Molecular motors that coordinate cellular functions in plants. *Annu. Rev. Plant Biol.* **69**, 329-361 (2018).

60. Ueda, H., Tamura, K. & Hara-Nishimura, I. Functions of plant-specific myosin XI: from intracellular motility to plant postures. *Curr. Opin. Plant Biol.* **28**, 30-38 (2015).

61. Avisar, D., Prokhnevsky, A.I., Makarova, K.S., Koonin, E.V. & Dolja, V.V. Myosin XI-K is required for rapid trafficking of Golgi stacks, peroxisomes, and mitochondria in leaf cells of Nicotiana benthamiana. *Plant Physiol.* **146**, 1098-1108 (2008).

62. Prokhnevsky, A.I., Peremyslov, V.V. & Dolja, V.V. Overlapping functions of the four class XI myosins in Arabidopsis growth, root hair elongation, and organelle motility. *Proc. Natl. Acad. Sci. U.S.A.* **105**, 19744-19749 (2008).

63. Peremyslov, V.V., Prokhnevsky, A.I., Avisar, D. & Dolja, V.V. Two class XI myosins function in organelle trafficking and root hair development in Arabidopsis. *Plant Physiol.* **146**, 1109-1116 (2008).

64. Madison, S.L. *et al.* Class XI myosins move specific organelles in pollen tubes and are required for normal fertility and pollen tube growth in Arabidopsis. *Plant Physiol.* **169**, 1946-1960 (2015).

65. Griffing, L.R., Gao, H.B.T. & Sparkes, I. ER network dynamics are differentially controlled by myosins XI-K, XI-C, XI-E, XI-I, XI-1, and XI-2. *Front Plant Sci* **5**, 218 (2014).

66. Kurth, E.G. *et al.* Myosin-driven transport network in plants. *Proc. Natl. Acad. Sci. U.S.A.* **114**, E1385-E1394 (2017).

67. Peremyslov, V.V., Klocko, A.L., Fowler, J.E. & Dolja, V.V. Arabidopsis myosin XI-K localizes to the motile endomembrane vesicles associated with F-actin. *Front Plant Sci* **3** (2012).

68. Peremyslov, V.V. *et al.* Identification of myosin XI receptors in Arabidopsis defines a distinct class of transport vesicles. *Plant Cell* **25**, 3022-3038 (2013).

69. Stefano, G. & Brandizzi, F. Advances in Plant ER Architecture and Dynamics. *Plant Physiol* **176**, 178-186 (2018).

70. Stefano, G. *et al.* ER network homeostasis is critical for plant endosome streaming and endocytosis. *Cell Discovery* **1**, 15033 (2015).

71. Deeks, M.J. *et al.* A superfamily of actin-binding proteins at the actin-membrane nexus of higher plants. *Curr. Biol.* **22**, 1595-1600 (2012).

72. Wang, P.W. *et al.* The plant cytoskeleton, NET3C, and VAP27 mediate the link between the plasma membrane and endoplasmic reticulum. *Curr. Biol.* **24**, 1397-1405 (2014).

73. Wang, P. *et al.* Plant VAP27 proteins: domain characterization, intracellular localization and role in plant development. *New Phytol.* **210**, 1311-1326 (2016).

74. Wang, P. & Hussey, P.J. NETWORKED 3B: a novel protein in the actin cytoskeleton-endoplasmic reticulum interaction. *J. Exp. Bot.* **68**, 1441-1450 (2017).

75. Lv, F.N. *et al.* GhCFE1A, a dynamic linker between the ER network and actin cytoskeleton, plays an important role in cotton fibre cell initiation and elongation. *J. Exp. Bot.* **66**, 1877-1889 (2015).

76. Zhu, Y.M. *et al.* Sec61 beta facilitates the maintenance of endoplasmic reticulum homeostasis by associating microtubules. *Protein & Cell* **9**, 616-628 (2018).

77. Wang, X., Li, S., Wang, H., Shui, W. & Hu, J. Quantitative proteomics reveal proteins enriched in tubular endoplasmic reticulum of Saccharomyces cerevisiae. *eLife* **6**, e23816 (2017).

78. Hoyer, M.J. *et al.* A novel class of ER membrane proteins regulates ER-associated endosome fission. *Cell* **175**, 254-265 (2018).

79. Bayer, E.M., Sparkes, I., Vanneste, S. & Rosado, A. From shaping organelles to signalling platforms: the emerging functions of plant ER-PM contact sites. *Curr. Opin. Plant Biol.* **40**, 89-96 (2017).

80. Wang, P.W., Hawes, C. & Hussey, P.J. Plant endoplasmic reticulum-plasma membrane contact sites. *Trends Plant Sci.* **22**, 289-297 (2017).

81. Stefano, G. *et al.* Plant endocytosis requires the ER membrane-anchored proteins VAP27-1 and VAP27-3. *Cell Reports* **23**, 2299-2307 (2018).

82. Saravanan, R.S. *et al.* The targeting of the oxysterol‐binding protein ORP3a to the endoplasmic reticulum relies on the plant VAP33 homolog PVA12. *Plant J.* **58**, 817-830 (2009).

83. Siao, W., Wang, P.W., Voigt, B., Hussey, P.J. & Baluska, F. Arabidopsis SYT1 maintains stability of cortical endoplasmic reticulum networks and VAP27-1-enriched endoplasmic reticulum-plasma membrane contact sites. *J. Exp. Bot.* **67**, 6161-6171 (2016).

84. Lewis, J.D. & Lazarowitz, S.G. Arabidopsis synaptotagmin SYTA regulates endocytosis and virus movement protein cell-to-cell transport. *Proc. Natl. Acad. Sci. U.S.A.* **107**, 2491-2496 (2010).

85. Lee, E. *et al.* Ionic stress enhances ER-PM connectivity via phosphoinositide-associated SYT1 contact site expansion in Arabidopsis. *Proc. Natl. Acad. Sci. U.S.A.* **116**, 1420-1429 (2019).

86. Chang, C.L., Chen, Y.J., Quintanilla, C.G., Hsieh, T.S. & Liou, J. EB1 binding restricts STIM1 translocation to ER-PM junctions and regulates store-operated Ca2+ entry. *J. Cell Biol.* **217**, 2047-2058 (2018).

87. van Vliet, A.R. *et al.* The ER stress sensor PERK coordinates ER-plasma membrane contact site formation through interaction with filamin-A and F-actin remodeling. *Mol. Cell* **65**, 885-899. e886 (2017).

88. del Dedo, J.E. *et al.* ORP-mediated ER contact with endocytic sites facilitates actin polymerization. *Dev. Cell* **43**, 588-602. e586 (2017).

89. Henne, W.M., Liou, J. & Emr, S.D. Molecular mechanisms of inter-organelle ER-PM contact sites. *Curr. Opin. Cell Biol.* **35**, 123-130 (2015).

90. Angelos, E., Ruberti, C., Kim, S.J. & Brandizzi, F. Maintaining the factory: the roles of the unfolded protein response in cellular homeostasis in plants. *Plant J.* **90**, 671-682 (2017).

91. Meagher, R.B. & Fechheimer, M. *The Arabidopsis cytoskeletal genome*, Vol. 2003. (BIOONE, 2003).

92. Szymanski, D.B. & Cosgrove, D.J. Dynamic coordination of cytoskeletal and cell wall systems during plant cell morphogenesis. *Curr. Biol.* **19**, R800-R811 (2009).

93. Feeney, M., Kittelmann, M., Menassa, R., Hawes, C. & Frigerio, L. Protein storage vacuoles originate from remodeled preexisting vacuoles in Arabidopsis thaliana. *Plant Physiol.* **177**, 241-254 (2018).

94. Cui, Y. *et al.* A whole-cell electron tomography model of vacuole biogenesis in Arabidopsis root cells. *Nature Plants* **5**, 95-105 (2019).

95. Zheng, J.M., Han, S.W., Rodriguez-Welsh, M.F. & Rojas-Pierce, M. Homotypic Vacuole Fusion Requires VTI11 and Is Regulated by Phosphoinositides. *Molecular Plant* **7**, 1026-1040 (2014).

96. Li, L.J., Ren, F., Gao, X.Q., Wei, P.C. & Wang, X.C. The reorganization of actin filaments is required for vacuolar fusion of guard cells during stomatal opening in Arabidopsis. *Plant Cell and Environment* **36**, 484-497 (2013).

97. Li, S.C. & Kane, P.M. The yeast lysosome-like vacuole: Endpoint and crossroads. *Biochim. Biophys. Acta* **1793**, 650-663 (2009).

98. Wickner, W. Membrane fusion: five lipids, four SNAREs, three chaperones, two nucleotides, and a rab, all dancing in a ring on yeast vacuoles. *Annu. Rev. Cell. Dev. Biol.* **26**, 115-136 (2010).

99. Takenawa, T. & Suetsugu, S. The WASP-WAVE protein network: connecting the membrane to the cytoskeleton. *Nature Reviews Molecular Cell Biology* **8**, 37-48 (2007).

100. Eitzen, G. Actin remodeling to facilitate membrane fusion. *Biochimica Et Biophysica Acta-Molecular Cell Research* **1641**, 175-181 (2003).

101. Eitzen, G., Wang, L., Thorngren, N. & Wickner, W. Remodeling of organelle-bound actin is required for yeast vacuole fusion. *J. Cell Biol.* **158**, 669-679 (2002).

102. Eitzen, G., Thorngren, N. & Wickner, W. Rho1p and Cdc42p act after Ypt7p to regulate vacuole docking. *EMBO J.* **20**, 5650-5656 (2001).

103. Muller, O., Johnson, D.I. & Mayer, A. Cdc42p functions at the docking stage of yeast vacuole membrane fusion. *EMBO J.* **20**, 5657-5665 (2001).

104. Bodman, J.A.R., Yang, Y., Logan, M.R. & Eitzen, G. Yeast translation elongation factor-1A binds vacuole-localized Rho1p to facilitate membrane integrity through F-actin remodeling. *J. Biol. Chem.* **290**, 4705-4716 (2015).

105. Isgandarova, S. *et al.* Stimulation of actin polymerization by vacuoles via Cdc42p-dependent signaling. *J. Biol. Chem.* **282**, 30466-30475 (2007).

106. Jones, L., Tedrick, K., Baier, A., Logan, M.R. & Eitzen, G. Cdc42p is activated during vacuole membrane fusion in a sterol-dependent subreaction of priming. *J. Biol. Chem.* **285**, 4298-4306 (2010).

107. Feiguelman, G., Fu, Y. & Yalovsky, S. ROP GTPases Structure-Function and Signaling Pathways. *Plant Physiol* **176**, 57-79 (2018).

108. Taiz, L. Plant cell expansion: regulation of cell wall mechanical properties. *Annu. Rev. Plant Physiol. Plant Mol. Biol.* **35**, 585-657 (1984).

109. Löfke, C., Dünser, K., Scheuring, D. & Kleine-Vehn, J. Auxin regulates SNARE-dependent vacuolar morphology restricting cell size. *eLife* **4**, e05868 (2015).

110. Scheuring, D. *et al.* Actin-dependent vacuolar occupancy of the cell determines auxin-induced growth repression. *Proc. Natl. Acad. Sci. U.S.A.* **113**, 452-457 (2016).

111. Ren, M. *et al.* Target of rapamycin signaling regulates metabolism, growth, and life span in Arabidopsis. *Plant Cell* **24**, 4850-4874 (2012).

112. Gosavi, P. & Gleeson, P.A. The function of the golgi ribbon structure - an enduring mystery unfolds! *Bioessays* **39**, 1700063 (2017).

113. Sparkes, I.A., Ketelaar, T., de Ruijter, N.C.A. & Hawes, C. Grab a golgi: Laser trapping of golgi bodies reveals in vivo interactions with the endoplasmic reticulum. *Traffic* **10**, 567-571 (2009).

114. Brandizzi, F., Snapp, E.L., Roberts, A.G., Lippincott-Schwartz, J. & Hawes, C. Membrane protein transport between the endoplasmic reticulum and the golgi in tobacco leaves is energy dependent but cytoskeleton independent: Evidence from selective photobleaching. *Plant Cell* **14**, 1293-1309 (2002).

115. Nebenfuhr, A. *et al.* Stop-and-go movements of plant Golgi stacks are mediated by the acto-myosin system. *Plant Physiol.* **121**, 1127-1141 (1999).

116. Avisar, D., Abu-Abied, M., Belausov, E. & Sadot, E. Myosin XIK is a major player in cytoplasm dynamics and is regulated by two amino acids in its tail. *J. Exp. Bot.* **63**, 241-249 (2012).

117. Wei, L.Q., Zhang, W., Liu, Z.H. & Li, Y. AtKinesin-13A is located on golgi-associated vesicle and involved in vesicle formation/budding in Arabidopsis root-cap peripheral cells. *BMC Plant Biol.* **9**, 138 (2009).

118. Lu, L., Lee, Y.R.J., Pan, R.Q., Maloof, J.N. & Liu, B. An internal motor kinesin is associated with the golgi apparatus and plays a role in trichome morphogenesis in Arabidopsis. *Mol. Biol. Cell* **16**, 811-823 (2005).

119. Akkerman, M., Overdijk, E.J.R., Schel, J.H.N., Emons, A.M.C. & Ketelaar, T. Golgi body motility in the plant cell cortex correlates with actin cytoskeleton organization. *Plant Cell Physiol.* **52**, 1844-1855 (2011).

120. Breuer, D. *et al.* System-wide organization of actin cytoskeleton determines organelle transport in hypocotyl plant cells. *Proc. Natl. Acad. Sci. U.S.A.* **114**, E5741-E5749 (2017).

121. Yadav, S. & Linstedt, A.D. Golgi positioning. *Cold Spring Harb. Perspect. Biol.* **3** (2011).

122. Uemura, T., Suda, Y., Ueda, T. & Nakano, A. Dynamic behavior of the trans-golgi network in root tissues of Arabidopsis revealed by super-resolution live imaging. *Plant Cell Physiol.* **55**, 694-703 (2014).

123. Baluska, F. *et al.* F-actin-dependent endocytosis of cell wall pectins in meristematic root cells. Insights from brefeldin A-induced compartments. *Plant Physiol.* **130**, 422-431 (2002).

124. Kim, H., Park, M., Kim, S.J. & Hwang, I. Actin filaments play a critical role in vacuolar trafficking at the Golgi complex in plant cells. *Plant Cell* **17**, 888-902 (2005).

125. Stephan, O. *et al.* RISAP is a TGN-associated RAC5 effector regulating membrane traffic during polar cell growth in tobacco. *Plant Cell* **26**, 4426-4447 (2014).

126. Granger, E., McNee, G., Allan, V. & Woodman, P. The role of the cytoskeleton and molecular motors in endosomal dynamics. *Semin. Cell Dev. Biol.* **31**, 20-29 (2014).

127. Simonetti, B. & Cullen, P.J. Actin-dependent endosomal receptor recycling. *Curr. Opin. Cell Biol.* **56**, 22-33 (2019).

128. Ambrose, C. *et al.* CLASP interacts with sorting nexin 1 to link microtubules and auxin transport via PIN2 recycling in Arabidopsis thaliana. *Dev. Cell* **24**, 649-659 (2013).

129. Rakusová, H., Han, H., Valošek, P. & Friml, J. Genetic screen for factors mediating PIN polarization in gravistimulated Arabidopsis thaliana hypocotyls. *Plant J.* (2019).

130. Kang, Y.S. *et al.* HopW1 from Pseudomonas syringae disrupts the actin cytoskeleton to promote virulence in Arabidopsis. *PLoS Path.* **10**, 1-10 (2014).

131. Beck, M., Zhou, J., Faulkner, C., MacLean, D. & Robatzek, S. Spatio-temporal cellular dynamics of the Arabidopsis flagellin receptor reveal activation status-dependent endosomal sorting. *Plant Cell* **24**, 4205-4219 (2012).

132. Friml, J. Subcellular trafficking of PIN auxin efflux carriers in auxin transport. *Eur. J. Cell Biol.* **89**, 231-235 (2010).

133. Geldner, N., Friml, J., Stierhof, Y.D., Jurgens, G. & Palme, K. Auxin transport inhibitors block PIN1 cycling and vesicle traficking. *Nature* **413**, 425-428 (2001).

134. Friml, J., Wisniewska, J., Benkova, E., Mendgen, K. & Palme, K. Lateral relocation of auxin efflux regulator PIN3 mediates tropism in Arabidopsis. *Nature* **415**, 806-809 (2002).

135. Kleine-Vehn, J., Dhonukshe, P., Swarup, R., Bennett, M. & Friml, J. Subcellular trafficking of the Arabidopsis auxin influx carrier AUX1 uses a novel pathway distinct from PIN1. *Plant Cell* **18**, 3171-3181 (2006).

136. Hu, Y.F. *et al.* Narciclasine, a potential allelochemical, affects subcellular trafficking of auxin transporter proteins and actin cytoskeleton dynamics in Arabidopsis roots. *Planta* **242**, 1349-1360 (2015).

137. Ivanov, R. *et al.* SORTING NEXIN1 is required for modulating the trafficking and stability of the Arabidopsis IRON-REGULATED TRANSPORTER1. *Plant Cell* **26**, 1294-1307 (2014).

138. Niemes, S. *et al.* Sorting of plant vacuolar proteins is initiated in the ER. *Plant J.* **62**, 601-614 (2010).

139. Pourcher, M. *et al.* Analyses of SORTING NEXINs reveal distinct retromer-subcomplex functions in development and protein sorting in Arabidopsis thaliana. *Plant Cell* **22**, 3980-3991 (2010).

140. Li, P. & Day, B. Battlefield cytoskeleton: Turning the tide on plant immunity. *Mol. Plant-Microbe Interact.* **32**, 25-34 (2019).

141. Bashline, L., Li, S.D. & Gu, Y. The trafficking of the cellulose synthase complex in higher plants. *Ann. Bot.* **114**, 1059-1067 (2014).

142. Gutierrez, R., Lindeboom, J.J., Paredez, A.R., Emons, A.M.C. & Ehrhardt, D.W. Arabidopsis cortical microtubules position cellulose synthase delivery to the plasma membrane and interact with cellulose synthase trafficking compartments. *Nat. Cell Biol.* **11**, 797-U743 (2009).

143. Crowell, E.F. *et al.* Pausing of golgi bodies on microtubules regulates secretion of cellulose synthase complexes in Arabidopsis. *Plant Cell* **21**, 1141-1154 (2009).

144. Zhu, X., Li, S., Pan, S., Xin, X. & Gu, Y. CSI1, PATROL1, and exocyst complex cooperate in delivery of cellulose synthase complexes to the plasma membrane. *Proc. Natl. Acad. Sci. U.S.A.* **115**, E5635-E5635 (2018).

145. Gu, Y. *et al.* Identification of a cellulose synthase-associated protein required for cellulose biosynthesis. *Proc. Natl. Acad. Sci. U.S.A.* **107**, 12866-12871 (2010).

146. Hashimoto-Sugimoto, M. *et al.* A Munc13-like protein in Arabidopsis mediates H+-ATPase translocation that is essential for stomatal responses. *Nature Communications* **4**, 2215 (2013).

147. Zhong, R.Q., Burk, D.H., Morrison, W.H. & Ye, Z.H. A kinesin-like protein is essential for oriented deposition of cellulose microfibrils and cell wall strength. *Plant Cell* **14**, 3101-3117 (2002).

148. Kong, Z.S. *et al.* Kinesin-4 functions in vesicular transport on cortical microtubules and regulates cell wall mechanics during cell elongation in plants. *Molecular Plant* **8**, 1011-1023 (2015).

149. Zhu, C.M. *et al.* The Fragile Fiber1 kinesin contributes to cortical microtubule-mediated trafficking of cell wall components. *Plant Physiol.* **167**, 780-792 (2015).

150. Spiegelman, Z., Lee, C.M. & Gallagher, K.L. KinG is a plant-specific kinesin that regulates both intra- and intercellular movement of SHORT-ROOT. *Plant Physiol.* **176**, 392-405 (2018).

151. Monastyrska, I., Rieter, E., Klionsky, D.J. & Reggiori, F. Multiple roles of the cytoskeleton in autophagy. *Biological Reviews* **84**, 431-448 (2009).

152. Kruppa, A.J., Kendrick-Jones, J. & Buss, F. Myosins, actin and autophagy. *Traffic* **17**, 878-890 (2016).

153. Pankiv, S. *et al.* FYCO1 is a Rab7 effector that binds to LC3 and PI3P to mediate microtubule plus end-directed vesicle transport. *J. Cell Biol.* **188**, 253-269 (2010).

154. Wang, Y. *et al.* Disruption of microtubules in plants suppresses macroautophagy and triggers starch excess-associated chloroplast autophagy. *Autophagy* **11**, 2259-2274 (2015).

155. Ketelaar, T., Voss, C., Dimmock, S.A., Thumm, M. & Hussey, P.J. Arabidopsis homologues of the autophagy protein Atg8 are a novel family of microtubule binding proteins. *FEBS Lett.* **567**, 302-306 (2004).

156. Zientara-Rytter, K. & Sirko, A. Selective autophagy receptor Joka2 co-localizes with cytoskeleton in plant cells. *Plant Signal Behav.* **9**, e28523 (2014).

157. Wang, P.W., Richardson, C., Hawes, C. & Hussey, P.J. Arabidopsis NAP1 regulates the formation of autophagosomes. *Curr. Biol.* **26**, 2060-2069 (2016).

CHAPTER 2. SYP73 ANCHORS THE ER TO THE ACTIN CYTOSKELETON FOR MAINTENANCE OF ER INTEGRITY AND STREAMING IN *ARABIDOPSIS*

The work presented in this chapter has been published:

Current Biology 26, no. 23 (2016): 3245-3254.

Pengfei Cao[1,2], Luciana Renna[1,2], Giovanni Stefano[1,2] and Federica Brandizzi[1,2,*]

[1]MSU-DOE Plant Research Lab, Michigan State University, East Lansing, MI 48824, USA.

[2]Department of Plant Biology, Michigan State University, East Lansing, MI 48824, USA.

*Corresponding author

2.1 ABSTRACT

The ER is an essential organelle that spreads throughout the cytoplasm as one interconnected network of narrow tubules and dilated cisternae that enclose a single lumen. The ER network undergoes extensive remodeling, which critically depends on membrane-cytoskeleton interactions [1]. In plants the ER is also highly mobile and its streaming significantly contributes to the movement of other organelles [2, 3]. The remodeling and motility of the plant ER rely mainly on actin [4] and to a minor extent on microtubules [5]. While a three-way interaction between the ER, cytosolic myosin-XI, and F-actin mediates the plant ER streaming [6], the mechanisms underlying stable interaction of the ER membrane with actin are unknown. Early electron microscopy studies suggested a direct attachment of the plant ER with actin filaments [7, 8], but it is plausible that yet-unknown proteins facilitate anchoring of the ER membrane with the cytoskeleton. We demonstrate that SYP73, a member of the plant Syp7 subgroup of SNARE proteins [9] containing actin-binding domains, is a novel ER membrane-associated actin-binding protein. We show that overexpression of SYP73 causes a striking rearrangement of the ER over actin and that, similar to mutations of myosin-XI [4, 10, 11], loss of SYP73 reduces ER streaming, affects overall ER network morphology and plant growth. We propose a novel model for plant ER remodeling whereby the dynamic rearrangement and streaming of the ER network depend on the propelling action of myosin-XI over actin coupled with a SYP73-mediated bridging, which dynamically anchors the ER membrane with actin filaments.

2.1 RESULTS

2.1.1 The ER-Localized SYP73 Reshapes the ER Network to Overlay Actin Cables

In order to identify an anchor between the plant ER membrane and actin cytoskeleton we set up to isolate proteins with similar domains and functional attributes to CLIMP-63/p63, the first

identified anchor between the ER membrane and cytoskeleton in mammalian cells. CLIMP-63/p63 is an integral ER membrane protein containing a central microtubule-binding domain that rearranges the ER over the microtubules when overexpressed [12]. We therefore scanned the Arabidopsis ER proteome [13] in search of protein sequences that analogously to CLIMP-63/p63 contained a putative membrane anchor as well as a cytosolic tail with cytoskeleton binding domain(s), specifically actin. We also expected that similar to the ER remodeling ability of CLIMP63/p63 over microtubules, a plant ER membrane-actin anchor would extensively rearrange the ER over actin when overexpressed. In our searches, we identified SYP73 a member of SYP7 family of plant-unique SNAREs that consists of three proteins (i.e., SYP71, SYP72 and SYP73) (Figures 2.5 A-C) predicted to contain a putative transmembrane domain with no harpin domain and a cytosolic region (Figures 2.5 D and 2.6 D) with actin-binding domains (Figures 2.6 A-C). SYP71 has been localized to the ER, plasma membrane and cell plate, and facilitates vesicular transport in cytokinesis [9, 14]. SYP71 is also involved in membrane fusion between virus-induced vesicles and chloroplasts [15]. However, the other two members of the SYP7 subgroup, SYP72 and SYP73, have not been yet functionally characterized. The three proteins share overall good degree of sequence similarity but marked differences in a central variable domain (Figure 2.5 B). This suggested to us the possibility of a functional diversification of among the SYP7-proteins. We confirmed the proteomics results that SYP73 is an ER protein through live-cell analyses of a green fluorescent protein fusion to SYP73 (SYP73-GFP) in co-expression with the established ER lumenal marker ERYK (Figure 2.1). SYP73 was distributed to the overall ER network, ER-plasma membrane anchoring sites (Figures 2.6 E and F), and, albeit only to minor extent, to points of yet-unknown nature in which ERYK was excluded (Figures 2.1 B and E). We also verified that in high-expressing cells (Figures 2.1 C and F) the pattern of SYP73-GFP distribution changed

substantially from that of cells with lower fluorescence levels (Figures 2.1 B and E). Specifically, in highly expressing cells the ER labelled by SYP73-GFP assumed a modified morphology with enhancement of the tubular network and visible reduction of the appearance of the cisternal ER (Figures 2.1 C, F and G). Such acquired ER network morphology strikingly resembled that of the organization of actin cables, which normally underlie the ER but do not completely overlap with the ER network [16] (Figures 2.2 A and B). Indeed, co-expression analyses of SYP73-GFP with either the F-actin marker YFP-ABD2 or the microtubule marker YFP-TUA6 indicated that the modified ER network labelled by SYP73-GFP largely overlapped with the actin network (Figures 2.2 D and G) but not with the microtubule cytoskeleton (Figures 2.6 G, H and I). The evidence that overexpression of an untagged SYP73 led to a similar ER rearrangement compared to overexpression of SYP73-GFP (Figures 2.7 A and B) indicated that the effect of SYP73 on the ER is not due to the presence of a fluorescent protein. Also, the evidence that high expression of the bulk membrane marker GFP-Calnexin did not lead to ER rearrangement to an actin-like organization besides a slight enlargement of the ER toward a more cisternal form (Figure 2.2 C) [17] further supported specificity of the ER shaping effect of SYP73.

We next aimed to test whether the verified ER rearrangement effect of SYP73 was due to overexpression of the transmembrane anchor of the protein. To do so, we constructed a SYP73-putative transmembrane domain and short luminal tail (residues 239-264) (SYP73TMC) and expressed it as a yellow fluorescent protein fusion (SYP73TMC-YFP) along with GFP-Calnexin to visualize the ER membrane. We established that SYP73TMC-YFP was distributed to the ER network whose morphology was not altered by the presence of this protein (Figure 2.7 C). This experiment indicates that the putative transmembrane domain of SYP73 functions to target SYP73 to the ER and that the ER-rearranging action of SYP73 is not due to over-representation of such a

domain in the ER. The results also support the likelihood that overexpression of SYP73 leads to ER rearrangement through mechanisms involving the cytoplasmic region of this protein.

A handful of plant ER-shaping proteins are currently known and these include ER membrane proteins such as reticulons [18] and RHD3 [19, 20]. Reticulons likely facilitate curvature of the ER tubules because of the wedge-like transmembrane topology of their conserved hydrophobic segments, which would force membrane tubulation by insertion into the lipid bilayer [3, 21]. Overexpression of reticulons leads to constrictions of the ER lumen and reduction of the fluidity of the luminal content [22]. The ER-anchored dynamin-like GTPase RHD3 on the other hand facilitates homotypic membrane fusion in virtue of the fusogenic action of the cytosolic domain [23]. Overexpression of RHD3 leads to elongated ER tubules [24], most likely because of excess of fusion events. In our work we have established that when overexpressed SYP73 modifies the ER into a network that mirrors the actin cytoskeleton. These data support that SYP73 is a novel modifier of the ER network shape. The evidence that overexpression of the transmembrane domain does not affect the ER morphology indicates that the ER shaping role of SYP73 necessitates the cytosolic domain. Indeed, contrarily to reticulons SYP73 transmembrane region is not predicted to assume a wedge-like structure (Figure 2.5 D), posing the possibility that the transmembrane domain is simply required to anchor the cytosolic domain to the ER, which in turn executes the ER rearranging effect.

2.1.2 SYP73 Binds F-Actin Directly

Based on the evidence of a striking ER remodeling ability of SYP73 to overlay the ER network over the actin cables and the stringent requirement of the presence of an ER membrane anchor for the ER remodeling effect of this protein, we hypothesized that SYP73 could bind actin and function as a tether between the ER membrane and the actin cytoskeleton. This hypothesis is strongly

supported by the presence of protein domains in SYP73 that are predicted to bind actin (Figures 2.6 B and C), and by the evidence that, unlike Cytosolic YFP (control, Figures 2.7 F and G), a fluorescent protein fusion to the cytosolic domain of SYP73 (YFP-SYP73ΔTM) associates with intact actin cables in plant cells (Figure 2.7 D), but it is distributed in the cytosol in cells with depolymerized actin (Figure S3E). Therefore, we next assayed the ability of the cytosolic domain of SYP73 to bind actin directly using high-speed co-sedimentation analyses with recombinant His-tagged SYP73ΔTM (His-SYP73ΔTM; MW= 30.6 KDa) and actin (MW= 42 KDa). The known actin-binding tropomyosin was used as positive control, while BSA was used as negative control. In this assay, actin-interacting proteins sediment with actin upon ultracentrifugation while non-interacting proteins remain mainly in the supernatant because of the lack of interaction with actin. After one hour's incubation with pre-polymerized F-actin, proteins were pelleted by 135,000*g* ultracentrifugation. As actin-free samples, we omitted actin in the incubation reaction with His-SYP73ΔTM, tropomyosin or BSA. SDS-PAGE runs followed by Coomassie blue staining verified that small amount of tropomyosin was detected in pellet after actin-free incubation, while most tropomyosin co-sedimented with actin (Figure 2.2 H, lanes 7-10). When we analyzed His-SYP73ΔTM samples, we found two bands that correspond to the MW of His-SYP73ΔTM monomers (*) and dimers (arrowhead) (Figure 2.2 H); the dimers were disrupted by urea treatment (Figure 2.2 K), suggesting that SYP73 may form strong dimers *in vivo*. Similary to tropomyosin, only a small amount of His-SYP73ΔTM was found in the pellet in the absence of actin (Figure 2.2 H, lanes 1-2). However upon incubation with actin, both monomer and dimer His-SYP73ΔTM forms co-sedimented with actin (Figure 2.2 H, lanes 5-6). The negative control BSA remained in supernatant even after incubation with actin (Figure 2.2 H, lanes 11-14). These data demonstrate a direct interaction between His-SYP73ΔTM and F-actin directly. Next we aimed to determine

whether the binding of SYP73ΔTM to F-actin was saturable, and therefore we performed high-speed co-sedimentation assays using increasing concentrations of His-SYP73ΔTM and constant amount of actin. After incubation, the supernatant and pellet were separated by ultracentrifugation, then subjected to SDS-PAGE and Coomassie blue staining (Figure 2.2 I). The amounts of bound and free His-SYP73ΔTM were quantified by gel densitometry, and the bound SYP73ΔTM values were plotted against those of free SYP73ΔTM for fitting to a hyperbolic function (Figure 2.2 L). We found that the binding of SYP73ΔTM to actin was indeed saturable, as it occurs for other plant actin-binding proteins. These results indicate that the cytosolic domain of SYP73 binds filamentous actin directly.

Together our data support a model whereby overexpression of SYP73 may lead to an enhanced anchoring of the ER to the actin cytoskeleton. To gain evidence for this model *in vivo,* we disrupted actin with the actin depolymerizing agent latrunculin B (Lat B) in cells expressing SYP73-GFP and YFP-ABD2. We hypothesized that loss of actin integrity would relieve the SYP73-mediated anchoring of the modified ER membrane network from actin and consequently that the ER would resume morphology. Indeed, we verified that disruption of actin led to remodeling of the ER to a network of collapsed cisternae and tubular ER (Figure 2.2 F) similar to the phenotype of Lat B-treated cells expressing GFP-Calnexin alone [4] (Figure 2.2 E). Therefore, together our results support that SYP73 is an ER protein that binds actin and anchors the ER to the underlying actin cytoskeleton. These results assign a cellular function to SYP73 which is analogous to that of the CLIMP-63/p63 in anchoring the ER membrane to the cytoskeleton in mammalian cells [25]. Nonetheless, substantial differences between SYP73 and CLIMP-63 exist. Besides the ability of the two proteins to anchor the ER to different cytoskeletal proteins, CLIMP-63 has been reported to be an ER sheet protein in mammalian cells, while proteins such as ER-shaping REEPs mediate

attachment of ER tubules with microtubules [26]. The evidence that SYP73 is not restricted to sheets or tubules highlights that plants have evolved unique mechanisms to anchor the ER to the cytoskeleton. In general, our results also highlight an unexpected role of a plant SNARE. Generally, SNAREs exert a membrane fusogenic role through the formation of complexes on juxtaposed membranes of donor and acceptor organelles. It is also well established that SNAREs facilitate membrane traffic by interacting with several tethers [27] and are required for cell homeostasis through direct interaction with ion channels [28]. Nonetheless, mammalian SNAREs can directly associate with actin [29, 30] and vimentin [31]. The evidence provided in this work that SYP73 can bind actin supports that the interaction of SNAREs with the cytoskeleton is a conserved feature of these proteins. In this work we have not tested the actin binding properties of SYP71 and SYP72, and do not exclude that also these other SYP7 proteins may have an ER remodeling function similar to SYP73, a possibility that we will test in the future.

2.1.3 A *SYP73* Knockout Mutant Has Defects in Early Plant Growth

We next aimed to gain further insights on the functional role of SYP73 as anchor between the ER membrane and actin. Based on the notion that mutations that affect directly actin-myosin-driven streaming negatively affect plant growth [32], we hypothesized that loss of ER-actin anchoring contacts due to cellular depletion of SYP73 would lead to compromised plant growth. To test this hypothesis, we isolated a T-DNA insertion line knockout of *SYP73* (*syp73*; Figures 2.8 A and B) and generated complemented lines expressing SYP73 under the control of the endogenous promoter (*syp73*/ProSYP73::SYP73-YFP) for quantitative analyses of plant phenotype. We observed that compared to wild type and complemented lines three day-after-germination (3DAG), *syp73* had shorter length of the primary root and reduced fresh weight of the whole seedling (Figures 2.7 A and B). Morphometric analyses of the root tip of *syp73* and wild type (Figures 2.3

D and E) indicated no differences in the length of the zone comprising the root apex and division zone but a significant reduction of the length of the elongation zone in *syp73* compared to wild type. Furthermore, the number of cells in the zone comprising the root apex and division zone was higher in *syp73* compared to wild type (Figures 2.3 D and E). Together these results support that the loss of SYP73 compromises cell elongation at the root tip. They also indicate that the SYP73 fusion is functional. The *syp73* defects at early stages of growth were restored later as at 6DAG no differences were observed between wild type, *syp73* and the complemented line (Figure 2.3 B). These results indicate that SYP73 functions early in plant development and that later it becomes less influential. Analyses of root hair elongation showed no significant increase in *syp73* root hair elongation compared to wild type (Figure 2.3 C). This phenotype is opposite to that of the loss-of-function mutants of the ER shaper RHD3[33]. These data indicate that the mechanisms underlying the ER defects in *syp73* and *rhd3* have different effect on cell elongation. This is consistent with the evidence that the ER defects due to loss of RHD3 are independent of actin [33]. We have not verified other obvious defects in *syp73* growth and development, and therefore we conclude that SYP73 assumes roles that are highly regulated during development. The Arabidopsis genome encodes about 60 SNARE genes, which can be subdivided in gene subgroups with multiple members that can show either functional redundancy or stringent requirements for survival [34, 35]. Several of the Arabidopsis SNARE proteins are yet functionally uncharacterized. Our data provide evidence for the requirement of SYP73 in vegetative plant growth. Based on the evidence that SYP73 anchors the ER to actin presented thus far, we propose that the phenotypic growth defects of *syp73* are likely associated with the role of this protein in bridging the ER membrane with the actin cytoskeleton. This hypothesis is consistent with the verified plant growth defects linked to loss of myosin XI, which functions as a motor between actin and ER membrane [6, 10]. The evidence

that SYP73 is required in a short interval during growth and that *syp73* is viable supports a development-specific role of SYP73 and the likelihood that the function of other SNARE proteins, such as SYP71 and SYP72 or others, partially compensate for the loss of SYP73 at later stages of development. Alternatively, it is also possible that either non-SNARE proteins share ER rearrangement roles and/or, albeit unlikely, that ER membrane-actin anchors become unnecessary if the ER interacts with actin directly at later stages of growth.

2.1.4 SYP73 Contributes to ER Morphogenesis and Streaming

ER morphology and streaming largely depend on actin [10]. Depletion of actin leads to enlargement of ER tubule and cisternae [4] (see also Figure 2.2 F) and reduced movement [4]. Analogously, genetic deletion of myosin-XI leads to defects in ER shape as well as reduced ER streaming [6, 10]. Therefore we set up to test whether loss of SYP73 could lead to alteration of the ER morphology and streaming velocity, which would be consistent with its role in bridging the ER membrane with the actin cytoskeleton. The evidence that SYP73 is required for plant growth between 3DAG and 6DAG informed us on the developmental stage in which to analyze the morphology and dynamics of the ER in the *syp73* background. Therefore, we proceeded with the analysis of wild-type and *syp73* lines stably expressing an ER luminal marker using quantitative laser scanning confocal microscopy. Because of the verified requirement for SYP73 in early stages of development, we analyzed hypocotyl cells, which enable clear imaging of the ER network in very young seedlings. We verified that in the hypocotyl epidermal cells of 4 DAG wild-type seedlings, the ER networks assumed a network appearance of tubules and cisternae; however, in the *syp73* the ER network appeared enlarged (Figure 2.4 A). To quantify this phenotype, we measured the cortical cell areas that were occupied and unoccupied by the ER (Figure 2.8 C and D) using ImageJ plugin to compare the percentage of the areas occupied by the ER in wild-type and *syp73* cells. We found that

compared to wild type, the area occupied by the ER in *syp73* was significantly greater (Figure 2.4 B), indicating that the *syp73* ER is enlarged compared to wild type. To ensure that the defects of the ER morphology were independent from large secretion defects, which may lead to an enlargement of the ER, we assayed the secretion of a bulk-flow marker SEC-RFP which is normally trafficked to the apoplast through the default pathway but retained in the ER or mis-targeted to the vacuole if secretion defects take place [36]. In the hypocotyl epidermal cells of 4 DAG *syp73*/SEC-RFP seedlings, we did not detect abnormal accumulation of SEC-RFP in either middle or cortical focal plane (Figure 2.8 E and F). These results indicate that SEC-RFP is not mislocalized and therefore support secretion homeostasis in *syp73* and that the ER morphology defects verified in the mutant are unlikely due to retention of bulk proteins in the ER.

We next hypothesized that if SYP73 was involved in anchoring the ER membrane to actin, loss of SYP73 would lead to reduced streaming due to depletion of anchoring points between the two cellular structures. To test this hypothesis we carried out quantitative analyses on ER movement using a velocity maps depicted by the KbiFlow software to obtain average and maximal velocity streaming measurements of the plant ER, as described before [10, 37]. We found that the ER in 4DAG *syp73* hypocotyl epidermal cells was characterized by a significantly reduced average and maximal velocities of ER streaming compared to wild type (Figure 2.4C). Together with the morphometric analyses of the ER network (Figures 2.4 A and B), these results support that SYP73 contributes to ER structure and streaming. Because of the demonstrated interaction of SYP73 with actin (Figure 2.2), we hypothesized that the verified effect of loss of SYP73 on ER morphology and streaming occurred in relation to the actin cytoskeleton. To gain support for this hypothesis, we aimed to assay the sensitivity of *syp73* to loss of actin integrity. Specifically, as actin is strictly required for cytoplasmic streaming [38] and the latter has a critical role in plant growth [32], we hypothesized that

syp73 would be more sensitive to loss of actin compared to wild type. To test this, wild-type, *syp73* and complemented seedlings were germinated on vertical plates for three days and then transferred onto vertical plates containing either DMSO (control) or 50 mM Lat B. After three days on control plates (i.e., 6 DAG), wild-type and *syp73* seedlings showed similar length of the primary root; however, on the Lat B plate *syp73* seedlings showed shorter primary roots compared to wild type (Figures 2.3 F and G). This difference in primary root elongation was even more significant when the seedlings were allowed to grow for nine days after transfer to plates containing either DMSO or Lat B (Figures 2.3 G and H). These data support our hypothesis for a close functional relationship between SYP73 and the actin cytoskeleton, which is reflected in hypersensitivity of the *syp73* mutant to depolymerization of filamentous actin compared to wild type.

2.2 DISCUSSION

In conclusion, our data identify SYP73 as a novel ER-associated actin binding protein that is required for ER morphology and streaming as well plant growth at early stages of development. Our functional assays in conditions of genetic ablation of *SYP73* show that SYP73 is required for ER shaping and streaming in relation to the actin cytoskeleton; on the other hand, overexpression of SYP73 molds the ER network onto the actin cytoskeleton. Based on these results we propose that SYP73 has a critical yet non-essential role in ER shaping and streaming in combination with the actin-myosin system. In this novel model for plant ER identity and movement, myosin would provide the force to propel ER streaming and organize actin into cables that guide the ER membrane in obtaining a dynamic cable-like network as suggested earlier [6, 10]; in addition however, SYP73 would anchor the ER membrane to the underlying actin cytoskeleton (Figure 2.4 D). This model is supported by the evidence that overexpression of SYP73 models the ER membrane to overlay actin, possibly by increasing the abundance of anchoring points. Nonetheless, based on

the evidence that the streaming is reduced in *syp73* compared to wild type, we propose that attachment points of the ER with the cytoskeleton mediated by SYP73 function as dynamic holders of the ER membrane onto the cytoskeleton that would anchor to and release from the ER membrane to provide links between the ER and the underlying cytoskeleton. Such links would likely be necessary to ensure vicinity of the ER to actin and enable efficient utilization of the propelling action of myosin over actin to promote ER movement (see model in Figure 2.4 D; see also [39]). Myosin XI has been found in association with the ER in biochemical analyses [10] but also with vesicles of unknown nature as a fluorescent protein fusion [40]. As an alternative model, we propose that SYP73 may contribute to actin polymerization and hence facilitate growth of the ER over the actin cytoskeleton independently from myosin (Figure 2.4 E). While our data do not exclude that SYP73 may also have a role in other cellular processes or later stages of development, we propose that these may be dispensable as they may be executed by other proteins or they may not be required at later stages of cell growth. In the future, it will be interesting to test whether also the other members of the SYP7 family bind actin and share the function of SYP73 in anchoring the ER to actin, a scenario that would be supported by the sequence similarity among SYP7-family members (Figures 2.5 B and C) [34] and ER localization of SYP71 [9].

2.3 METHODS

2.3.1 Molecular Cloning

The coding sequence of *SYP73* was amplified from *Arabidopsis thaliana* Col-0 using Phusion High-Fidelity DNA Polymerase (NEB) and subcloned into the pVKH18-En6 vector for plant expression [41] between *Xba*I and *Sal*I restriction sites to generate a SYP73-GFP construct. To produce a ProSYP73:SYP73-YFP construct, the coding sequence of *SYP73* was overlapped with 2kb upstream of the start codonand YFP sequence, the full sequence was subcloned into pGWB1

vector [42]. The coding sequence of SYP73ΔTM (1-238) and SYP73TMC (239-264) were introduced into pCR8/GW/TOPO vector and then subcloned into pEarleyGate104 and pEarleyGate101 [43] respectively using Gateway cloning system (Invitrogen) to generate YFP-SYP73ΔTM and SYP73TMC-YFP constructs. For His-tag fused protein, the coding sequence of SYP73ΔTM was cloned into the pET-28b vector (Novagen) between *BamH*I and *Not*I sites. The plasmid for protein expression was transformed into *Escherichia coli* strain BL21 (DE3).

2.3.2 RNA Extraction and RT-PCR Analysis

The total RNA was extracted using RNeasy Plant Mini Kit (Qiagen). Reverse transcription was performed using iScript cDNA Synthesis Kit (Bio-Rad) and PCR analysis was conducted using GoTaq DNA Polymerase (Promega).

2.3.3 Plant Materials and Growth Conditions

Tobacco plants (*Nicotiana tabacum* cv. Petit Havana) were grown in 25°C chamber and Arabidopsis seedlings were grown at 21°C in 16h light: 8h dark cycle. The T-DNA insertion mutants Salk_134631 (*syp73*) was obtained from the ABRC at Ohio State University. The seeds of *Arabidopsis* Col-0 and *syp73* mutant (Col-0 background) were plated on vertical culture plates (half-strength Murashige and Skoog (PhytoTech) and phytagel (Sigma)). The 3DAG and 6DAG seedlings were sampled to measure primary root length and whole seedling fresh weight. To assess plant growth on Lat B-containing media, the three days-after-germination wild-type and *syp73* mutant seedlings were transferred onto half-strength Murashige and Skoog agar media containing either DMSO or 50 nM Lat B for further analyses as detailed in Figure 2.3.

2.3.4 Transient and Stable Plant Transformation

Four-week-old *N. tabacum* plants were infiltrated with the *Agrobacterium tumefaciens* strain GV3101 (OD_{600} = 0.05) for transient expression analyses [44]. Transformation of Col-0 and *syp73* Arabidopsis plants was performed through floral dip method [45]

2.3.5 Confocal Laser Scanning Microscopy

A Nikon A1Rsi and a Zeiss LSM 510 META laser scanning confocal microscope were used for analyzing fluorescence constructs transiently expressed in lower epidermis of tobacco leaves. Samples from Arabidopsis stable lines were analyzed by the Nikon A1Rsi confocal microscope. NIS-Elements Advanced Research software (Nikon) and ImageJ were used for image handling. ImageJ and JACoP plugin [46] were used to compute the Manders' Colocalization Coefficient (MCC) [47]. First, a region of interest (ROI) was selected in the merged GFP-and-YFP image. Then the GFP channel image and YFP channel image were separated and opened in JACoP plugin. The thresholds for GFP and YFP were automatically selected to remove background and noise to calculate MCC [46].

The fluorescent protein fusions used in this study were ERYK [48], YFP-ABD2 and CFP-ABD2 [49], GFP-Calnexin [33], YFP-TUA6 [50], PVA12-YFP [51], Cytosolic YFP [52], SEC-RFP [53]. Lat B treatment was performed as described earlier [54].

2.3.6 Analyses of ER Morphology and Dynamics

For quantification of ER cisternae, we considered a cisterna as an enlarged ER region fitting within a circle with a diameter of 3-5 µm (20.55–34.25 pixel). Regions of interest (ROIs) with size of 150 × 150 pixels were analyzed from the original 512 × 512 pixel confocal images, and then number of cisternae was counted in each ROI. Number of cell analyzed was 15. Number of 150 × 150 ROI analyzed was 30.

For the analysis of ER streaming, time-lapse series were acquired in the cortical ER using a Plan Apo 60× oil objective and 10× digital zoom. Each series contains 50 frames, each frame is 256×256 pixel resolution and the frame interval is 0.50s. The Nikon A1Rsi Perfect Focus System was used to keep acquiring frames in the same focal plane. Based on the time-lapse series, maximal and average velocities of ER streaming were assessed in ImageJ using the LPX Flow plugin [10].

2.3.7 Root and Root Hair Measurements

The roots of Arabidopsis seedlings were stained using 1 μg/ml propidium iodide [55] for 5 min. Confocal images of propidium iodide stained root tip were analyzed using Cell-O-Tape [56] to segment different zones in the root tip, and the transition zone and mature zone are defined by previous descriptions [57]. Cell numbers in different zones were also automatically counted by the software. The method used for root hair measurement was modified from a previously described procedure [58]. In brief, 20 Arabidopsis seedling were germinated vertically at the interspace between a glass microscope slide and a coverslip outdistanced by a spacer and filled up with ½ MS and phytagel media. Z-stacks of roots were acquired with a 10× objective, 6 days after germination using a Zeiss Axio Vert microscope. Root hair length was measured using Fiji (ImageJ)

2.3.8 Protein Expression and Purification

A method described earlier [59] was used to express the His-tagged SYP73ΔTM recombinant protein. TALON Metal Affinity Resin (Clontech) was used to purify His-SYP73ΔTM from cell lysate and the experimental procedure was based on the manufacturer's manual.

2.3.9 F-Actin High-Speed Co-Sedimentation Assay

F-actin preparation and F-actin cosedimentation assays were performed based on a previously described method [60]. In detail, 1 mg actin (AKL95, Cytoskeleton Inc., >95% rabbit skeletal muscle

actin) was dissolved in 1ml buffer 1 (general actin buffer, 1 M Tris pH 8.0, 1 M $CaCl_2$, 50 mM ATP and 1 M DTT) to prepared 1 mg/ml actin stock. For each assay, 300 µl 1 mg/ml actin stock was diluted by adding 450 µl buffer 1 to obtain 0.4 mg/ml actin. After 20,000*g* centrifugation for 10 min at 4°C, 720 µl supernatant was transferred into a new tube and left on ice for 1 hour. F-actin polymerization was allowed by adding 80 µl buffer 2 (actin polymerization buffer, 500 mM KCl, 20 mM $MgCl_2$ and 10 mM ATP) and incubating at 24°C for 1 hour.

For preparation of the tested proteins, purified His-SYP73ΔTM were subjected to dialysis using buffer 3 (tested protein preparation buffer, a 9:1 mixture of buffer 1 and buffer 2) using Amicon Ultra-15 Centrifugal Filter Units (Merck Millipore Ltd.). The protein concentrations were measured using Bio-Rad Protein Assay Dye (Bio-Rad) and BioMate 3 spectrophotometer (Thermo). Tropomyosin (T2400, Sigma) and BSA were also dissolved in buffer 3. All tested proteins were 135,000*g* pre-centrifuged for 30 min at 4°C.

For each F-actin binding reaction, the tested proteins were incubated with 80 µl 0.4 mg/ml actin and buffer 3 was added to reach a total volume of 100 µl. The reaction occurred at room temperature for 60 min. After 135, 000*g* centrifugation for 30 min at 24°C, the supernatant was transferred to a new tube and mixed with 6x SDS sample buffer, the pellet was resuspended with 2x SDS sample buffer. The proteins were boiled for 5 min and subjected to SDS-PAGE and visualized by Coomassie Brilliant Blue R-250 (Bio-Rad) staining.

To determine the dissociation constant K_d, the F-actin cosedimentation assay described above was repeated three times using increasing concentrations of His-SYP73ΔTM (0, 0.3, 0.5, 0.7, 1.0 and 1.5 µM) and 3µM polymerized F-actin. The separated supernatants and pellets were subjected to SDS-PAGE and later staining with Coomassie Brilliant Blue

2.4 ACKNOWLEDGEMENTS

We acknowledge support by the Chemical Sciences, Geosciences and Biosciences Division, Office of Basic Energy Sciences, Office of Science, U.S. Department of Energy (award number DE-FG02-91ER20021) and National Science Foundation (MCB1243792) and AgBioResearch. We are grateful to Mr. Robert Loepp (MSU) for the construction of a SYP73-GFP fusion.

APPENDIX

Primer Name	Sequence (5'→3')
pVKH18-En6 SYP73-GFP, F	CAGGACGTCTAGATGGGCGTAATTGATTTGATCACTAGG
pVKH18-En6 SYP73-GFP, R	CATGACCGTCGACTTCTTCACAGAGTTGTATATGAAGGC
SYP73 promoter, F	CTCAAATTAATGGTGAATCAAGAGTTTCTTACCCTCTGAATTTGATGC
Promoter-SYP73, R	AATTACGCCCATCTTCGCCGCTCG
Promoter-SYP73, F	CGAGCGGCGAAGATGGGCGTAATT
SYP73-YFP, R	CTTCACCTTTAGACATCTTCACAGAGTTG
SYP73-YFP, F	CAACTCTGTGAAGATGTCTAAAGGTGAAG
YFP, R	TTATTTGTACAATTCATCCATACCATGGGTAATAC
pEarleyGate101 SYP73TMC, F	AGCCGCAACTTCTGCATAGACATCATCCT
pEarleyGate101 SYP73TMC, R	GGATCTCAACTTTGTTACAGTATCCTTGAG
pEarleyGate104 SYP73ΔTM, F	ATGGGCGTAATTGATTTGATCACTAGGGTTGATTCCATCTG
pEarleyGate104 SYP73ΔTM, R	TCAGGATCTCAACTTTGTTACAGTATCCTTGAGCCTCACATTG
pET-28b His-SYP73ΔTM, F	GGTGCTGGATCCCATG GGC GTAATTGATTTGATCACTAG
pET-28b His-SYP73ΔTM, R	GCGCAGGCGGCCGCTCAGGATCTCAACTTTGTTACAGTAT
pVKH18E-n6 CFP-SKL+SYP73, F	CAGGACGTCTAGATGGGCGTAATTGATTTGATCACTAGGGTTG
pVKH18E-n6 CFP-SKL+SYP73, R	GCGCCGGAGCTCTCACTTCACAGAGTTGTATATGAAGG
genotyping of Salk_134631, LP	TATCCTTGAGCCTCACATTGG
genotyping of Salk_134631, RP	CGAAACTGTTCTTCAGGTTCG
genotyping of Salk_134631, LBb1.3	ATTTTGCCGATTTCGGAAC
RT-PCR SYP73, F	ATGGGCGTAATTGATTTGATCACTAGGGTTGATTCCATCTG
RT-PCR SYP73, R	CTTCACAGAGTTGTATATGAAGGCAGCGATTCCCAG

Table 2.1 Primers used in this study.

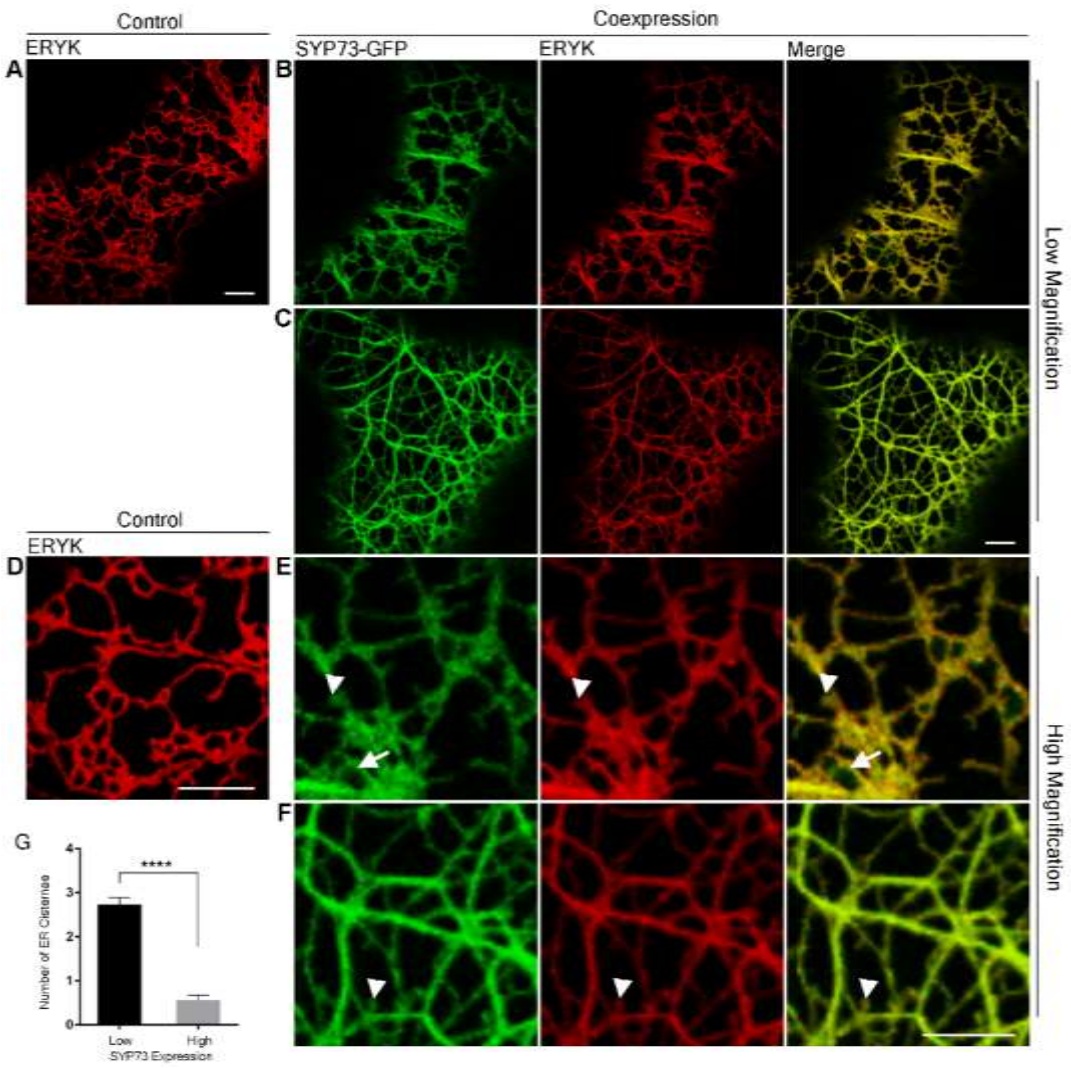

Figure 2.1 SYP73 is localized to the ER network, which it remodels in high-expressing cells.

(A) A confocal image of tobacco leaf epidermal cells expressing the ER marker ERYK (control). Scale bar = 5 µm.
(B and C) Confocal images of tobacco leaf epidermal cells co-expressing SYP73-GFP and ERYK. When SYP73-GFP is highly expressed (**C**), the appearance of the tubular ER is enhanced while that of the cisternal ER is reduced. Scale bar = 5 µm.
(D, E and F) High-magnification images of **A**, **B** and **C**, respectively, to illustrate details of SYP73 distribution. SYP73 is localized at the ER network and punctate structures. Most of these structures are largely immotile and represent ER-plasma membrane contact sites (arrowhead). Although to a minor extent, SYP73-GFP is also distributed to structures of unknown nature in which ER-YK is excluded (arrow). Scale bars = 5 µm.
(**G**) Quantification of the number of cisternae of the ER in cells with low or high levels of SYP73-GFP fluorescence. Values are mean and SEM (****$p < 0.0001$, unpaired t-test).

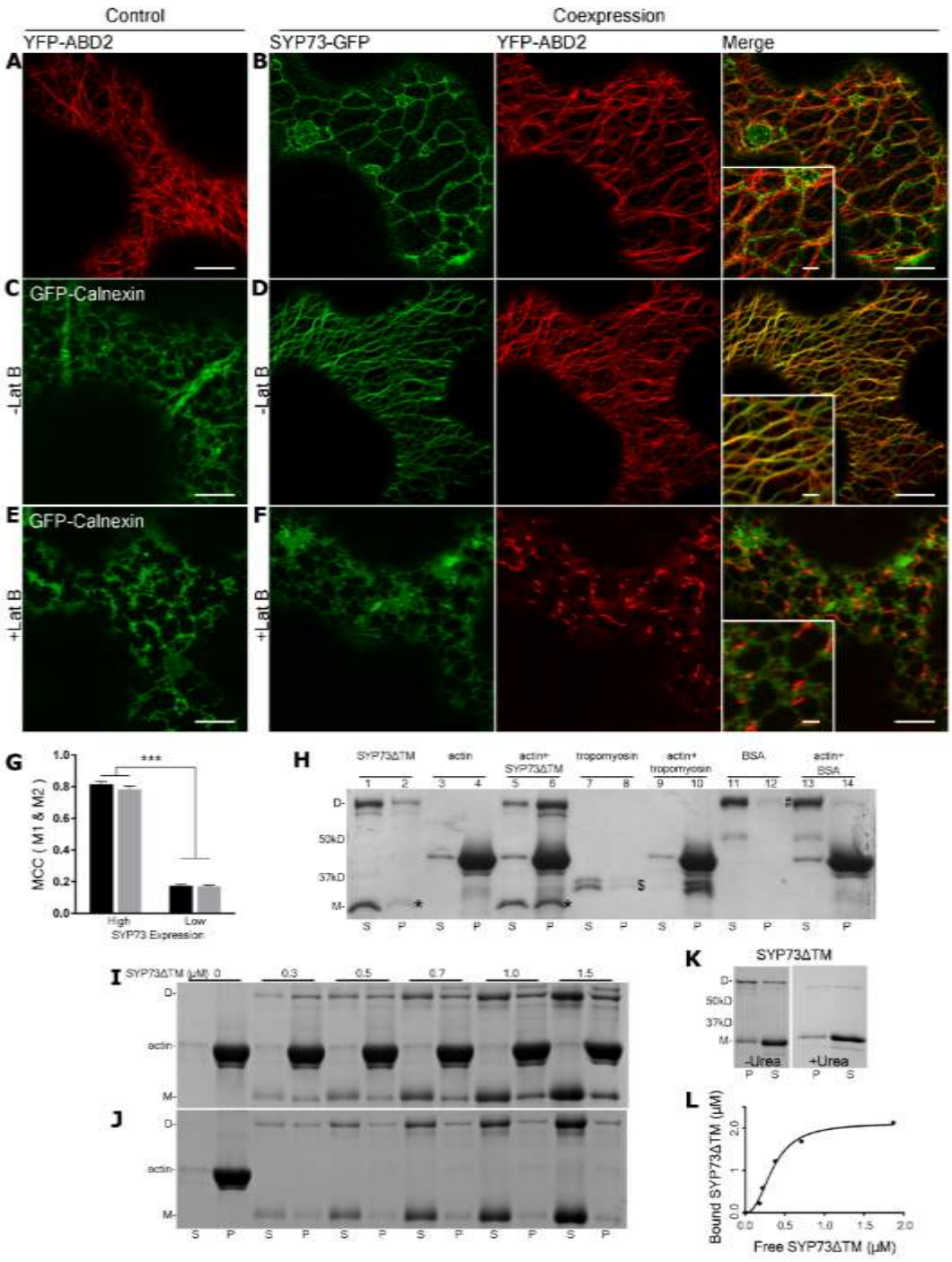

Figure 2.2 SYP73 remodels the ER over the actin cytoskeleton and binds actin directly.

(A and C) Confocal images of tobacco leaf epidermal cells transiently expressing the actin marker YFP-ABD2 (**A**) and ER membrane marker GFP-Calnexin (**C**). Scale bars = 10 μm.
(B and D) Confocal images of tobacco leaf epidermal cells transiently co-expressing YFP-ABD2 and SYP73-GFP. (**B**) In cells expressing SYP73-GFP at low levels, the ER network is only

Figure 2.2 (cont'd) partially overlapping with the actin cytoskeleton (see detail in inset in Merge image). (**D**) In cells expressing higher levels of SYP73-GFP, the ER network modified by SYP73-GFP overlaps almost completely with the actin cytoskeleton cables (see details in inset in Merge image). **B** and **D** were acquired with identical confocal microscope settings; in post-acquisition the signal of the SYP73-GFP in **B** was digitally increased to enable visual comparison of the SYP73-GFP signal between **B** and **D** in relation to actin. Scale bars = 10 µm, scale bars in the inset represent 2 µm.

(E and F) After 1hr Lat B treatment (+Lat B) of cells with high expression of SYP73-GFP (**F**), the ER network displayed similar morphology to that of cells expressing the ER membrane marker GFP-Calnexin (**E**). Scale bars = 10 µm, scale bar in the inset represents 2 µm.

(**G**) Manders' Colocalization Coefficients (MCCs) as measurement of colocalization between YFP-ABD2 and SYP73-GFP indicate that in cells expressing high levels of SYP73-GFP, YFP-ABD2 and SYP73-GFP largely overlapped and that the degree of overlap was significantly higher than in cells expressing low levels of SYP73-GFP . M1 (black column) indicates the fraction of SYP73-GFP fluorescence overlapping YFP-ABD2 fluorescence, and M2 (gray column) indicates the fraction of YFP-ABD2 fluorescence overlapping SYP73-GFP fluorescence. The MCC values were calculated as M1 = 0.81 ± 0.02, M2 = 0.78 ± 0.02, n = 24 in high SYP73-GFP expressors, and M1 = 0.17 ± 0.01, M2 = 0.17 ± 0.01, n = 16 in low SYP73-GFP expressors. Values are mean and SEM (***$p < 0.001$, one-way ANOVA analysis).

(H) High-speed co-sedimentation assays were used to test SYP73ΔTM binding to F-actin. Tropomyosin ($) and SYP73ΔTM (*), which are normally recovered in the supernatant fraction (S) in the absence of F-actin, were detected in the pellet (P) fraction after incubation with actin. After incubation with or without actin, BSA (#) was recovered primarily in the S fraction.

(I and J) High-speed co-sedimentation assays using either 4µM actin or no actin and increasing concentrations of His-SYP73ΔTM (0-1.5 µM) showed that after centrifugation to separate supernatant (S) and pellet (P), increasing amounts of His-SYP73ΔTM monomers (M) and dimers (D) were recovered in the pellet up to saturation (**I**). (**J**) Increasing concentrations of His-SYP73ΔTM (0-1.5 µM) were used to further ensure that enrichment of the protein in the P fraction is specific to the presence of actin in the reaction.

(K) Urea (4M) treatment of His-SYP73ΔTM samples led to dissolution of the dimer His-SYP73ΔTM (D) form and recovery of monomers (M).

(L) Gel densitometry analyses were conducted on four independent actin-SYP73ΔTM binding experiments to measure the concentrations of free and bound SYP73ΔTM and to estimate the dissociation constant (*K*d) and binding stoichiometry. The gel band intensities were plotted to fit a hyperbolic function. The graph is representative of one of the actin-SYP73ΔTM binding experiment replicates. For this experiment, the *K*d was calculated as 0.35 µM. At saturation, the stoichiometry was 0.52 mole of His-SYP73ΔTM per mole of actin.

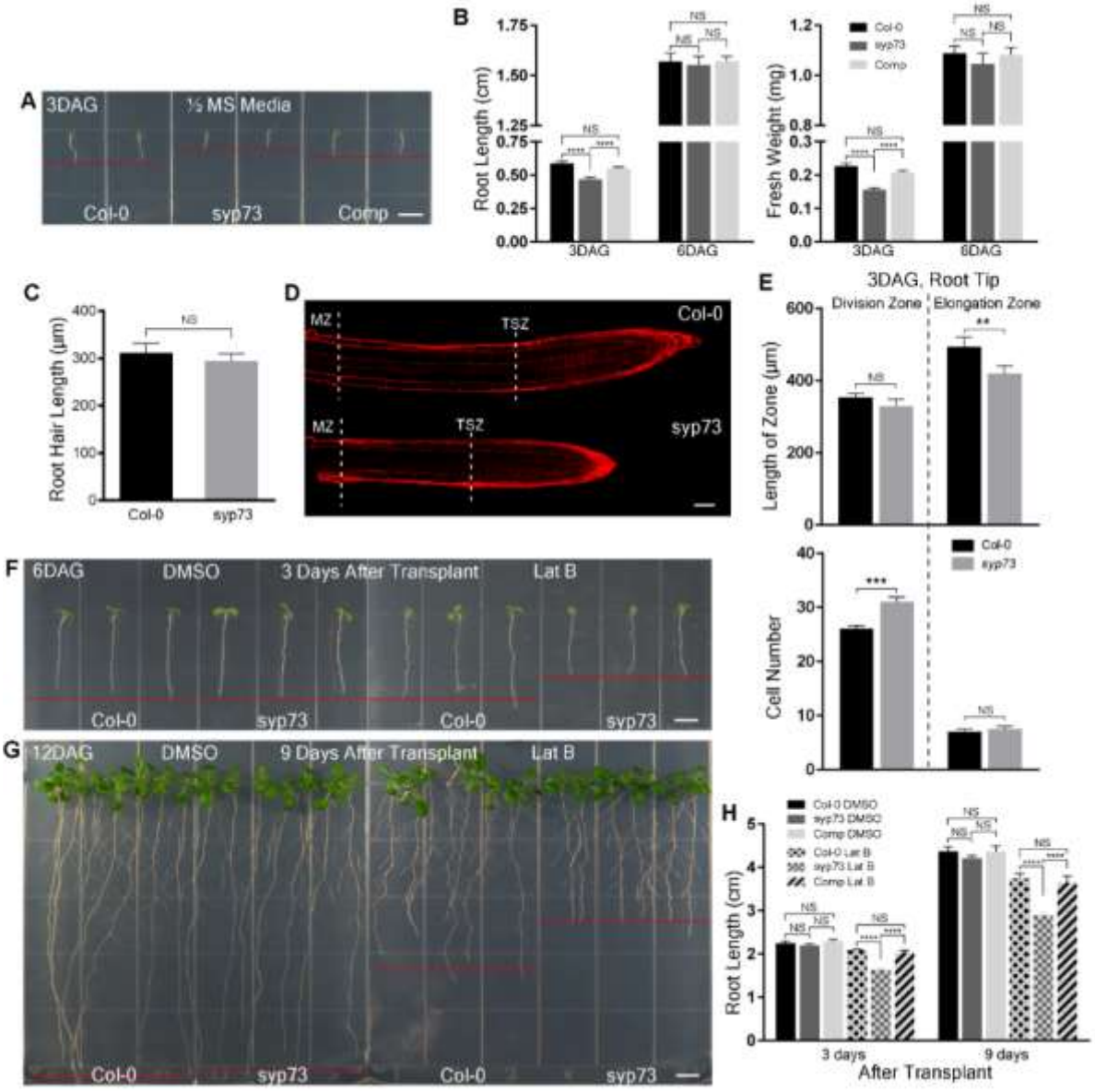

Figure 2.3 *syp73* mutant displays defects at early developmental stages.

(A) An image of wild-type, *syp73* and Comp (*syp73*/ProSYP73::SYP73-YFP) seedlings growing on ½ MS media three days after germination (3DAG). Scale bar = 0.5 cm.
(B) Quantification of primary root length and fresh weight for 3DAG wild-type, *syp73* and Comp (*syp73*/ProSYP73::SYP73-YFP) seedlings. Values are mean and SEM (n > 40) (****p < 0.0001, unpaired t tests; NS, not significant).
(C) Quantification of root hair length of 3DAG wild-type (n=12) and *syp73* (n=17) seedlings (NS, not significant).

Figure 2.3 (cont'd) (D) Representative images of propidium iodide staining of root tips of 3DAG wild-type and *syp73* seedlings to highlight the cell contours. The transition zone (TSZ) and the mature zone (MZ) are indicated. Scale bar = 50 µm.
(E) Cell-O-Tape software-based quantification of the root length between the root apex and the TSZ that contains the apex-division zone, as well as of the length of the elongation zone which resides between the TSZ and the MZ. The number of cells in each zone was also quantified. Values are mean and SEM (n of roots >20 for each genotype). Unpaired t tests indicate a significant difference between Col-0 and *syp73* (**$p < 0.01$; NS, not significant).
(F and G) At 3DAG wild-type and *syp73* seedlings were transplanted to ½ MS media containing either DMSO or 50 nM Lat B, and grew for another 3 days (**F**) or 9 days (**G**). Scale bars = 0.5 cm.
(H) Quantification of the primary root length of wild-type, *syp73* and Comp (*syp73*/ProSYP73::SYP73-YFP) seedlings after transplant to DMSO or Lat B. Graph shows mean and SEM (n = 30 for each genotype; ****$p < 0.0001$, unpaired t tests; NS, not significant).

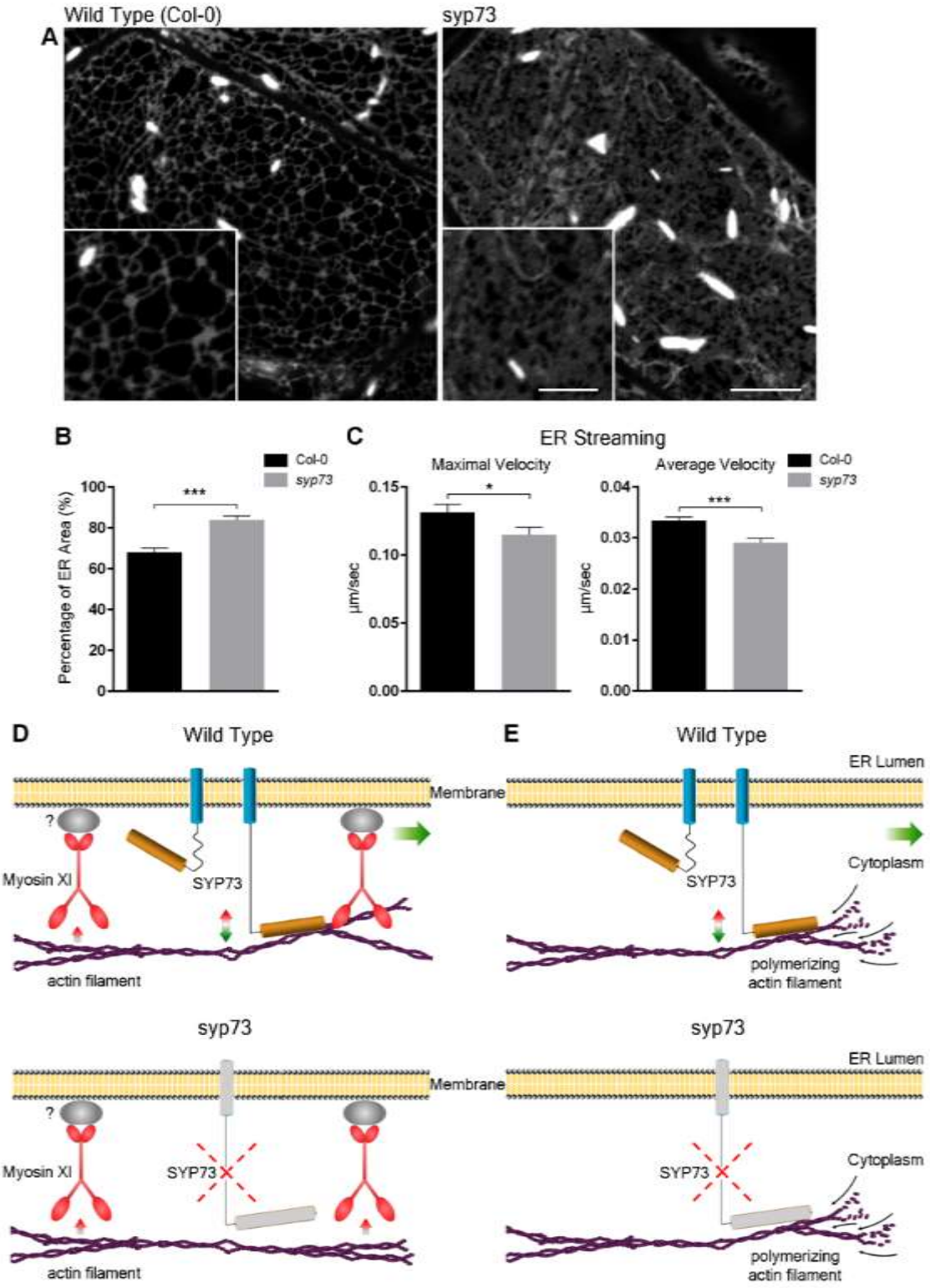

Figure 2.4 SYP73 is functionally involved in ER morphology and dynamics.

(A) Confocal images of hypocotyl epidermal cells of 4DAG wild type (Col-0) and *syp73* expressing the ER marker ERYK. The ER network appears enlarged in the *syp73* mutant

Figure 2.4 (cont'd) compared to wild type. Insets, magnified areas of main panels. The bright spindle-shaped structures interspersed in the ER network are ER bodies. Scale bar = 10 µm, scale bar in the inset represents 5 µm.

(B) Quantification of the percentage of ER area in the whole cell. The hypocotyl epidermal cells of 4DAG Col-0/ERYK and *syp73*/ERYK plants were subjected to confocal imaging. At the cortical confocal plane of each cell, the area occupied by the ER was measured using Image J and divided by the whole area of the cell cortex. Values are mean and SEM (n of cells = 30 for each line; ***$p < 0.001$, unpaired t test; NS, not significant).

(C) Maximal and average velocity of ER streaming measurements in hypocotyl epidermal cells of 4DAG Col-0/ERYK and *syp73*/ERYK seedlings were gathered from time-lapse images of the ER network. Values are mean and SEM (*n* of cells = 35-40 for each genotype). Unpaired t tests indicate significant differences of maximal velocity (*$p < 0.05$) and average velocity (***$p < 0.001$) compared to Col-0.

(D) Hypothetical model of the function of SYP73 at the interface of the ER and actin. In wild-type cells, SYP73 is associated to the ER and bridges dynamically the ER membrane to the actin cytoskeleton in virtue of the actin-binding ability of its cytosolic domain. This function may facilitate interaction of actin-myosin with the ER, which occurs through yet-unknown mechanisms (question mark in the Figure) and is necessary for ER integrity and movement. In the absence of SYP73, the ER is no longer in close association with actin, which in turn renders the action of actin-myosin system insufficient for ER shaping and streaming.

(**E**) An alternative model for the role of SYP73 in ER movement views the ER as being driven, at least in part, by actin polymerization. In this model through its binding SYP73 may stabilize actin filaments and promote ER movement independently from myosin.

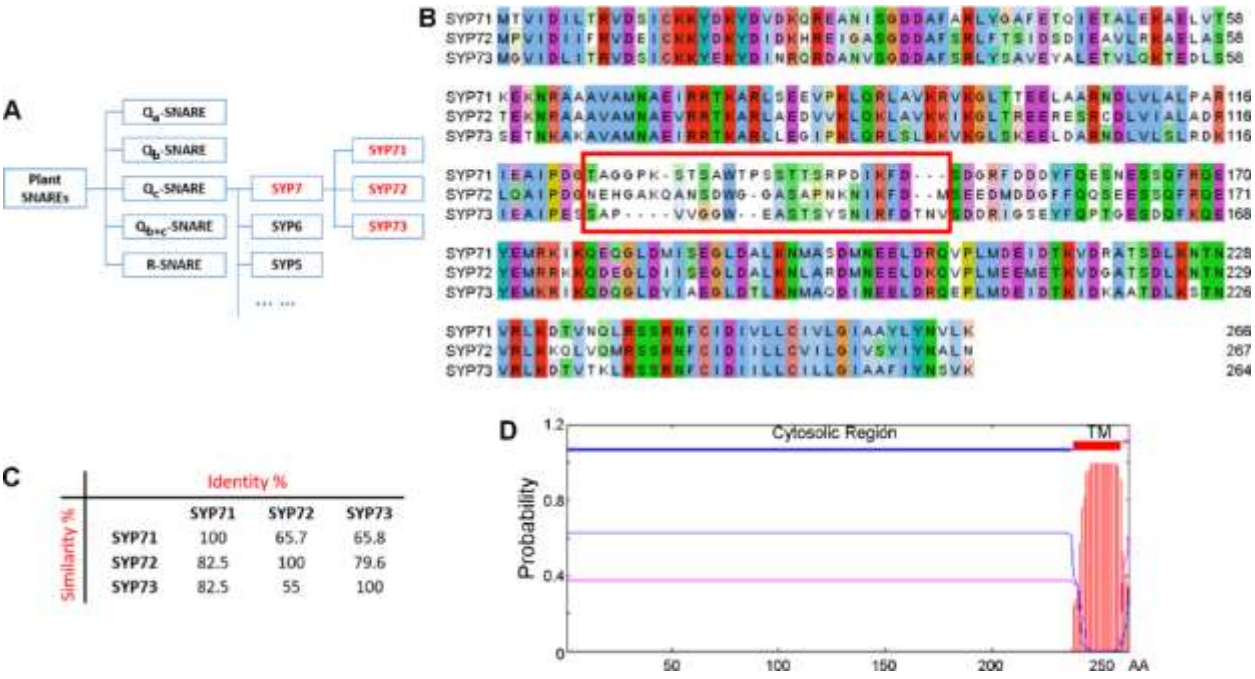

Figure 2.5 SYP73 is a distinct member in plant-specific SYP7 family.

(A) Phylogenetic diagram showing the position of SYP73 in the plant SNARE family, based on Sanderfoot et al., 2000 [41], with modifications. The SYP7 family is depicted in red font.
(B) Amino acid sequence alignment of full-length SYP71, SYP72 and SYP73 using MUSCLE [42] in Jalview (http://www.jalview.org/). The alignment indicates that the SYP proteins have a variable region (marked by a red box). Amino acids are color-coded with ClustalX according to the similarity of physicochemical properties.
(C) The identity % vs. similarity % scores of the amino acid sequences of SYP71, SYP72 and SYP73 are indicated in the matrix.
(D) The amino acid sequence of SYP73 was submitted to TMHMM [43] to estimate the probability of protein orientation with the respect to a membrane (inside/outside of a subcellular compartment) and the presence of transmembrane helices. The top blue line indicates the protein N-terminus faces cytoplasm (cytosolic region), the red thick line indicates the position of predicted transmembrane (TM), and the pink line indicates a C-terminal tail in the organelle lumen.

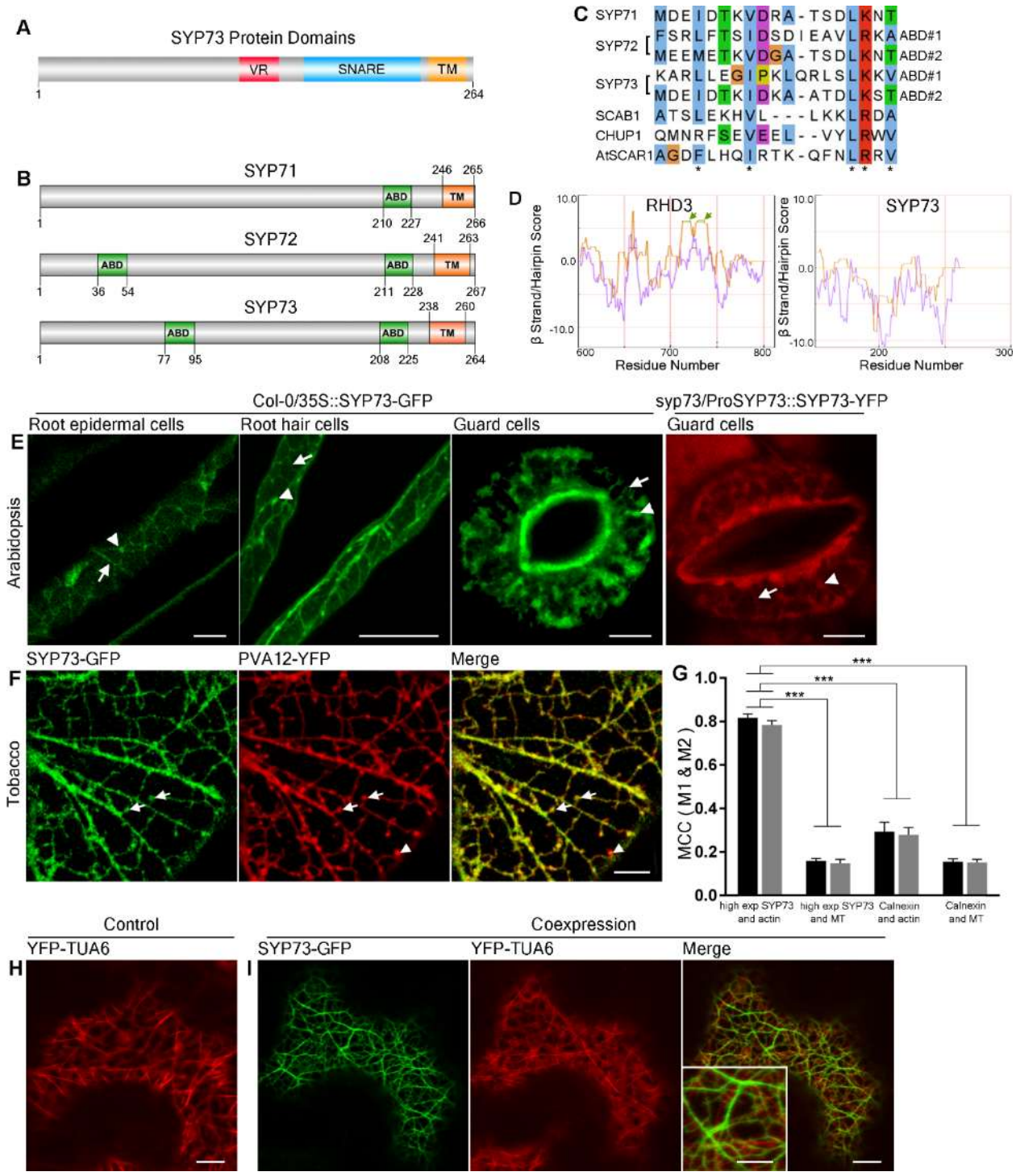

Figure 2.6 SYP73 has predicted actin-binding domains and in high expression does not modify the ER over the microtubules.

Figure 2.6 (cont'd) (A) Schematic diagram of SYP73 demonstrating the variable region (VR), a SNARE domain and a transmembrane domain (TM).
(B) Predicted actin-binding domains have been identified in SYP71, SYP72 and SYP73 by the Eukaryotic Linear Motif (ELM) program[44], which detected multiple matches of the actin-binding domain (ABD) LIG_Actin_WH2_2. The ELM program also detected WH2_2 motif in several other plant actin-binding proteins[45,46,47,48,49], which is consistent with experimentally identified actin-binding domain positions of CHUP1[46] and SCAB1[45].
(C) Alignment of the predicted actin-binding domains in SYP7 proteins and other plant actin-binding proteins. The WH2_2 motif was first identified in animal WAVE/SCAR family proteins and the predicted SYP73 actin-binding domains share similarity in several highly-conserved residues (marked by asterisks), which were also identified in the actin binding protein AtSCAR1[50].
(D) Analyses of the C-terminal region comprising the transmembrane domain of SYP73 (aa 150-264) and RHD3 (aa 600-802) using MPEX Tool (www.blanco.biomol.uci.edu) did not identify a hairpin domain in SYP73 but one in RHD3, which is known to contain a hairpin domain[23,24]. These analyses support that the SYP73 anchor to the ER membrane is mediated by a single-pass transmembrane domain.
(E) Confocal images of Arabidopsis seedlings (Col-0/35S::SYP73-GFP) show distribution of SYP73-GFP at the ER (arrows) and punctate structures (arrowheads) in root epidermal cells (left panel, scale bar = 5 µm), root hair cells (middle panel, scale bar = 100 µm) and stomata (right panel, scale bar = 5 µm). A confocal image of *syp73*/ProSYP73::SYP73-YFP shows distribution of SYP73-YFP at the ER (arrow) and punctate structures (arrowhead) in stomata (scale bar = 5 µm). Note that the fluorescence was clearly visible in the cell types indicated here. The ability of SYP73-YFP to complement the *syp73* phenotype (Figure 2.3) suggests that the protein is expressed also in other tissues but likely at levels that are below the detection limit of the confocal microscope.
(F) Confocal images of a tobacco leaf epidermal cell coexpressing SYP73-GFP with the ER and ER-PM contact site marker PVA12-YFP[51,52] shows colocalization at the ER-PM interface (colocalizing structures, arrows; non-colocalizing structures, arrowhead). Scale bar = 5 µm.
(G) Manders' Colocalization Coefficient (MCC) measurements indicate high level of colocalization between SYP73-GFP (high expression) and YFP-ABD2 (actin), but a much lower level of colocalization between SYP73-YFP (high expression) and YFP-TUA6 (MT, microtubules). A similar trend was observed compared to GFP-Calnexin and YFP-ABD2 (actin), GFP-Calnexin and YFP-TUA6 (MT). M1 (black column) indicates the fraction of **Figure 2.6 (cont'd)** GFP fluorescence overlapping YFP fluorescence, and M2 (gray column) indicates the fraction of YFP fluorescence overlapping GFP fluorescence. Values are means and SEM (***$p < 0.001$, one-way ANOVA analysis).
(H and I) Confocal images of tobacco leaf epidermal cells transiently expressing the microtubule marker YFP-TUA6 alone **(H)** or with SYP73-GFP **(I)**. The two markers showed distinct localization indicating that the ER network modified by overexpression of SYP73-GFP does not overlap with the microtubule cytoskeleton. Scale bars = 10 µm, scale bar in the inset represents 5 µm.

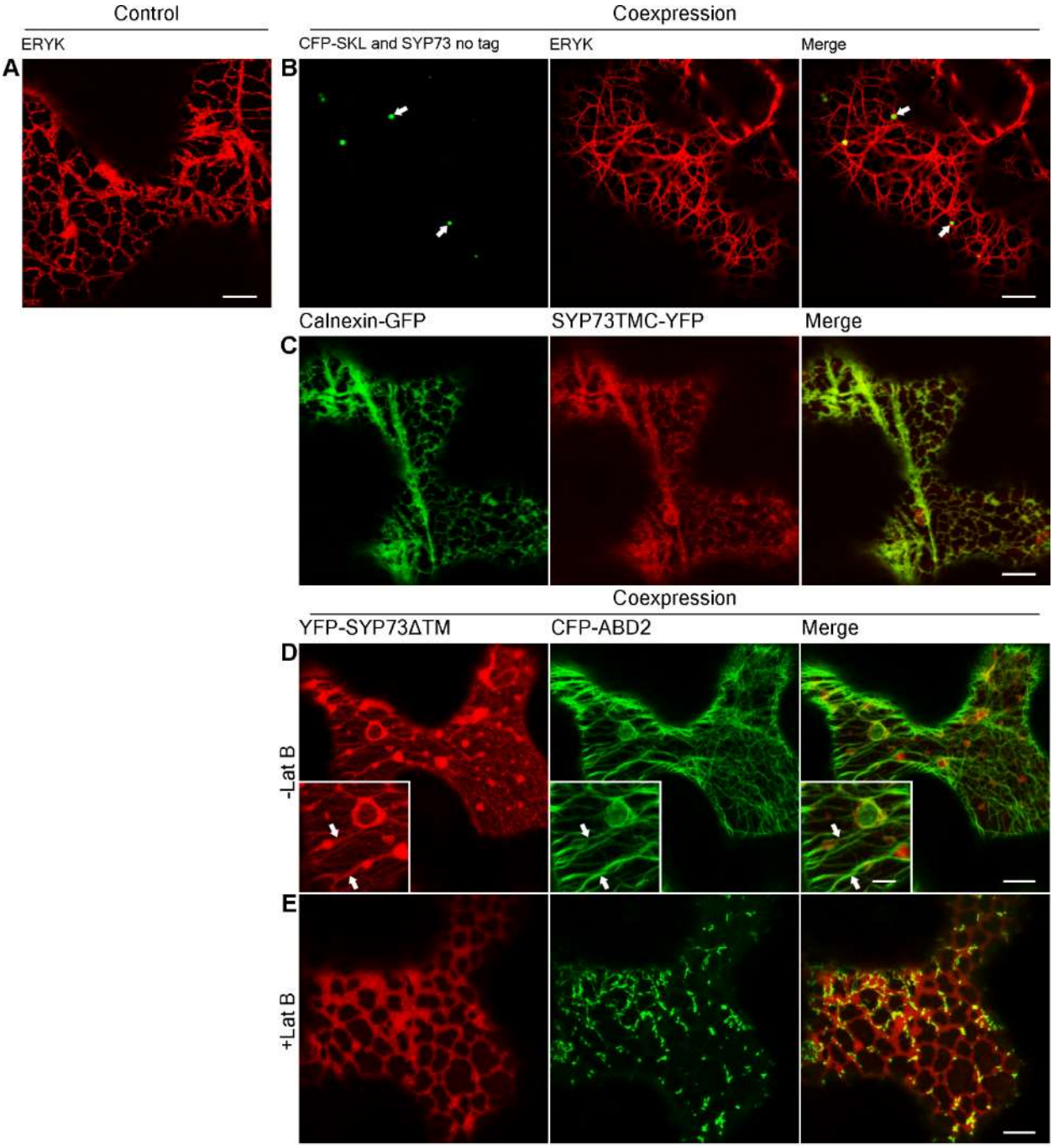

Figure 2.7 The N-terminal portion of SYP73 is required and sufficient for actin binding.

Figure 2.7 (cont'd)

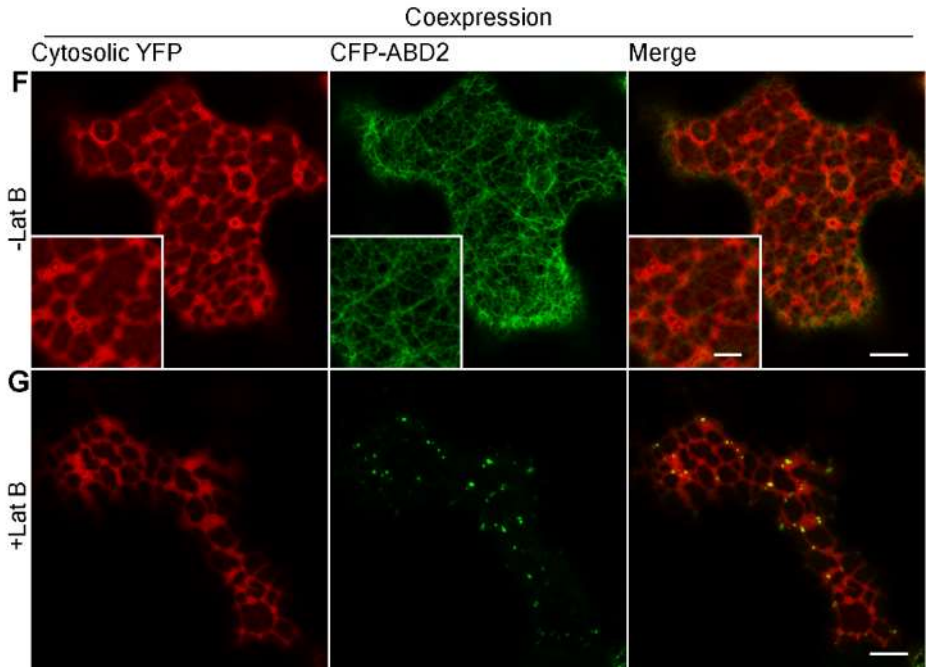

(A and B) Confocal images of tobacco leaf epidermal cells transiently expressing either ERYK alone (**A**) or with the peroxisome marker CFP-SKL and untagged SYP73. Note that CFP-SKL and untagged SYP73 are expressed in the same bicistronic vector (**B**). By visualizing the peroxisomes (arrows), this approach[53] allows identifying cells that express untagged SYP73. Cells expressing untagged SYP73 show rearrangement of the ER network similar to cells expressing SYP73-GFP. Scale bars = 10 µm.
(C) Confocal images of tobacco leaf epidermal cells transiently co-expressing GFP-Calnexin (ER membrane marker) and YFP-tagged SYP73TMC, which contains the transmembrane domain and C-terminal ER luminal tail of SYP73. Scale bar = 10 µm.
(D-G) Confocal images of tobacco leaf epidermal cells co-expressing SYP73ΔTM-YFP and the actin marker CFP-ABD2. In control cells (**D**; -Lat B), SYP73ΔTM-YFP is visibly distributed to the cytosol as well as to cable-like structures that overlap with actin filaments (see insets, arrows). When cells are treated with Lat B, SYP73ΔTM-YFP is redistributed in the cytosol and the cable-like distribution is lost (**E**), supporting that the cytosolic region of SYP73 interacts with actin. The control (cytosolic YFP) does not assume the cable-like distribution of SYP73ΔTM-YFP (**F)** and Lat B treatment does not affect the distribution of this marker (**G**) indicating that the distribution of SYP73ΔTM- **Figure 2.4 (cont'd)** YFP is specific for this protein chimaera. Insets: magnified image of areas pointed by arrows. Scale bars = 10 µm, scale bar in the inset represents 5 µm.

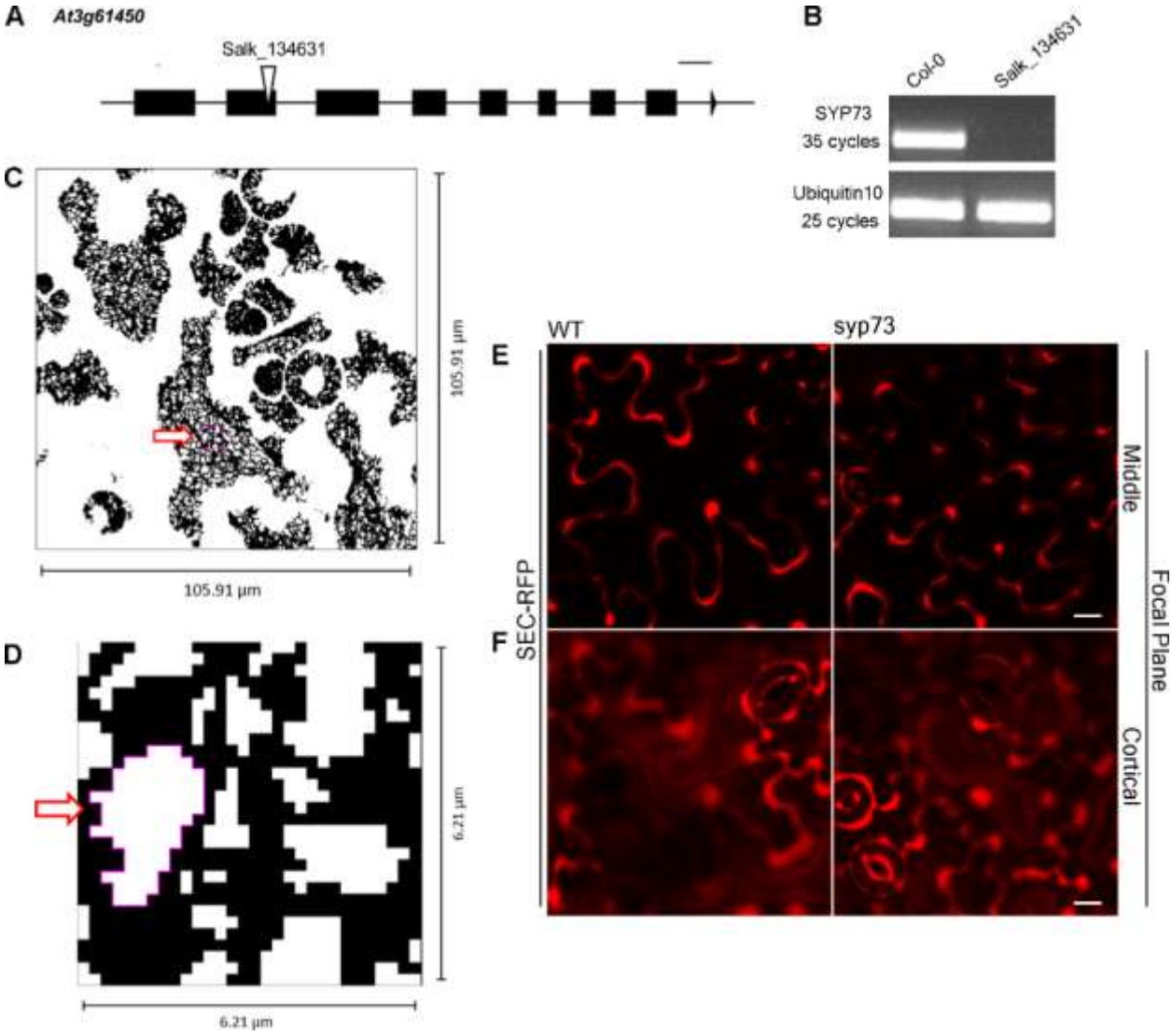

Figure 2.8 In a *SYP73* knockout mutant, ER morphology and dynamics are compromised, but constitutive secretion is not affected.

(A) Diagrams of *SYP73* (*At3g61450*) genomic region showing positions of exons (black boxes), introns (lines) and T-DNA insertion (inverted triangle). Scale length = 100 bp.
(B) RT-PCR analysis on genomic DNA of wild-type Col-0 and T-DNA insertion mutant (Salk_134631). Two-week-old plants were used for total RNA extraction. UBQ10 was used as a control. Contrarily to wild type, the *SYP73* gene was not amplified in the insertion line indicating that this line is likely a knock-out allele.
(C) In order to measure the percentage of ER area in the cell cortex, the cortical focal plane image of single cells was cropped, and a threshold was set and in the binary color image. The resultant black area was considered as ER. The area occupied by the ER was estimated as percentage over the entire cropped area.
(D) Magnified image of the cropped area that shows how the ER area was selected.

Figure 2.8 (cont'd) (E and F) Confocal images of cotyledon pavement cells of 4 DAG wild type and *syp73* mutant in the middle (**E**) and cortical (**F**) focal planes indicate no visible retention of the bulk secretion marker SEC-RFP inside the cells supporting that loss of SYP73 does not affect constitutive secretion. Scale bars = 10 µm.

REFERENCES

REFERENCES

1. Westrate, L.M., Lee, J.E., Prinz, W.A., and Voeltz, G.K. (2015). Form follows function: the importance of endoplasmic reticulum shape. Annu Rev Biochem 84, 791-811.

2. Stefano, G. et al. ER network homeostasis is critical for plant endosome streaming and endocytosis. Cell Discovery 1 (2015).

3. Voeltz, G.K., Prinz, W.A., Shibata, Y., Rist, J.M. & Rapoport, T.A. A class of membrane proteins shaping the tubular endoplasmic reticulum. *Cell* **124**, 573-586 (2006).

4. Sparkes, I., Runions, J., Hawes, C. & Griffing, L. Movement and remodeling of the endoplasmic reticulum in nondividing cells of tobacco leaves. *Plant Cell* **21**, 3937-3949 (2009).

5. Hamada, T., Ueda, H., Kawase, T. & Hara-Nishimura, I. Microtubules contribute to tubule elongation and anchoring of endoplasmic reticulum, resulting in high network complexity in Arabidopsis thaliana. *Plant physiology*, pp. 114.252320 (2014).

6. Ueda, H., Tamura, K. & Hara-Nishimura, I. Functions of plant-specific myosin XI: from intracellular motility to plant postures. *Curr Opin Plant Biol* **28**, 30-38 (2015).

7. Staehelin, L.A. The plant ER: a dynamic organelle composed of a large number of discrete functional domains. *The Plant Journal* **11**, 1151-1165 (1997).

8. Lichtscheidl, I.K., Lancelle, S.A. & Hepler, P. Actin-endoplasmic reticulum complexes inDrosera. *Protoplasma* **155**, 116-126 (1990).

9. Suwastika, I.N., Uemura, T., Shiina, T., Sato, M.H. & Takeyasu, K. SYP71, a plant-specific Qc-SNARE protein, reveals dual localization to the plasma membrane and the endoplasmic reticulum in Arabidopsis. *Cell Struct Funct* **33**, 185-192 (2008).

10. Ueda, H. *et al.* Myosin-dependent endoplasmic reticulum motility and F-actin organization in plant cells. *Proceedings of the National Academy of Sciences* **107**, 6894-6899 (2010).

11. Griffing, L.R., Gao, H.T. & Sparkes, I. ER network dynamics are differentially controlled by myosins XI-K, XI-C, XI-E, XI-I, XI-1, and XI-2. *Front Plant Sci* **5**, 218 (2014).

12. Sandoz, P.A. & Van der Goot, F.G. How many lives does CLIMP-63 have? *Biochemical Society Transactions* **43**, 222-228 (2015).

13. Dunkley, T.P. *et al.* Mapping the Arabidopsis organelle proteome. *Proceedings of the National Academy of Sciences* **103**, 6518-6523 (2006).

14. El Kasmi, F. *et al.* SNARE complexes of different composition jointly mediate membrane fusion in Arabidopsis cytokinesis. *Molecular biology of the cell* **24**, 1593-1601 (2013).

15. Wei, T., Zhang, C., Hou, X., Sanfaçon, H. & Wang, A. The SNARE protein Syp71 is essential for turnip mosaic virus infection by mediating fusion of virus-induced vesicles with chloroplasts. (2013).

16. Brandizzi, F., Snapp, E.L., Roberts, A.G., Lippincott-Schwartz, J. & Hawes, C. Membrane protein transport between the endoplasmic reticulum and the Golgi in tobacco leaves is energy dependent but cytoskeleton independent: evidence from selective photobleaching. *Plant Cell* **14**, 1293-1309 (2002).

17. Irons, S.L., Evans, D.E. & Brandizzi, F. The first 238 amino acids of the human lamin B receptor are targeted to the nuclear envelope in plants. *Journal of Experimental Botany* **54**, 943-950 (2003).

18. Sparkes, I. *et al.* Five Arabidopsis reticulon isoforms share endoplasmic reticulum location, topology, and membrane-shaping properties. *The Plant Cell* **22**, 1333-1343 (2010).

19. Stefano, G. & Brandizzi, F. Unique and conserved features of the plant ER-shaping GTPase RHD3. *Cell Logist* **4**, e28217 (2014).

20. Ueda, H. *et al.* Phosphorylation of the C-terminus of RHD3 has a critical role in homotypic ER membrane fusion in Arabidopsis. *Plant Physiol* (2015).

21. Shibata, Y., Hu, J., Kozlov, M.M. & Rapoport, T.A. Mechanisms shaping the membranes of cellular organelles. *Annu Rev Cell Dev Biol* **25**, 329-354 (2009).

22. Tolley, N. *et al.* Overexpression of a plant reticulon remodels the lumen of the cortical endoplasmic reticulum but does not perturb protein transport. *Traffic* **9**, 94-102 (2008).

23. Ueda, H. *et al.* Phosphorylation of the C Terminus of RHD3 Has a Critical Role in Homotypic ER Membrane Fusion in Arabidopsis. *Plant Physiology* **170**, 867-880 (2016).

24. Stefano, G., Renna, L., Moss, T., McNew, J.A. & Brandizzi, F. In Arabidopsis, the spatial and dynamic organization of the endoplasmic reticulum and Golgi apparatus is influenced by the integrity of the C-terminal domain of RHD3, a non-essential GTPase. *Plant J* **69**, 957-966 (2012).

25. Klopfenstein, D.R., Kappeler, F. & Hauri, H.P. A novel direct interaction of endoplasmic reticulum with microtubules. *EMBO J* **17**, 6168-6177 (1998).

26. Schlaitz, A.-L., Thompson, J., Wong, C.C., Yates, J.R. & Heald, R. REEP3/4 ensure endoplasmic reticulum clearance from metaphase chromatin and proper nuclear envelope architecture. *Developmental cell* **26**, 315-323 (2013).

27. Allan, B.B., Moyer, B.D. & Balch, W.E. Rab1 recruitment of p115 into a cis-SNARE complex: programming budding COPII vesicles for fusion. *Science* **289**, 444-448 (2000).

28. Honsbein, A. *et al.* A tripartite SNARE-K+ channel complex mediates in channel-dependent K+ nutrition in Arabidopsis. *The Plant Cell* **21**, 2859-2877 (2009).

29. Woronowicz, K. *et al.* The platelet actin cytoskeleton associates with SNAREs and participates in alpha-granule secretion. *Biochemistry* **49**, 4533-4542 (2010).

30. Jewell, J.L., Luo, W., Oh, E., Wang, Z. & Thurmond, D.C. Filamentous actin regulates insulin exocytosis through direct interaction with Syntaxin 4. *J Biol Chem* **283**, 10716-10726 (2008).

31. Faigle, W., Colucci-Guyon, E., Louvard, D., Amigorena, S. & Galli, T. Vimentin filaments in fibroblasts are a reservoir for SNAP23, a component of the membrane fusion machinery. *Mol Biol Cell* **11**, 3485-3494 (2000).

32. Tominaga, M. *et al.* Cytoplasmic streaming velocity as a plant size determinant. *Dev Cell* **27**, 345-352 (2013).

33. Stefano, G., Renna, L., Moss, T., McNew, J.A. & Brandizzi, F. In Arabidopsis, the spatial and dynamic organization of the endoplasmic reticulum and Golgi apparatus is influenced by the integrity of the C‐terminal domain of RHD3, a non‐essential GTPase. *The Plant Journal* **69**, 957-966 (2012).

34. Sanderfoot, A.A., Assaad, F.F. & Raikhel, N.V. The Arabidopsis genome. An abundance of soluble N-ethylmaleimide-sensitive factor adaptor protein receptors. *Plant Physiol* **124**, 1558-1569 (2000).

35. Kim, S.J. & Brandizzi, F. News and Views into the SNARE Complexity in Arabidopsis. *Front Plant Sci* **3**, 28 (2012).

36. Renna, L. *et al.* Golgi traffic and integrity depend on N-myristoyl transferase-1 in Arabidopsis. *Plant Cell* **25**, 1756-1773 (2013).

37. Stefano, G., Renna, L. & Brandizzi, F. The endoplasmic reticulum exerts control over organelle streaming during cell expansion. *Journal of cell science* **127**, 947-953 (2014).

38. Shimmen, T. The sliding theory of cytoplasmic streaming: fifty years of progress. *J Plant Res* **120**, 31-43 (2007).

39. Griffing, L.R., Lin, C., Perico, C., White, R.R. & Sparkes, I. Plant ER geometry and dynamics: biophysical and cytoskeletal control during growth and biotic response. *Protoplasma*, 1-14 (2016).

40. Peremyslov, V.V. *et al.* Identification of myosin XI receptors in Arabidopsis defines a distinct class of transport vesicles. *The Plant Cell* **25**, 3022-3038 (2013).

41. Sparkes, I.A., Runions, J., Kearns, A. & Hawes, C. Rapid, transient expression of fluorescent fusion proteins in tobacco plants and generation of stably transformed plants. *Nature protocols* **1**, 2019-2025 (2006).

42. Nakagawa, T. *et al.* Development of series of gateway binary vectors, pGWBs, for realizing efficient construction of fusion genes for plant transformation. *Journal of bioscience and bioengineering* **104**, 34-41 (2007).

43. Earley, K.W. *et al.* Gateway‐compatible vectors for plant functional genomics and proteomics. *The Plant Journal* **45**, 616-629 (2006).

44. Batoko, H., Zheng, H.-Q., Hawes, C. & Moore, I. A Rab1 GTPase is required for transport between the endoplasmic reticulum and Golgi apparatus and for normal Golgi movement in plants. *The Plant Cell* **12**, 2201-2217 (2000).

45. Clough, S.J. & Bent, A.F. Floral dip: a simplified method forAgrobacterium‐mediated transformation ofArabidopsis thaliana. *The plant journal* **16**, 735-743 (1998).

46. Bolte, S. & Cordelieres, F. A guided tour into subcellular colocalization analysis in light microscopy. *Journal of microscopy* **224**, 213-232 (2006).

47. Manders, E., Verbeek, F. & Aten, J. Measurement of co‐localization of objects in dual‐colour confocal images. *Journal of microscopy* **169**, 375-382 (1993).

48. Nelson, B.K., Cai, X. & Nebenführ, A. A multicolored set of in vivo organelle markers for co‐localization studies in Arabidopsis and other plants. *The Plant Journal* **51**, 1126-1136 (2007).

49. Sheahan, M.B., Rose, R.J. & McCurdy, D.W. Organelle inheritance in plant cell division: the actin cytoskeleton is required for unbiased inheritance of chloroplasts, mitochondria and endoplasmic reticulum in dividing protoplasts. *The Plant Journal* **37**, 379-390 (2004).

50. Ueda, K., Matsuyama, T. & Hashimoto, T. Visualization of microtubules in living cells of transgenic Arabidopsis thaliana. *Protoplasma* **206**, 201-206 (1999).

51. Saravanan, R.S. *et al.* The targeting of the oxysterol‐binding protein ORP3a to the endoplasmic reticulum relies on the plant VAP33 homolog PVA12. *The Plant Journal* **58**, 817-830 (2009).

52. LP daSilva, L. *et al.* Endoplasmic Reticulum Export Sites and Golgi Bodies Behave as Single Mobile Secretory Units in Plant Cells W. *The Plant Cell* **16**, 1753 (2004).

53. Faso, C. *et al.* A missense mutation in the Arabidopsis COPII coat protein Sec24A induces the formation of clusters of the endoplasmic reticulum and Golgi apparatus. *The Plant Cell* **21**, 3655-3671 (2009).

54. Brandizzi, F., Snapp, E.L., Roberts, A.G., Lippincott-Schwartz, J. & Hawes, C. Membrane protein transport between the endoplasmic reticulum and the Golgi in tobacco leaves is energy dependent but cytoskeleton independent evidence from selective photobleaching. *The Plant Cell* **14**, 1293-1309 (2002).

55. Lai, Y.-S., Stefano, G. & Brandizzi, F. ER stress signaling requires RHD3, a functionally conserved ER-shaping GTPase. *Journal of cell science* **127**, 3227-3232 (2014).

56. French, A.P. *et al.* Identifying biological landmarks using a novel cell measuring image analysis tool: Cell-o-Tape. *Plant Methods* **8**, 1 (2012).

57. Verbelen, J.-P., Cnodder, T.D., Le, J., Vissenberg, K. & Baluška, F. The root apex of Arabidopsis thaliana consists of four distinct zones of growth activities: meristematic zone, transition zone, fast elongation zone and growth terminating zone. *Plant signaling & behavior* **1**, 296-304 (2006).

58. Schapire, A.L. *et al.* Arabidopsis synaptotagmin 1 is required for the maintenance of plasma membrane integrity and cell viability. *The Plant Cell* **20**, 3374-3388 (2008).

59. Renna, L. *et al.* Golgi traffic and integrity depend on N-myristoyl transferase-1 in Arabidopsis. *The Plant Cell* **25**, 1756-1773 (2013).

60. van de Meerakker, J.B. *et al.* A novel alpha-tropomyosin mutation associates with dilated and non-compaction cardiomyopathy and diminishes actin binding. *Biochimica et Biophysica Acta (BBA)-Molecular Cell Research* **1833**, 833-839 (2013).

CHAPTER 3. HOMEOSTASIS OF BRANCHED-CHAIN AMINO ACIDS IS CRITICAL FOR THE ACTIVITY OF TOR SIGNALING IN *ARABIDOPSIS*

The work presented in this chapter has been submitted as a manuscript

Pengfei Cao[1,2], Sang-Jin Kim[3], Anqi Xing[4], Craig A. Schenck[4], Lu Liu[1], Nan Jiang[4], Jie Wang[2], Robert L. Last[2,4], and Federica Brandizzi[1,2,3*]

[1]MSU-DOE Plant Research Lab; [2]Department of Plant Biology; [3]Great Lakes Bioenergy Research Center; [4]Department of Biochemistry and Molecular Biology, Michigan State University, East Lansing, USA

[*]For correspondence: fb@msu.edu

3.1 ABSTRACT

The target of rapamycin (TOR) kinase is an evolutionarily conserved hub of nutrient sensing and metabolic signaling. In plants, a functional connection of TOR with glucose availability has been demonstrated but it is yet unclear whether branched-chain amino acids (BCAAs) are a primary input of TOR signaling as they are in yeast and mammalian cells. Here, we report on the characterization of an Arabidopsis mutant over-accumulating BCAAs. Through chemical interventions targeting TOR and by examining mutants of BCAA biosynthesis and TOR signaling, we found that BCAA over-accumulation leads to up-regulation of TOR activity, which causes reorganization of the actin cytoskeleton and actin-associated endomembranes. Finally, we show that activation of TOR is concomitant with alteration of cell expansion, proliferation and specialized metabolism, leading to pleiotropic effects on plant growth and development. These results demonstrate that BCAAs contribute to plant TOR activation and reveal previously uncharted downstream subcellular processes of TOR signaling.

3.2 INTRODUCTION

In eukaryotes, target of rapamycin (TOR) is a conserved master regulator of metabolic signaling that integrates nutrient, energy, hormone, growth and stress inputs with cell growth and metabolism[1-3]. In yeast and mammalian cells, TOR associates with different interactors to form two functional complexes, TOR complex 1 (TORC1) and TOR complex 2 (TORC2)[1]. The Arabidopsis genome encodes functional homologs of TOR (AtTOR) and two TOR-interactors: LST8 (AtLST8-1 and AtLST8-2) and a specific component of TORC1, RAPTOR (AtRAPTOR1A and AtRAPTOR1B)[3]. The Arabidopsis homologs of TORC2-specific components have not been identified yet.

The yeast and mammalian TORC1 and TORC2 receive specific inputs and regulate distinct downstream processes. For example, sensors of leucine (Leu) and other amino acids provide input signals to TORC1[1, 2], while mammalian TORC2 is primarily regulated by the insulin-PI3K signaling and is inhibited by mTORC1 effectors[1, 4]. The current model of plant TOR signaling is built upon the three TORC1 components identified to date and envisions that TORC1 has essential functions, including promoting synthesis of proteins, nucleotides and lipids, and inhibiting autophagy for cell growth and proliferation[3].

In plants, TOR has assumed critical and specific roles, including involvement in phytohormone signaling pathways (i.e., auxin[5-7], cytokinin[8], brassinosteroid[9, 10] and abscisic acid[11]), as well as metabolic signaling (e.g., glucosinolates[12], sulfur sensing[13]). Despite these advances, it is not well elucidated which inputs activate plant TOR signaling. In yeast and mammalian models, nutrient sensing of amino acids, especially the branched-chain amino acids (BCAAs) Leu, isoleucine (Ile) and valine (Val), is the primary input underlying activation of TOR signaling[1, 2]. Recent studies in plants revealed a glucose-TOR signaling pathway that integrates light and sugar availability to control meristem activation in root and shoot[5, 6, 8, 14], connecting TOR signaling to the generation and availability of photosynthates. Therefore, the level of conservation of TOR signaling input across kingdoms and in plant cells specifically is still a significant question.

Investigating the relationship between BCAAs and plant TOR signaling has been generally hindered by the innate capacity of plant cells to produce BCAAs[15]. In the chloroplast, the allosterically regulated enzymes threonine deaminase (TD), acetohydroxyacid synthase (AHAS) and isopropylmalate synthase (IPMS) are subjected to feedback inhibition, and contribute to BCAA homeostasis[15]. Mammalian cells are unable to synthesize BCAAs; consequently, starvation and repletion of BCAAs in the culture serum can be effective in stimulating TOR signaling[16, 17].

In contrast, for plant cells, exogenous feeding of a limited concentration of amino acids to the growth medium may not perturb BCAA homeostasis and trigger detectable activation of TOR signaling[14]. Moreover, supplementation of a single or a combination of multiple amino acids may confer intertwined feedback inhibition to the biosynthetic pathway, and lead to unpredictable disruption of amino acid homeostasis[18, 19]. Additionally, because TOR is the main negative regulator of autophagy and promotes protein synthesis, chemical inhibition of either BCAA biosynthesis or TOR activity does not specifically affect BCAAs but leads to substantial increases in almost all types of amino acids in plant cells[20-22]. In light of these considerations, it is therefore not surprising that little is known about the functional and physiological consequences of an up-regulation of TOR signaling in plants, especially at a subcellular level. In yeast and mammalian cells, induced activation of TOR governs numerous cellular processes, most evidently the inhibition of autophagy by TORC1 and the reorganization of actin cytoskeleton by TORC2[1]. Although the mechanistic basis is not fully understood, it has been proposed that mTORC2 regulates reorganization of actin cytoskeleton through the AGC family protein kinases and Rho signaling[4]. Plants express AGC family-like homologs with specialized functions[23] and Rho of Plants (ROP) members that signal to the cytoskeleton system[23, 24]. Nonetheless, direct functional connections between TOR signaling, cytoskeleton in plant growth and development are yet to be established[20, 25-31].

In this work, we report on the characterization of *eva1*, a mutant with defects in vacuole morphogenesis and organization of actin filaments and endomembranes, which are associated mainly with actin in plant cells[32]. The *eva1* mutation is a loss-of-function allele of *IPMS1*, which encodes the first committed enzyme of Leu biosynthesis, resulting in elevated free Val levels. Through phenotypic and functional analyses of *eva1* and a series of other mutants of BCAA

biosynthesis and TOR signaling, we demonstrate that the subcellular phenotypes of *eva1* specifically hinge upon up-regulation of TOR signaling, which in turn affects organization of actin and endomembranes, and plant development. Therefore, by focusing on mutants with constitutive TOR signaling mis-regulation due to altered endogenous BCAA levels, we demonstrated that plant TOR signaling is linked to BCAAs and is critical for the homeostasis of actin, endomembranes and growth. The broader implications of these findings are that, despite the acquisition of specialized functions of TOR signaling in plants, the activating inputs of TOR signaling and the subcellular consequences of TOR signaling mis-regulation are conserved across eukaryotes.

3.3 RESULTS

3.3.1 Identification of a mutant with defects in vacuole morphogenesis

We pursued a confocal microscopy-based screen on an EMS-mutagenized population to identify mutants with defects in the subcellular distribution of the tonoplast marker GFP-δTIP[33, 34]. We focused on *eva1*, a mutant characterized by severe defects in vacuole morphology early in development. During the first 10 days after germination, in wild-type (WT) cotyledon epidermal cells, small vacuoles undergo membrane fusion to form a large central vacuole[35] (Figure 3.1a). In contrast, 10-day old *eva1* cotyledon epidermal cells displayed prominent *trans*-vacuolar strands (TVSs) and numerous small vacuoles (Figure 3.1a). This phenotype was attenuated in 20-day old *eva1* cotyledons, which closely resembled WT (Figure 3.1b). The *eva1* vacuole phenotypes were verified in 10-day old *eva1* cotyledons expressing γTIP-YFP[36], which labels the large central vacuole and other vacuolar structures not marked by GFP-δTIP[37] (Figure 3.2b). These results support that the tonoplast organization and vacuolar morphology are compromised in *eva1* in early stages of growth independently from the tonoplast marker used for the analyses.

We next aimed to identify the causative mutation in *eva1*. Bulked segregant analysis and whole-genome resequencing narrowed down the *eva1* mutation to a G-to-A transition in *IPMS1* (*AT1G18500*) causing an aspartate (Asp)-to-asparagine (Asn) residue substitution (Figure 3.1c, d; Figure 3.3a). IPMS1 catalyzes condensation of 2-oxoisovalerate and acetyl-CoA into 2-isopropylmalate, the committed step for Leu biosynthesis[38] (Figure 3.4a). Homology modeling of IPMS1 predicted that the mutated Asp228 is located in the acetyl-CoA binding surface near the pocket for 2-oxoisovalerate substrate (Figure 3.3b, c). Three other *IPMS1* alleles have been characterized thus far: two recessive loss-of-function mutants, *ipms1-4* and *ipms1-5*, and the gain-of-function *ipms1-1D*, with a point mutation that impairs allosteric regulation (Figure 3.1c)[15, 38]. 10-day old *eva1*, *ipms1-4* and *ipms1-5* seedlings exhibited similar delay in the emergence of true leaves (Figure 3.1e). These growth and developmental phenotypes, as well as the subcellular phenotypes (Figure 3.1a, b), were attenuated by 20 days of growth (Figure 3.1f). The presence of the *eva1* phenotypes in the *eva1* $\times$ *ipms1-5* F1 progeny confirmed allelism of *eva1* to *IPMS1* (Figure 3.3d, e). Together, these results support that the *eva1* vacuole and plant growth phenotypes are correlated to a loss of functional IPMS1, which has a consistent subcellular impact on early stages of growth.

3.3.2 *eva1* over-accumulates Val

The role of IPMS1 in BCAA biosynthesis has been well characterized as directing flux towards Leu biosynthesis, and away from the competing product Val[15, 38] (Figure 3.4a). The Arabidopsis genome encodes two IPMS isoforms: IPMS1 mRNA accumulates to higher levels than IPMS2 mRNA through most stages of plant growth[38]. Earlier work examined four-week old plants and found that Val and Ile were increased in both *ipms1-4* and *ipms1-5* but Leu was decreased in *ipms1-4* and increased in *ipms1-5*[15]. To determine the impact of the *eva1* mutation on amino acid

homeostasis at earlier stages of growth, we conducted free amino acid analysis of 10- and 20-day old WT and *ipms1* mutants. Notably, we found that *eva1*, *ipms1-4* and *ipms1-5* had similar increases in Val and total BCAAs and decreases in Leu, consistent with our findings that *eva1* is a loss-of-function allele of *IPMS1* (Figure 3.4b, c; Figure 3.2). In addition, in these mutants we found similar changes of Asp-derived amino acids (threonine-Thr, methionine-Met, lysine-Lys and Ile) and aromatic amino acids (phenylalanine-Phe, tryptophan-Trp and tyrosine-Tyr) (Figure 3.4b, c). Consistent with a disappearance of the subcellular phenotypes of the mutants during growth (Figure 3.1a, b), the impact of *ipms1* mutations on amino acid homeostasis was mitigated at 20 days of growth, with the fold change of Val becoming smaller in the mutants *versus* WT, and the types of amino acids significantly changed in the mutants compared to WT becoming fewer (Figure 3.4b, c). Taken together, these data indicate that *eva1* is a loss-of-function mutant of *IPMS1* equivalent to *ipms1-4* and *ipms1-5* and that the alteration in BCAA levels is most notable for an increased in Val levels.

3.3.3 Disruption of BCAA homeostasis leads to pleiotropic defects on plant growth and development

Next, we asked whether the transient changes in BCAA accumulation and vacuole morphology affected early plant growth. At 10 days following germination, the *IPMS1* loss-of-function mutants displayed retardation of growth and development (Figure 3.1e, f), showing approximately 30-40% decrease in aerial tissue fresh weight and 40-50% decrease in primary root length compared to WT (Figure 3.6a, b). Propidium iodide staining showed a strikingly delayed formation of root hairs in *ipms1* mutants compared to WT (Figure 3.7a), which was accompanied by an increase in both cell length and number in the elongation zone (Figure 3.7b, c). At 20 days of growth, the difference in fresh weight between *ipms1* alleles and WT became not significant, though the primary roots of

the *ipms1* mutants were still slightly shorter than WT (Figure 3.6c, d). In contrast, two independent lines of dominant *ipms1-1D* feedback-insensitive mutant, which have limited Val decrease and Leu increase[15], exhibited indistinguishable primary root elongation, but increased fresh weight compared to WT (Figure 3.6a - d). Additionally, we did not observe notable difference between six-week old WT and *IPMS1* loss-of-function mutants growing in soil (Figure 3.6e). The transient retardation of overall plant growth of *IPMS1* loss-of-function mutants correlated with the emergence-and-disappearance period of both vacuole morphology and BCAA homeostasis perturbation phenotypes (Figure 3.1a, b; Figure 3.4b - e).

We then examined the development of cotyledons, which constituted most of the aerial tissue for amino acid profiling and were used for confocal microscopy analyses. Cotyledons of *ipms1* mutants were thicker and larger than WT (Figure 3.5a - c). Despite a delay of true leaf emergence (Figure 3.1e), the expanded first pair of true leaves in these mutants were larger than WT (Figure 3.1f). Transmission electron microscopy analyses revealed an absence of connecting stroma thylakoids in chloroplasts of the cotyledons of *IPMS1* loss-of-function mutants compared to WT (Figure 3.5d, e). Additionally, we noticed purple pigmentation in 10-day old *IPMS1* loss-of-function mutants, particularly in cotyledon petioles and emerging true leaves (Figure 3.8a). Anthocyanin extraction and measurement confirmed that these mutants contained higher levels of total anthocyanins compared to WT (Figure 3.8b, c). These results indicate that the growth of certain tissues of the *ipms1* mutants is particularly promoted but the overall plant growth and development are temporarily inhibited.

3.3.4 The organization of ER network and actin cytoskeleton is altered in *eva1*

To gain more insights into the *eva1* vacuolar phenotypes, we extended our analyses to other endomembrane compartments. The endoplasmic reticulum (ER) is the most extensively

distributed organelle of the plant secretory pathway, and it is closely associated with several other membrane-bound organelles, including the vacuole[32]. In the *eva1* mutant, the ER luminal marker ERYK[36] revealed a pronounced appearance of the cortical ER network with strikingly thickened strands compared to WT (Figure 3.9a; see arrows). The thickened ER strands did not completely overlap with the TVSs (Figure 3.10). High-magnification confocal microscopy images of the cortical ER revealed a pronounced cisternation in *eva1* compared to WT (Figure 3.9b). Quantitative analyses of the surface area occupancy of the ER in the total field of view confirmed these observations (i.e., larger ER-occupied area in *eva1* compared to WT) (Figure 3.9d). The appearance of the Golgi apparatus, which in plant cells is organized in disperse stacks of cisternae in close association with the ER[39], also was abnormal. Indeed, the Golgi marker GFP-CASP[40] revealed increased clustering and higher abundance of Golgi stacks at the cell cortex in *eva1* compared to WT (Figure 3.11). Next, we examined secretion to the apoplast with the bulk flow marker SEC-RFP[41]. We found no intracellular retention of the marker in *eva1* (Figure 3.12), as it would be expected for mutants with defective secretion[42, 43]. These results and the absence of retention of the vacuolar marker in the ER (Figure 3.10) document that the morphology of the vacuole, organization of the Golgi and the ER network are markedly affected by the *eva1* mutation, while bulk-flow traffic is unaffected.

Collectively, the root-related defects of the *ipms1* mutants, including delayed formation of root hairs and reduced number of lateral roots (Figure 3.7; Figure 3.13), are reminiscent of mutants with impaired actin depolymerization or promoted actin bundling[44, 45], consistent with the possibility that re-organization of actin cytoskeleton may be causative of the observed developmental phenotypes. Furthermore, because the establishment and maintenance of the TVSs, ER network and Golgi subcellular distribution are dependent on the actin cytoskeleton[32], we

hypothesized that the organization of actin cytoskeleton may be altered in *eva1*. Indeed, confocal microscopy in cells expressing the actin filament (F-actin) marker YFP-ABD2[46] revealed coalescence of actin cables compared to WT (Figure 3.9c). Furthermore, quantitative analyses of actin organization identified higher skewness, suggesting enhanced bundling, and lower density, suggesting decreased occupancy of F-actin in the cytoplasm in *eva1* compared to WT (Figure 3.9e, f). These results imply that the prominent phenotypes of the endomembranes in *eva1* may be due to their connections with F-actin, whose organization is largely altered in the *eva1* mutant.

We next sought to validate this hypothesis by testing the sensitivity of the *ipms1* alleles to the F-actin depolymerizing reagent latrunculin B (Lat B)[47]. The primary root length of 10-day old *ipms1-4* and *ipms1-5* was approximately 50% of WT (Figure 3.13a, c). Seedlings of all genotypes were then transferred to medium containing DMSO or 50 nM or 100 nM Lat B in DMSO. After another 8 days, we found that the Lat B treatment promoted the formation of lateral roots in WT seedlings, but not in *ipms1* alleles (Figure 3.13b). Additionally, the primary root length of *ipms1-4* and *ipms1-5* was approximately 65% compared to WT on DMSO medium; however, this difference was reduced in the presence of increasing levels of Lat B in the growth medium (i.e., 80% to WT on 50 nM Lat B, and not significantly different from WT on 100 nM Lat B) (Figure 3.13d). These results demonstrate that the *ipms1* alleles are less sensitive to F-actin depolymerization compared to WT, supporting a functional connection between the disruption of *IPMS1* and altered organization of the actin cytoskeleton.

3.3.5 The vacuole phenotypes of *eva1* are rescued by PI3K/TOR dual inhibitors and partially recovered by disruption of F-actin

To gain insights into the mechanisms by which *eva1*defects in BCAA biosynthesis led to alteration of the organization of subcellular structures, we employed chemicals known to alter the vacuolar

morphogenesis and cytoskeleton integrity. We hypothesized that the persistence of small vacuoles in *eva1* could be due to delayed vacuole membrane fusion during vacuole morphogenesis. To test this, we first employed wortmannin (Wm), an inhibitor of phosphoinositide 3-kinases (PI3Ks) that disrupts the balance of phosphoinositides and promotes homotypic tonoplast fusion[48-50]. We found that treatment of 10-day old WT and *eva1* seedlings for two hours suppressed the *eva1* phenotypes (Figure 3.14a - d; Figure 3.15a - d). The effects of Wm were mirrored by treatment with another PI3K inhibitor, LY294002[48] (Figure 3.15e - h). We then investigated a relationship between TVSs and integrity of the cytoskeleton in *eva1*. After a two-hour treatment with Lat B, we found that TVSs disappeared but the small vacuoles persisted in *eva1* cotyledon epidermal cells (Figure 3.14e, f). By contrast, a two-hour treatment with oryzalin, a microtubule disrupting reagent[48], did not lead to discernable change of vacuole morphology (Figure 3.14g, h). Together these results indicate that the unfused vacuole and enhanced TVS phenotypes in *eva1* are both responsive to Wm and LY294002, but only the enhanced TVS phenotype is related to the verified reorganization of F-actin.

3.3.6 Loss of function of IPMS1 leads to up-regulation of TOR activation

Through chemical interventions, we confirmed that homotypic membrane fusion and F-actin bundling are two processes directly involved in the *eva1* Leu biosynthetic mutant phenotypes (Figure 3.14). This creates a quandary given that the role of IPMS1 in chloroplast BCAA biosynthesis is both functionally disconnected with – and spatially isolated from – the endomembrane compartments and actin cytoskeleton. Although the functions of Wm and LY294002 in inhibiting PI3Ks and promoting homotypic vacuolar membrane fusion have been established in plant cells[48, 49, 51, 52], in mammalian cell studies these chemicals have been used to inhibit TOR signaling[16, 53]. This is because TOR belongs to the phosphoinositide kinase-related

kinase (PIKK) family, whose members share similar kinase domains with PI3Ks[54]. Indeed, Wm and LY294002 are effective inhibitors of mammalian TOR[53], and thus are considered as PI3K/TOR dual inhibitors[55]. These considerations and our results led us to hypothesize that the effects of Wm and LY294002 in suppressing the *eva1* vacuole phenotypes could be related to TOR inhibition.

To test this hypothesis, we employed two TOR inhibitors with high selectivity for TOR over PI3Ks: AZD-8055 and Torin2[55-57]. We transferred 10-day old WT and *eva1* seedlings to liquid growth medium containing 5 μM AZD-8055. Compared to untreated samples, WT cells did not exhibit significant changes in the morphology of the central vacuole and the few thin TVSs after 2 or 4 hours of incubation, although numerous fluorescent punctae appeared (Figure 3.16a, c, e). Because TOR is the major negative regulator of autophagy[58], the punctae are presumably autophagic structures resulting from the TOR inhibition by the chemicals. Untreated *eva1* cells contained numerous small vacuoles and conspicuous TVSs (Figure 3.16b); however, by 2-hour treatment with AZD-8055, these structures were reduced in appearance (Figure 3.16d). By 4-hour treatment, the *eva1* cells were indistinguishable from WT, including the appearance of the small punctae (Figure 3.16e, f). These results were mirrored by Torin2 treatment: unfused vacuoles and TVSs were no longer present in the *eva1* cells by 2 hours of 1 μM Torin2 treatment (Figure 3.17). This result is in line with the higher *in vitro* TOR inhibitory activity of Torin2 compared to AZD-8055[56, 57]. Together these results indicate that chemical inhibition of TOR suppresses the subcellular defects of *ipms1* and thus suggest a functional connection between TOR activity and BCAA homeostasis.

We next sought to confirm these results by testing the activation status of TOR in *ipms1*. Based on the evidence that TOR inhibition rescued the *ipms1* subcellular phenotypes, we predicted to

find an increased level of TOR activity in *ipms1* compared to WT. S6K is a conserved substrate of TOR protein kinase and its phosphorylation status has been adopted as an indicator of TOR activity in plants[8, 11, 13, 31]. Indeed, immunoblot analyses with specific antisera for either phosphorylated or total S6K[8, 11, 13, 31] revealed increased levels of TOR-phosphorylated S6K in *eva1* and *ipms1-4* compared to WT, despite similar levels of total S6K in three genotypes (Figure 3.16g). These data indicate that TOR signaling is up-regulated in the *ipms1* background. To validate this conclusion, we monitored DNA synthesis in root tips because a stimulated TOR signaling promotes cell proliferation in the root apical meristem, which can be detected by EdU staining of newly synthesized DNA[5, 13, 14]. Consistent with our hypothesis, the EdU staining displayed enhanced labeling in the root apical meristem of *ipms1-4* and *ipms1-5* compared to WT (Figure 3.16h). This result was supported by propidium iodide staining and morphometric analyses of root tips showing increased cell numbers in the root apical meristem of *eva1*, *ipms1-4* and *ipms1-5* compared to WT (Figure 3.7b, c).

Taken together, the results indicating suppression of vacuole phenotypes by TOR inhibition, increased levels of S6K phosphorylation and root apical meristem activity (i.e., increased DNA synthesis and cell number) in the *ipms1* mutants support the hypothesis that TOR signaling is up-regulated in the *IPMS1* loss-of-function mutants.

Next, we aimed to test a role of TOR signaling and its specificity in the verified BCAA over-accumulation-induced phenotypes. To do so, we utilized an estradiol-inducible TOR mutant (*tor-es*)[31] and a loss-of-function mutant of *AtRAPTOR1B* (*raptor1b*, SALK_022096)[28], a locus encoding the functional TORC1 component RAPTOR in Arabidopsis[27, 29]. Before silencing induction, similar to WT (Figure 3.18a, d), *tor-es* seedlings grown on BCAA-supplemented medium showed enhanced F-actin bundling compared to *tor-es* grown on normal medium (Figure

3.18g, j). After induction of TOR silencing, *tor-es* grown on either medium exhibited similarly low levels of bundling (Figure 3.18h, k). These results confirm a functional dependence of TOR signaling and the actin cytoskeleton phenotype due to mis-regulated TOR. By contrast, in *raptor1b* BCAA feeding led to F-actin bundling (Figure 3.18i, l). Together, these results not only indicate that reorganization of F-actin induced by over-accumulation of BCAAs is dependent on functional TOR but also underlie a cause of the subcellular phenotype linked to BCAA on TOR signaling components other than RAPTOR.

3.3.7 Over-accumulation of BCAAs alters the subcellular organization of the actin cytoskeleton and endomembranes

Next, we aimed to test the generality of the connection between over-accumulation of BCAAs, morphological alteration of cellular structures and functional TOR signaling. To do so, we used a variety of previously characterized BCAA mutants[15], combined with BCAA feeding. For example, *ipms1-1*^{D} was chosen because it has a modest Val decrease and Leu increase; *ahass1-1* has a limited Val increase; *ahass2-7* has decreased Val and Leu; *omr1-11*^{D} has a >140 fold Ile increase compared to WT. Confocal microscopy analyses of cotyledon epidermal cells revealed that the organization of F-actin in *ipms1-1*^{D} and *ahass1-1* mutants resembled that of WT (Figure 3.18a - c). By contrast, enhanced actin bundling was observed following BCAA feeding (1 mM Val, Leu and Ile) and in the *ipms1-5* and *omr1-11*^{D} mutants (Figure 3.18d - f). Interestingly also, we found that the mutants showed reorganization of F-actin and remodeling of the ER network. Specifically, mutants with moderate increase or decrease in BCAAs showed ER morphology similar to WT (Figure 3.19a - d), while WT grown with BCAA supplementation and mutants that over-accumulate BCAAs showed compromised ER organization with longer and thicker ER strands compared to WT (Figure 3.19e - g). The striking phenotype of enhanced ER strands in *omr1-11*^{D}

was recovered by a 2-hour Torin2 treatment (Figure 3.19h). In addition to bundling of F-actin and enhancement of ER strands, supplementation of BCAAs also induced the formation of prominent TVSs (Figure 3.20). Together, these results support a general correlation between over-accumulation of BCAAs and distorted actin cytoskeleton and endomembranes.

3.4 DISCUSSION

In eukaryotic cells, the TOR kinase coordinates cell growth and metabolism with nutrient sensing[1, 2]. In mammalian cells, the availability of BCAAs and other amino acids – as well as glucose and mammalian growth factors – regulates TOR signaling, which generally promotes growth via several downstream cellular processes, including mRNA translation, metabolism of nucleotides, sugar and lipids, protein turnover and cytoskeletal reorganization[1, 2]. Prior to this work, in plant cells a functional connection between glucose availability and TOR activation as well as crosstalk between TOR and major hormone signaling pathways had been established[3], but a role for BCAAs in TOR signaling was yet unknown. Furthermore, it was still unclear whether TOR signaling is connected to the morphogenesis and remodeling of subcellular structures, other than autophagic bodies. We demonstrated that TOR signaling senses BCAA homeostasis and modulates the organization of subcellular structures, including actin cytoskeleton and endomembranes. Indeed, we provide evidence that over-accumulation of BCAAs up-regulates TOR signaling, inducing actin bundling with formation of aberrant endomembrane structures and compromising overall growth (Figure 3.21).

3.4.1 Endogenous BCAAs influence TOR signaling in plant cells

In yeast and mammalian cells, TOR signaling is modulated directly by changes in amino acid levels, especially BCAAs, and indirectly by glucose levels and growth factors[1, 2]. In plants, TOR-mediated meristem activation by sugar and light signals has been established[5, 6, 8, 14], but a

connection between TOR signaling and levels of endogenous amino acid was yet unexplored. Plants produce BCAAs *de novo* and their biosynthesis is stringently controlled[15]. In this study, through the characterization of mutants with altered BCAA homeostasis and TOR signaling, we provide evidence for a functional correlation between BCAA accumulation and TOR activity in plant cells. Indeed, we found that in early stages of growth (i.e., 10 days) BCAA over-accumulating mutants showed up-regulation of TOR, a phenotype that was recreated by BCAA feeding. Furthermore, a reduction in TOR signaling activation via dual and specific TOR inhibitors restored the actin and endomembrane phenotypes. Our results establish that plant TOR senses over-accumulation of BCAAs, and that up-regulation of TOR signaling alters the organization of actin cytoskeleton and associated endomembranes and controls plant growth. Our results indicate that plant TOR signaling and TOR-dependent growth regulation are highly responsive to BCAA availability, at least in early stages of growth, underscoring a previously unappreciated but significant role of these amino acids in TOR biology.

3.4.2 TOR signaling controls actin organization in plant cells

In mammalian cells, a reorganization of actin cytoskeleton was the first identified downstream effect specific to TORC2, which was also found to be independent of TORC1[16, 17, 59]. In yeast and mammalian cells, TORC2 phosphorylates other protein kinases, which signal to the Rho-coordinated cytoskeletal signaling[4, 60]. Recently, it has been demonstrated that Arabidopsis ROP2 interacts with TOR and mediates an auxin-to-TOR signaling[5, 7], suggesting an interplay among TOR, ROPs and the cytoskeleton in plant cells. The evidence provided in our work for promoted actin bundling phenotype in mutants with BCAA over-accumulation or upon BCAA supplementation to WT provides direct support for a functional interaction between TOR and the actin cytoskeleton. Furthermore, our evidence that the BCAA-induced actin reorganization relies

on functional TOR but not RAPTOR, which defines TORC1, extends these conclusions at a mechanistic level by excluding TORC1 in TOR-depended actin reorganization in plant cells.

3.4.3 Plant endomembrane homeostasis is correlated with TOR activity

The vacuole and the ER are the two organelles of largest membrane extension in plant cells[35, 61]. The central vacuole is for essential cellular functions such as providing turgor pressure, protein turnover and metabolite storage[35]. The ER is the gateway to the secretory pathway and a membrane network that weaves through nearly all the other types of organelles[61, 62]. Despite of the essential roles of the vacuole and the ER[35, 61], the mechanisms underpinning their morphogenesis are still largely undefined although homotypic membrane fusion is known to be required[35, 52, 63]. It is also yet unclear whether and how the dynamics of plant ER and vacuoles are controlled in response to different developmental and environmental clues. The dynamics of endomembrane system in plant cells are mechanistically different from mammalian cells. In the latter, the ER morphology, organization and dynamics are mainly driven by microtubules and microtubule-related motor proteins[64]. In net contrast, the ER is primarily anchored to and mobilized by the actomyosin system[32, 35, 65]. Furthermore, plant vacuoles are in close proximity to the actin cytoskeleton[35] and the integrity of the TVSs depends on actin[32]. We have shown that an over-accumulation of BCAAs affects the morphology of the tonoplast, ER and Golgi distribution. Our results also showed that attenuation of TOR signaling in BCAA over-accumulating mutants leads to a restoration of the defective actin cytoskeleton and endomembrane morphology. We propose therefore that in plant cells a stringent relationship exists between endomembrane organization and TOR-signaling, which occurs via a functional connection of TOR with the actin cytoskeleton. Depending on nutrient status, TORC1 regulates the size and number of yeast vacuoles and mammalian lysosomes[66, 67]. In light of the conserved functions of nutrient storage and turnover that are shared

by plant and yeast vacuoles[35], a TORC1-dependent control of the vacuolar homeostasis may be conserved in plant cells. An auxin-dependent actin remodeling has been also recently invoked in controlling vacuole occupancy in the plant cell[68, 69]. In this work, we provided evidence for a remodeling of actin through TORC1-independent TOR signaling. Therefore, we propose that TOR activity is involved in morphogenesis of the central vacuole, but this may occur through mechanisms that are not conserved.

3.4.4 Plant growth and TOR signaling

BCAAs are crucial nutrients that humans and other animals must obtain from diets. Significant deficits exist in the amino acid composition of plant feed sources for livestock[70]. Moreover, BCAAs serve as human dietary supplements, because they potently promote protein synthesis through TOR activity[71]. Fortification of crops with BCAAs is therefore desirable to improve plant nutritional content. However, studies in Arabidopsis reported that BCAA over-accumulation due to exogenous feeding or genetic manipulation of biosynthetic or catabolic pathways resulted in various defects in plant growth and development[15, 72-74]. In this study, we established a functional connection between BCAA over-accumulation and plant growth inhibition, which is likely linked to alteration of TOR signaling and disruption of subcellular structures. Despite an overall retardation of early plant development compared to WT, *ipms1* seedlings exhibited up-regulation of the growth-promoting TOR signaling in concert with locally promoted growth, such as larger and thicker cotyledons and higher activity of root apical meristem. At the subcellular level, we showed that BCAA over-accumulation via exogenous feeding or genetic mutations caused severe remodeling of the actin cytoskeleton and endomembranes, which underlies certain growth defects such as delayed formation of root hairs and reduced abundance of lateral roots[44, 45, 63]. Together, these results indicate that an inconsistency between nutrient status and the activity of metabolic

signaling is detrimental to plant growth and development. By adding new insights into the fundamental understanding of plant growth control by metabolic signaling, our study supports that developmentally controlled manipulation of TOR signaling may be required for successful engineering of crops with improved yield and nutritional values.

3.5 METHODS

3.5.1 Plant growth conditions

Except for chronical treatments with specified chemicals, Arabidopsis seeds were stratified and grown on medium containing half-strength Linsmaier & Skoog nutrients (½ LS; Caisson Labs, LSP03), 1% sucrose and 0.4% phytagel (Sigma-Aldrich, P8169) in chambers conFigured with 21℃ and 16h light: 8h dark cycle.

To examine the effect of latrunculin B (Lat B; Sigma-Aldrich, L5288) on root elongation, wild type (Col-0), *ipms1-4* and *ipms1-5* lines germinated and grew on horizontally staged Petri dishes containing normal Arabidopsis growth medium (½ LS, 1% sucrose and 0.4% phytagel). 10 days old seedlings were transplanted to Petri dishes containing ½ LS, 1% sucrose and 1% Agar (Sigma-Aldrich, A1296) medium containing DMSO or 50 nM Lat B or 100 nM Lat B. Photographs were acquired immediately after the transplant and the Petri dishes were vertically staged in a Percival chamber. Photographs were also acquired 8 days after the transplant.

Exogeneous feeding of 1mM BCAA was performed by stratification and germination of seeds on ½ LS, 1% sucrose and 1% Agar medium containing 1 mM equal concentrations of Ile, Val and Leu. L-Isoleucine (Sigma-Aldrich, I2752), L-Valine (Sigma-Aldrich, V0500) and L-Leucine (Sigma-Aldrich, L8000) were dissolved in water to prepare 1M stock solutions, which were then filtered by Millex-GS 0.22 μm filter unit (Millipore, SLGS033SS).

3.5.2 Confocal microscopy

A Zeiss LSM 510 META and a Nikon A1Rsi laser scanning confocal microscope were used for imaging. Acquired images were handled by NIS-Elements Advanced Research (Nikon), ZEN (Zeiss) and Fiji (ImageJ)[71]. The fluorescent protein fusions used in this study are GFP-δTIP[72], ERYK[73], YFP-ABD2[74], GFP-CASP[75], SEC-RFP[74] and γTIP-YFP[73]. Transformation of Arabidopsis plants were conducted using floral dip method[76].

3.5.3 Quantitative analysis of ER morphology and actin cytoskeletal organization

Image acquisition and further evaluation of the ER cisternae was conducted using a previously described method that measures the occupancy of ER area in a region of interest[77]. Analysis of the actin cytoskeletal organization were performed following a previously described procedure[78]. Briefly, Z-stack images with 0.5 μm intervals were acquired to cover the whole epidermal cell. The Z-stack series were converted to maximal projection images using NIS-Elements Advanced Research (Nikon) and Fiji (ImageJ)[71]. Utilizing two ImageJ macros that were previously generated[78], skewness was measured to present the distribution of YFP-ABD2 fluorescence intensity and occupancy was measured for the density of skeletonized YFP-ABD2 fluorescence signal.

3.5.4 Chemical stocks and treatments

All temporal chemical treatments were performed using 10 days old seedlings. Each of the following chemicals was first dissolved in DMSO to prepare a stock solution, and then diluted in Arabidopsis growth medium (½ LS and 1% sucrose) to reach the specific working concentration. 33 μM Wortmannin (Sigma-Aldrich, W1628) and 100 μM LY294002 (MedChemExpress, HY-10108) were used to treat seedlings for 2 hours. Latrunculin B (Sigma-Aldrich, L5288) and Oryzalin (Chem Service Inc., N-12729) were diluted to 25 μM and 40 μM, respectively, for 2

hours treatments. For TOR inhibition, seedlings were incubated with 5 μM AZD-8055 (MedChemExpress, HY-10422) or 1 μM Torin2 (MedChemExpress, HY-13002) for 2 or 4 hours as the Figure legends indicated. 10 μM solution of β-estradiol (Sigma-Aldrich, E8875) was used to induce gene silencing.

3.5.5 Amino acid extraction and LC-MS/MS analysis

Plants used for amino acid extraction were grown under standard conditions for 10 or 20 days. The aerial tissue (fresh weight around 10 mg) was harvested into a 2 mL tube with two 3 mm steel beads and flash frozen in liquid N2. Tissue was either used immediately or stored at -80℃ until extraction. Tissue was pulverized using Retsch Mill (MM400) for 1 minute at 30 times per second. Amino acids were extracted as previously reported[13, 79]. Briefly, an amino acid extraction buffer was prepared with ~ 2 M heavy labeled amino acids standards (13C, 15N, Sigma-Aldrich), 10 M 1,4-dithiothreitol (DTT, Sigma-Aldrich), and 10 mM perfluoroheptanoic acid (PFHA, Sigma-Aldrich). To the ground tissue, 350 L of extraction buffer was added, vortexed for 10 seconds and heated at 90℃ for 10 minutes. Tubes were cooled on ice for 5 minutes and centrifuged for 10 minutes at 4℃ at 13,000 × g. The supernatant was applied to a low-binding hydrophilic 0.2 μm centrifugal polytetrafluoroethylene (PTFE) filter (Millipore, UFC30LG25) and centrifuged for 5 minutes at 3,500 × g. 150 L flow through was transferred to 2 mL glass vials with glass insert for LC-MS analysis.

Amino acid detection and quantification by LC-MS/MS was performed as previously reported[79, 80]. Briefly, a dilution series (12.2 nM to 250 μM) of each individual amino acid standard was made containing the same concentration of the heavy standards as was in the amino acid extraction buffer. Samples were injected into a Quattro micro API LC/MS/MS (Waters) equipped with an Acquity UHPLC HSS T3 1.8 μm column (Waters) using a three-function method. The 13-minute

LC method with solvent A (10 mM PFHA) and solvent B (acetonitrile) at a flow rate of 0.3mL/minute is provided in supplementary file (Supplementary file 1). Amino acids were quantified by comparison to their standard curves using QuanLynx.

3.5.6 EdU staining

EdU (5-ethynyl-2'-deoxyuridine) staining of root meristem was performed using Click-iT EdU Alexa Fluor 488 Imaging Kit (Invitrogen, C10337), following a protocol that was adapted for plant tissues[81]. Labeling was performed by incubating 10 days old Arabidopsis seedlings in 10 μM EdU in Arabidopsis growth medium (½ LS and 1% sucrose) for 30 min in a Percival chamber for Arabidopsis growth. All samples were then incubated with fixation buffer (4% formaldehyde, 0.1% Triton X-100, 1× PBS) for 30 min. All samples were washed for three times, 10 min each, with 1× PBS after fixation. The EdU detection was conducted by 30 min incubation in dark with the Click-iT cocktail, which was prepared according to the manual of Click-iT EdU Alexa Fluor 488 Imaging Kit. Each sample was immediately washed for three times, 10 min each, with 1× PBS before imaging.

3.5.7 PI staining of root tip and measurement

PI (propidium iodide) staining was conducted by 3 min incubation of Arabidopsis seedlings in propidium iodide (Invitrogen, P3566) diluted to 1 μg/mL using Arabidopsis growth medium (½ LS and 1% sucrose). After staining, all samples were immediately washed for 1 min and then subjected to imaging. Confocal images of propidium iodide stained root tips were analyzed using Cell-O-Tape[82], which is a plugin of ImageJ that automatically segments three zones in a root tip (the meristem, the transition zone and the mature zone) by comparing the lengths of adjacent cells in the same cortical layer. Adjacent cells with significant increase in cell length belong to the transition zone. Cells before and after the transition zone are categorized as cells in the meristem

and the mature zone respectively. The program records the length of each cell and the cell number in each zone.

3.5.8 Protein preparation and immunoblotting

To detect the phosphorylation status of S6K, 50 mg plant aerial tissue was used for protein extraction using 1.5 mL extraction buffer of 1 × PBS, pH 7.4, containing 250 mM sucrose, Protease Inhibitor Cocktail (100 μL per 10 mL extraction buffer; Sigma-Aldrich, P9599) and PhosSTOP phosphatase inhibitor (1 tablet per 10 mL extraction buffer; Roche, 4906845001). Three times of centrifugation, 1 k × g for 5 min, 14 k × g for 5 min and 135 k × g for 60 min, were conducted to separate the soluble proteins. The supernatant from the last centrifugation was separated, concentrated to 200 μL using an Amicon Ultra centrifugal unit (Millipore, UFC501024), and then mixed with 40 μL 6× Laemmli buffer. Proteins were denatured by incubation at 95℃ for 10 min. Protein samples were separated on 8% SDS-PAGE and blotted to PVDF membranes (Bio-Rad, 1620177). Blots were blocked with 5% milk for 1 h at room temperature. Blots were incubated with primary antibodies of either anti-S6K (Agrisera, AS12 1855) or anti-S6K-phosphorylated (Agrisera, AS13 2664) overnight at 4 ℃ and subsequently with secondary HRP conjugated goat anti-rabbit antibody (Sigma-Aldrich, A0545) for 1 h at room temperature.

3.5.9 Extraction and measurement of anthocyanins

The aerial parts of 10 days old Arabidopsis seedlings were collected, and then lyophilized and measured for dry weight. Total anthocyanins were extracted using 1 μL extraction buffer (50% methanol containing 3% formic acid) per 50 μg dry weight. After overnight incubation with extraction buffer at room temperature, the supernatant was collected and measured absorbance of 532 nm.

3.5.10 TEM and measurement of leaf thickness

The electron microscopic imaging of the endomembrane structures and chloroplasts were performed following an established protocol[83]. In brief, 1 mm × 1 mm pieces of cotyledon samples were cut and fixed in TEM fixative buffer (2.5% paraformaldehyde and 2.5% glutaraldehyde in 0.1 M cacodylate buffer, pH 7.4) with vacuum infiltration. The fixed samples were stained with 1 % osmium tetroxide overnight at 4 ℃. After series of dehydration with acetone, the samples were infiltrated and embedded in Spurr's Resin. Sections with 50 nm thickness were cut and mounted on the copper grid and 10 well slides. For TEM the grids were post-stained in 2% uranyl-acetate for 30 min and then treated with 1 % lead citrate for 15 min. JEOL 100CX TEM (JEOL USA) was used to observe the ultrastructure of cotyledon.

The thickness of cotyledons was measured as previously described[84]. Briefly, 2 mm × 1 mm samples cut from center of the cotyledons were fixed in fixative buffer (4% paraformaldehyde and 0.5% glutaraldehyde in 1 × PBS, pH 7.4) with vacuum infiltration. The fixed samples were stained with 1 % osmium tetroxide overnight at 4 ℃. After series of dehydration with acetone, the samples were infiltrated and embedded in Spurr's Resin. Sections with 500 nm thickness were cut and mounted on the copper grid and 10 well slides. For leaf thickness analysis, the sections stained with 1% toluidine blue for 1 min and washed with running water. Images were taken using Axio Imager M2 (Zeiss), and measurement of leaf thickness was performed using AxioVision SE64 Rel. 4.9.1 (Zeiss) software. Three biological samples with three technical replicates were used to measure leaf thickness.

3.6 ACKNOWLEDGMENTS

We thank Dr. Natasha Raikhel for the kind donation of the *eva1* line. We thank the members of the Brandizzi laboratory for critical inputs and Dr. Xiayan Liu for helpful discussions. We thank

Drs. Brad Day and Yi-Ju Lu for assistance of quantitative evaluation of the actin cytoskeleton. We thank the MSU Mass Spectrometry and Metabolomics Core Facility for assistance in amino acid analysis. We acknowledge support by the Chemical Sciences, Geosciences and Biosciences Division, Office of Basic Energy Sciences, Office of Science, US Department of Energy (award number DE-FG02-91ER20021) for infrastructure, and the National Science Foundation (MCB1727362).

APPENDIX

Stage	Genotype	Ile (nmol/mg FW[a])	Ileu (FC[b])	Val (nmol/mg FW)	Val (FC)	Leu (nmol/mg FW)	Leu (FC)
10 days old	WT	0.029 ± 0.0012		0.12 ± 0.003		0.035 ± 0.0013	
	eva1	0.052 ± 0.0021***	1.76	0.97 ± 0.040***	7.90	0.024 ± 0.0032**	0.66
	ipms1-4	0.047 ± 0.0013***	1.62	0.64 ± 0.024***	5.29	0.027 ± 0.0016**	0.77
	ipms1-5	0.044 ± 0.00055***	1.50	0.70 ± 0.016***	5.70	0.016 ± 0.00071***	0.46
20 days old	WT	0.026 ± 0.00067		0.087 ± 0.0048		0.020 ± 0.0014	
	eva1	0.028 ± 0.0020	1.05	0.24 ± 0.016***	2.74	0.012 ± 0.0014**	0.58
	ipms1-4	0.041 ± 0.0060	1.55	0.26 ± 0.022***	3.02	0.020 ± 0.0038	0.97
	ipms1-5	0.040 ± 0.0019***	1.51	0.29 ± 0.025***	3.30	0.021 ± 0.0017	1.02

Stage	Genotype	Thr (nmol/mg FW)	Thr (FC)	Leu/(Val+Leu) (ratio × 100)	BCAA (nmol/mg FW)	BCAA (FC)	BCAA/FAA[c] (ratio × 100)
10 days old	WT	0.55 ± 0.033		22 ± 0.43	0.19 ± 0.0054		0.64 ± 0.05
	eva1	0.82 ± 0.044***	1.51	2.3 ± 0.22***	1.05 ± 0.044***	5.58	1.8 ± 0.14***
	ipms1-4	0.81 ± 0.025***	1.48	4.0 ± 0.20***	0.73 ± 0.026***	3.87	1.5 ± 0.07***
	ipms1-5	0.76 ± 0.023***	1.40	2.3 ± 0.13***	0.76 ± 0.016***	4.06	1.4 ± 0.07***
20 days old	WT	0.34 ± 0.013		19 ± 0.48	0.13 ± 0.0063		0.77 ± 0.04
	eva1	0.29 ± 0.017*	0.85	4.6 ± 0.36**	0.28 ± 0.019***	2.21	1.9 ± 0.08***
	ipms1-4	0.35 ± 0.021	1.03	6.0 ± 1.5*	0.32 ± 0.026***	2.55	1.9 ± 0.14***
	ipms1-5	0.45 ± 0.033*	1.31	6.8 ± 0.75*	0.35 ± 0.026***	2.77	2.1 ± 0.04***

Table 3.1 The BCAA biosynthesis pathway is up-regulated in young seedlings of *eva1* and *IPMS1* loss-of-function mutants.

Amino acids were extracted from aerial tissues of 10 days old seedlings and rosette leaves of 20 days old plants. Each value represents the mean ± SEM. The asterisks indicate significant difference compared to the GFP-δ TIP as wild type (WT) (*p ⩽ 0.05, **p ⩽ 0.01, ***p ⩽ 0.001, unpaired t test).
aFW, fresh weight; bFC, fold change compared to GFP-δTIP; cFAA, total 19 free amino acids without cysteine.

Reagent type (species)	Designation	Source or reference	Identifiers
Gene (*Arabidopsis thaliana*)	*AtIPMS1*		TAIR: AT1G18500
Gene (*Arabidopsis thaliana*)	*AtOMR*		TAIR: AT3G10050
Gene (*Arabidopsis thaliana*)	*AtAHASS1*		TAIR: AT2G31810
Gene (*Arabidopsis thaliana*)	*AtAHASS2*		TAIR: AT5G16290
Gene (*Arabidopsis thaliana*)	*AtTOR*		TAIR: AT1G50030
Gene (*Arabidopsis thaliana*)	*AtRaptor1B*		TAIR: AT3G08850
Genetic reagent (*Arabidopsis thaliana*)	*eva1*	this paper	
Genetic reagent (*Arabidopsis thaliana*)	*ipms1-4*	Xing and Last, 2017	SALK_101771
Genetic reagent (*Arabidopsis thaliana*)	*ipms1-5*	Xing and Last, 2017	WiscDsLoxHs221_05F
Genetic reagent (*Arabidopsis thaliana*)	*tfl111 (ipms1-1^{D})*	Xing and Last, 2017	TAIR: CS69734
Genetic reagent (*Arabidopsis thaliana*)	*tfl102 (ipms1-1^{D})*	Xing and Last, 2017	TAIR: CS69733
Genetic reagent (*Arabidopsis thaliana*)	*ahass1-1*	Xing and Last, 2017	SALK_096207
Genetic reagent (*Arabidopsis thaliana*)	*ahass2-7*	Xing and Last, 2017	WiscDsLoxHs009_02G
Genetic reagent (*Arabidopsis thaliana*)	*ahass2-1^{D}*	Xing and Last, 2017	TAIR: CS69724
Genetic reagent (*Arabidopsis thaliana*)	*omr1-11^{D}*	Xing and Last, 2017	TAIR: CS69720
Genetic reagent (*Arabidopsis thaliana*)	*tor-es*	Xiong and Sheen, 2012; TAIR	TAIR: CS69829
Genetic reagent (*Arabidopsis thaliana*)	*raptor1B*	Salem et al., 2017; TAIR	SALK_022096
Antibody (Rabbit polyclonal)	Anti-S6K	Agrisera	AS12 1855
Antibody (Rabbit polyclonal)	Anti-S6K-phosphorylated	Agrisera	AS13 2664
Antibody (secondary)	HRP conjugated goat anti-rabbit	Sigma-Aldrich	A0545
Commercial assay or kit	Click-iT EdU Alexa Fluor 488 Imaging Kit	Invitrogen	C10337

Table 3.2 Key resources.

Time (minutes)	% Solvent A	% Solvent B
0	100	0
1.75	100	0
8	25	75
8.01	10	90
9	10	90
9.01	100	0
13	100	0

Table 3.3 LC gradient used for amino acid separation.

Sequence name	Nucleotide sequence	Description
ipms1-4_LP	TTTCAATAAGCGATGACCCAC	Genotyping of *ipms1-4* (SALK_101771)
ipms1-4_RP	ATGGAATGCTGAAACACAAGG	Genotyping of *ipms1-4* (SALK_101771)
ipms1-5_LP	GTGCCTAACGGTCCTCTTTTC	Genotyping of *ipms1-5* (WiscDsLoxHs221_05F)
ipms1-5_RP	CCAGTTCCAATAGAACAAGCG	Genotyping of *ipms1-5* (WiscDsLoxHs221_05F)
ahass1-1_LP	TAAGGTCGTCAACAACCGAAC	Genotyping of *ahass1-1* (SALK_096207)
ahass1-1_RP	CAGAAGTCTGAAACCCACAGG	Genotyping of *ahass1-1* (SALK_096207)
ahass2-7_LP	AAGTCTCTCCAGGATTCGCTC	Genotyping of ahass2-7 (WiscDsLoxHs009_02G)
ahass2-7_RP	TCTTTTTCTCACCCCACATTG	Genotyping of ahass2-7 (WiscDsLoxHs009_02G)
raptor1B_LP	CAATATGAAGCTGCGGCTAAC	Genotyping of *raptor1B* (SALK_022096)
raptor1B_RP	CATCGGATCAAGTTGCTTACC	Genotyping of *raptor1B* (SALK_022096)
LBb1.3	ATTTTGCCGATTTCGGAAC	Genotyping of SALK lines
LB4	TGATCCATGTAGATTTCCCGGACATGAAG	Genotyping of WiscDsLoxHs lines
IPMS1_F1	TGCTCAATCTCAGATCCTTCTC	Amplification of the coding sequence of IPMS1 catalytic domain
IPMS1_R1	CTAATACATGATCTCCACGGCA	Amplification of the coding sequence of IPMS1 catalytic domain
IPMS1_F2	GGCTATTGTAGGAGCGAATG	Amplification of the coding sequence of IPMS1 allosteric domain
IPMS1_R2	CTCTTTTGACATGCAACTTCG	Amplification of the coding sequence of IPMS1 allosteric domain
AHASS2_F	TCCGTTTTGGAGATTTTCAG	Amplification of the coding sequence of AHASS2 ACT2 domain
AHASS2_R	GAGACATCAATGGCTTTAGCAC	Amplification of the coding sequence of AHASS2 ACT2 domain
OMR1_F	GGACGTGAATGTCGTAGCC	Amplification of the coding sequence of OMR1 ACT2 domain
OMR1_R	ACGCTCATCCGACAGACAC	Amplification of the coding sequence of OMR1 ACT2 domain

Table 3.4 Primers used in this study.

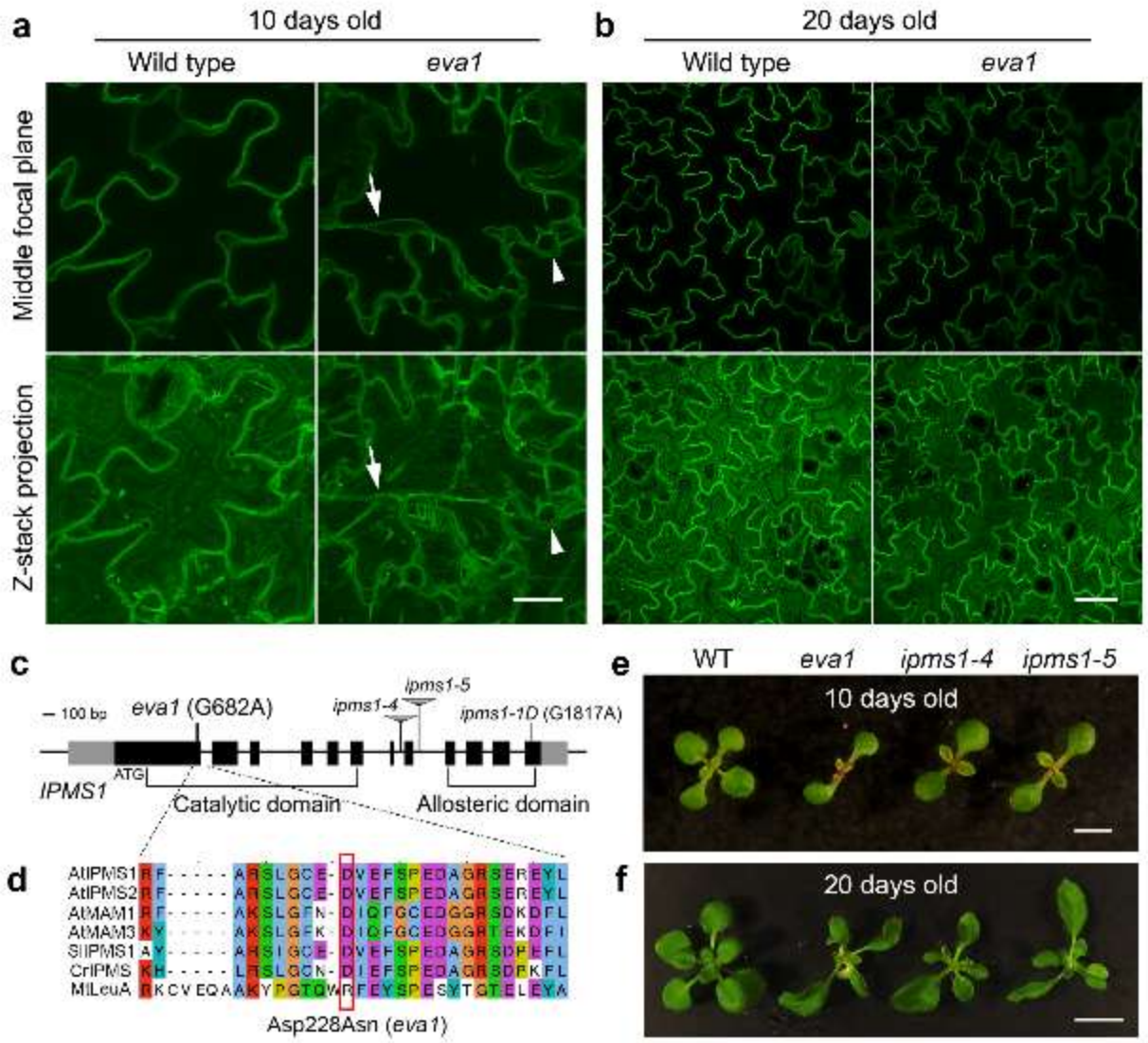

Figure 3.1 Identification of a mutant with defects in vacuole morphogenesis.

a and **b**, Confocal images of cotyledon epidermal cells expressing tonoplast marker GFP-δTIP in 10 days old (**a**) and 20 days old (**b**) wild type and *eva1* plants. The top panel presents single images of the middle focal plane, and the bottom panel presents Z-stack maximal projections. Arrows point to enhanced transvacuolar strands, arrowheads indicate unfused vacuolar structures. Scale bar in **a**, 20 μm. Scale bar in **b**, 50 μm.

c, Genomic structure of *IPMS1* (AT1G18500). Grey boxes indicate UTRs, black boxes indicate exons, black lines indicate introns.

d, Amino acid sequence alignment of IPMS1 homologs using T-COFFEE in Jalview. Amino acids are colored with ClustalX based on their similarity of physicochemical properties. At, *Arabidopsis thaliana*; Sl, *Solanum lycopersicum*; Cr, *Chlamydomonas reinhardtii*; Mt, *Mycobacterium tuberculosis*. The amino acid substitution of *eva1* is denoted by a red box.

e and **f**, Photographs of 10 days old (**c**) and 20 days old (**d**) plants. Scale bar in **c**, 0.5 cm. Scale bar in **d**, 1 cm.

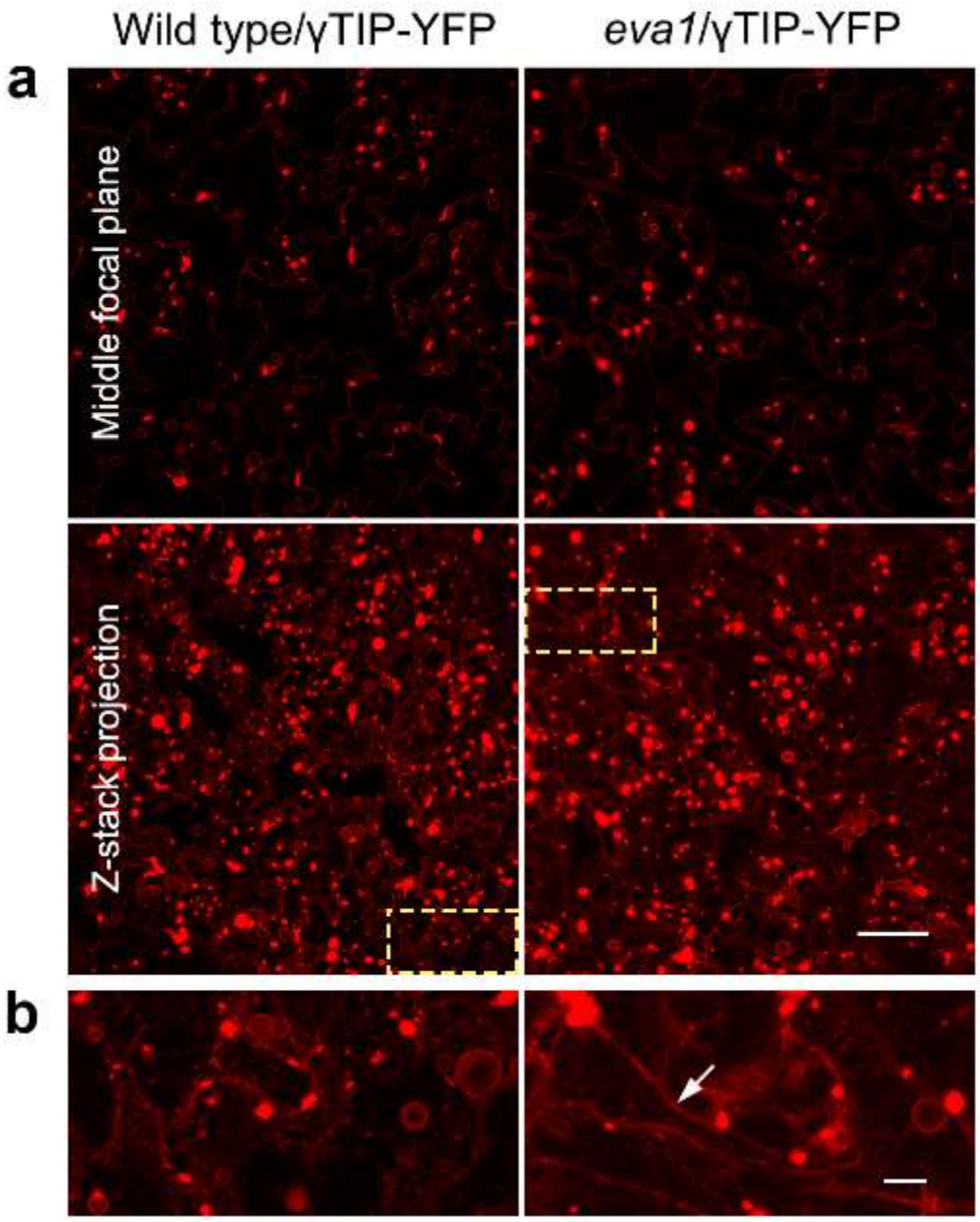

Figure 3.2 Reviewing the *eva1* vacuolar mutant phenotypes using another tonoplast marker γTIP-YFP.

a, Confocal images of cotyledon epidermal cells expressing γTIP-YFP in 10 days old wild type and *eva1* plants. Scale bar, 50 μm.
b, Enlargement of the regions of interest in (**a**), which are marked by dash-line yellow boxes. The arrow indicates enhanced transvacuolar strands. Scale bar, 10 μm.

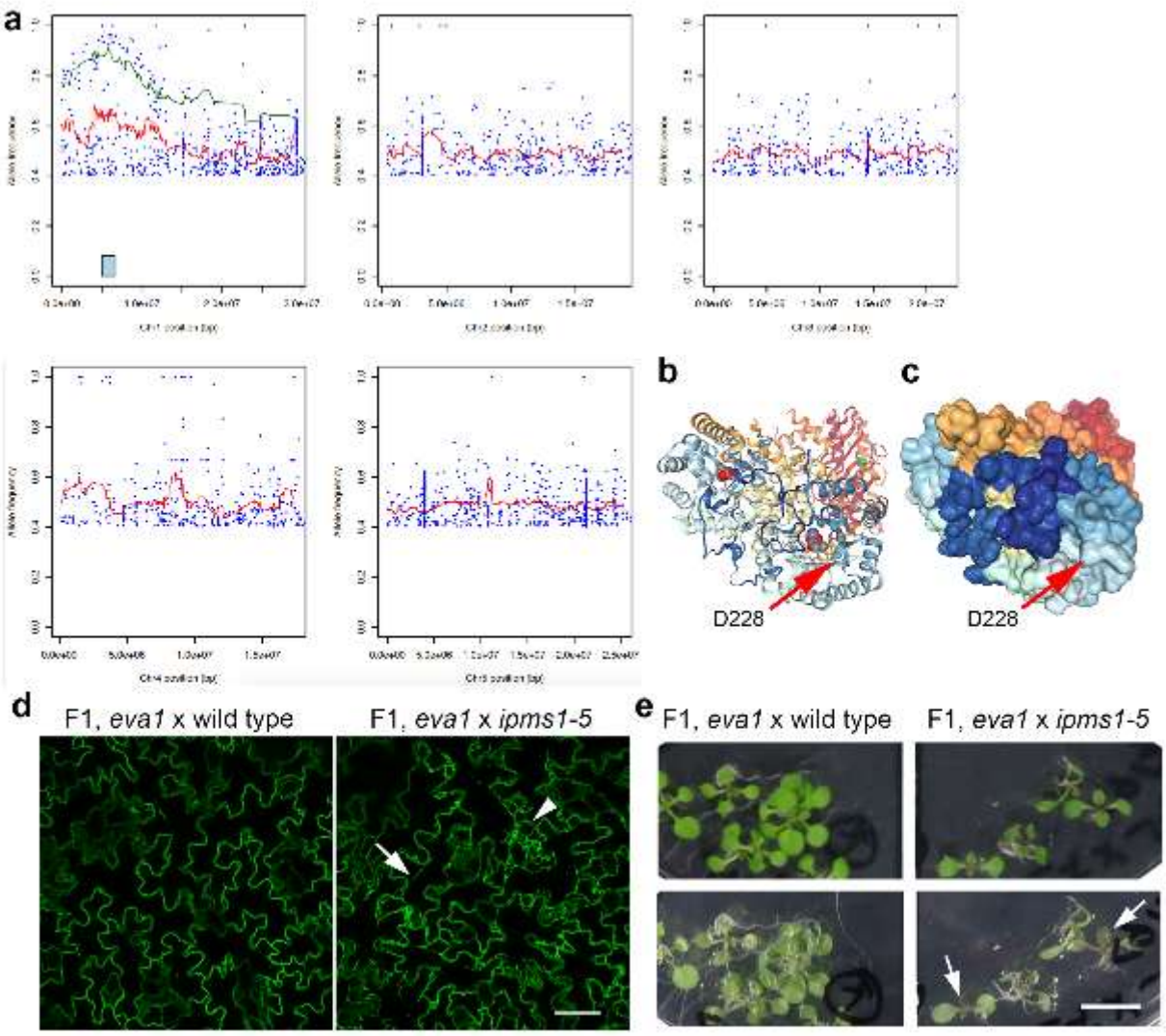

Figure 3.3 The causal mutation of *eva1* mutant is mapped to *IPMS1*.

a, Mapping the causal mutation using bulk sergeant analysis. Horizontal and vertical axes are genomic position and observed allele frequency, respectively. Blue dots represent the SNPs identified from a pool of F2 population with mutant phenotypes. Red lines represent smoothed curves over 100 SNP windows with SNPs whose allele frequency are greater than 0.4. The green line represents a smoothed curve over 10 SNP windows with SNPs whose allele frequency are greater than 0.6. The light blue box indicates the mapping interval.
b and **c**, Cartoon (**b**) and space-filling (**c**) models of the IPMS1 dimers that were generated by fitting Arabidopsis IPMS1 to the *Mycobacterium tuberculosis* homolog structure (PDB: 1SR9) using Phyre2 program. The models are rainbow colored from N-terminus as blue to C-terminus as red. Red arrows point to the position of residue D228. Leucine is shown by a green ball, 2-oxoisovalerate substrate is depicted as a space-filling model. The models of IPMS1 dimers are rotated towards acetyl-CoA, which is approaching from the viewer's perspective.

Figure 3.3 (cont'd) d and **e**, Examination of vacuolar phenotypes (**d**) and growth phenotypes (**e**) of 10 days old plants of F1 generation after crossing *eva1* with either wild type (Col-0) or *ipms1-5*. **d**, Single-plane confocal images of cells expressing GFP-δTIP. Arrow indicates enhanced transvacuolar strands, arrowhead indicates unfused vacuolar structures. Scale bar, 50 μm. **e**, Photographs that view seedlings from adaxial and abaxial sides. Arrows point to visible accumulation of anthocyanins in cotyledon petioles and emerging true leaves. Scale bar, 1 cm.

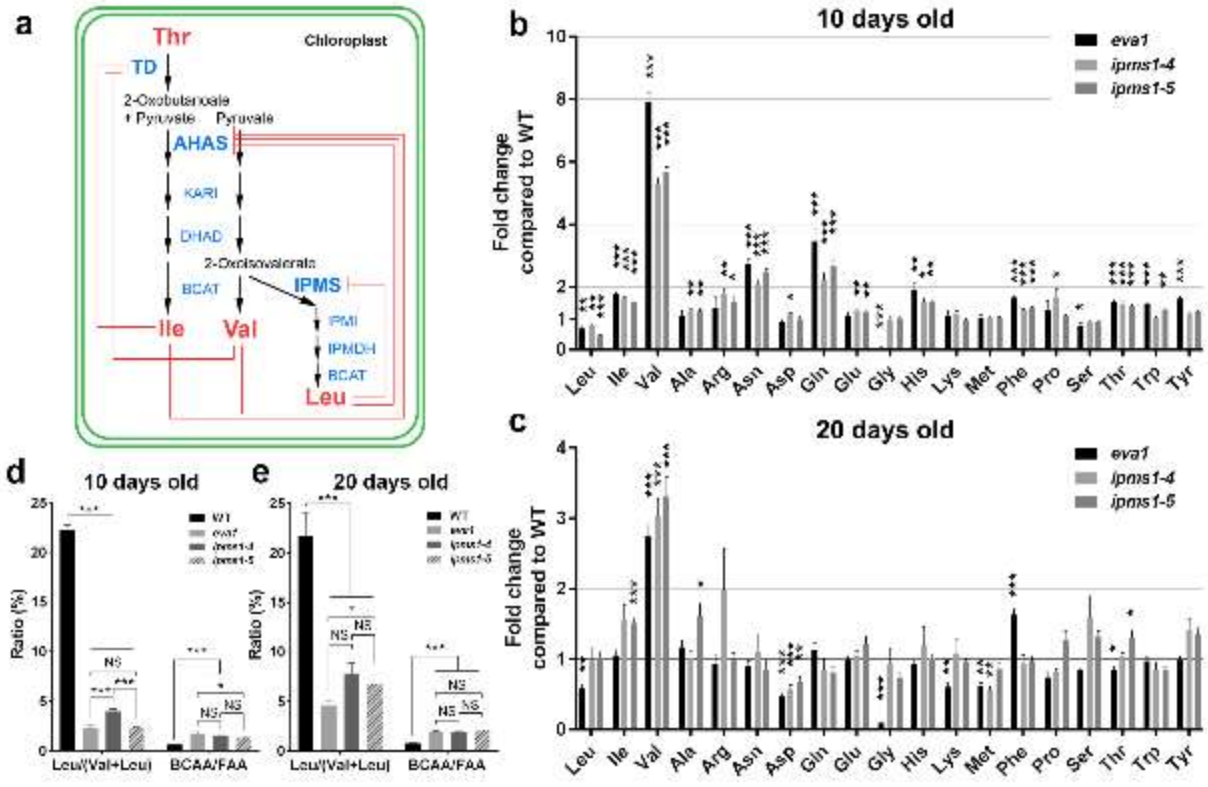

Figure 3.4 *eva1* and two loss-of-function mutants of *IPMS1* show similar patterns of BCAA overaccumulation.

a, Schematic of the BCAA biosynthetic pathway in the chloroplast. Red lines show known feedback inhibitions of enzymes of committed steps by end products. TD, threonine deaminase; AHAS, acetohydroxyacid synthase; KARI, ketolacid reductoisomerase; DHAD, dihydroxyacid dehydratase; BCAT, branched-chain aminotransferase; IPMS, isopropylmalate synthase; IPMI, isopropylmalate isomerase; IPMDH, isopropylmalate dehydrogenase.
b and **c**, Fold change of each free amino acid in *eva1*, *ipms1-4* and *ipms1-5* mutants compared to wild type.
d and **e**, Critical ratios reflecting the activities of Leu biosynthesis and BCAA biosynthesis.
For all the charts in (**b - e)**, values are mean ± SEM. For 10 days old sampling, n = 7 for WT, n = 5 for *eva1*, n = 8 for *ipms1-4*, n = 7 for *ipms1-5*. For 20 days old sampling, n = 6 for each genotype. The asterisks indicate significant differences compared to the wild type (*p ≤ 0.05, **p ≤ 0.01, ***p ≤ 0.001, NS, p > 0.05 and not significant, unpaired *t* test).

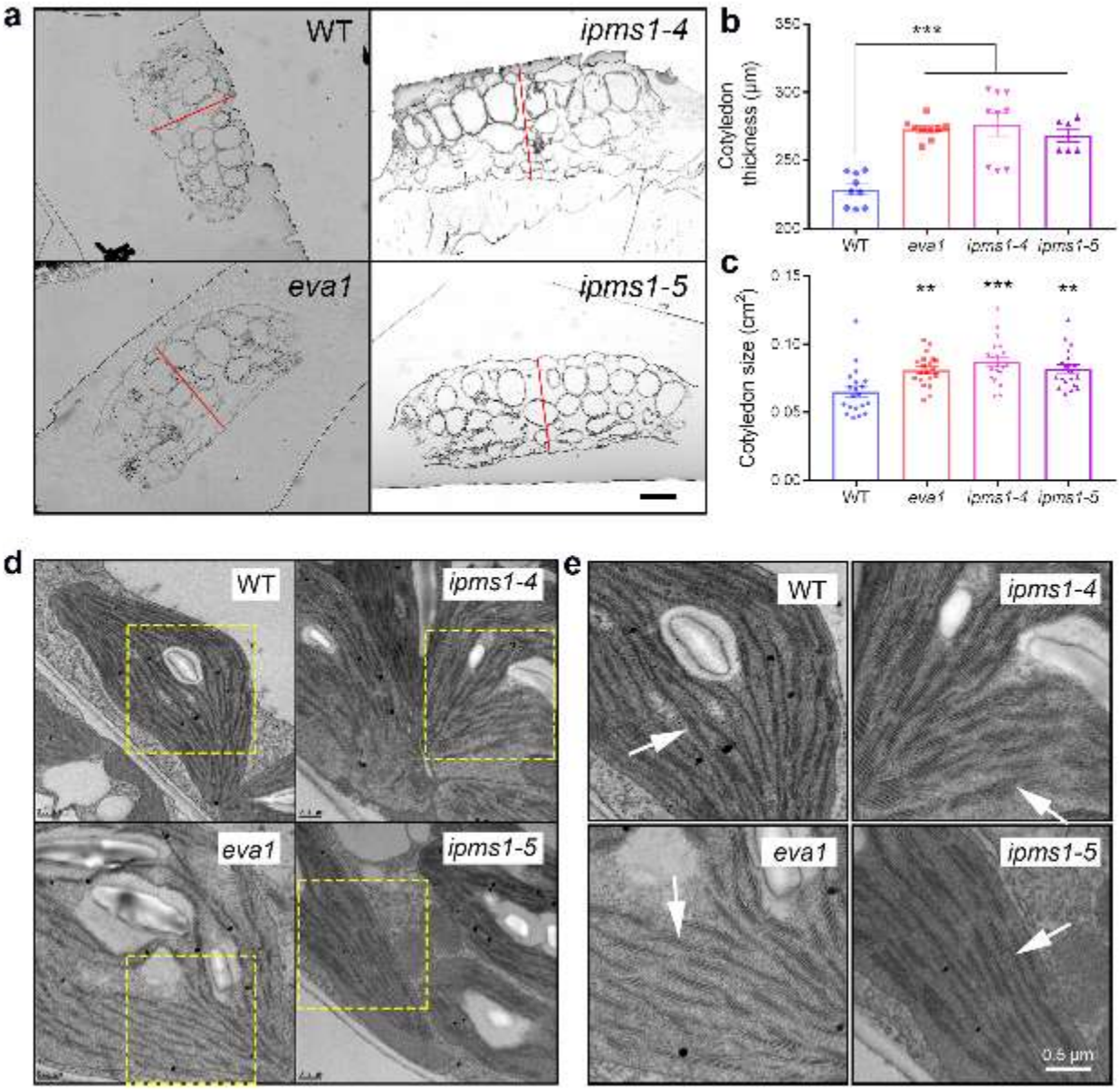

Figure 3.5 Mutants of *IPMS1* show defects in cotyledon architecture and chloroplast ultrastructure.

a, light microscopic images of cotyledon cross sections. Cotyledon thickness is denoted by red lines. Scale bar, 100 µm.
b, Measurement of cotyledon thickness. Values are mean ± SEM. n = 9 for WT, *eva1* and *ipms1-4;* n= 6 for *ipms1-5*. The asterisks indicate significant differences of each mutant compared to wild type (***p < 0.001, unpaired *t* test).
c, Measurement of cotyledon size. Values are mean ± SEM. n = 20 for each genotype. The asterisks present significant differences of each mutant compared to wild type (**p < 0.01, ***p < 0.001, unpaired *t* test).

Figure 3.5 (cont'd) d, Representative transmission electron microscopic images of chloroplasts. Dash-line rectangles highlight regions that are subsequently magnified. Scale bars, 0.5 μm.
e, High-magnification images of the highlighted regions in (**d**). Arrows point to thylakoids. Scale bar, 0.5 μm.

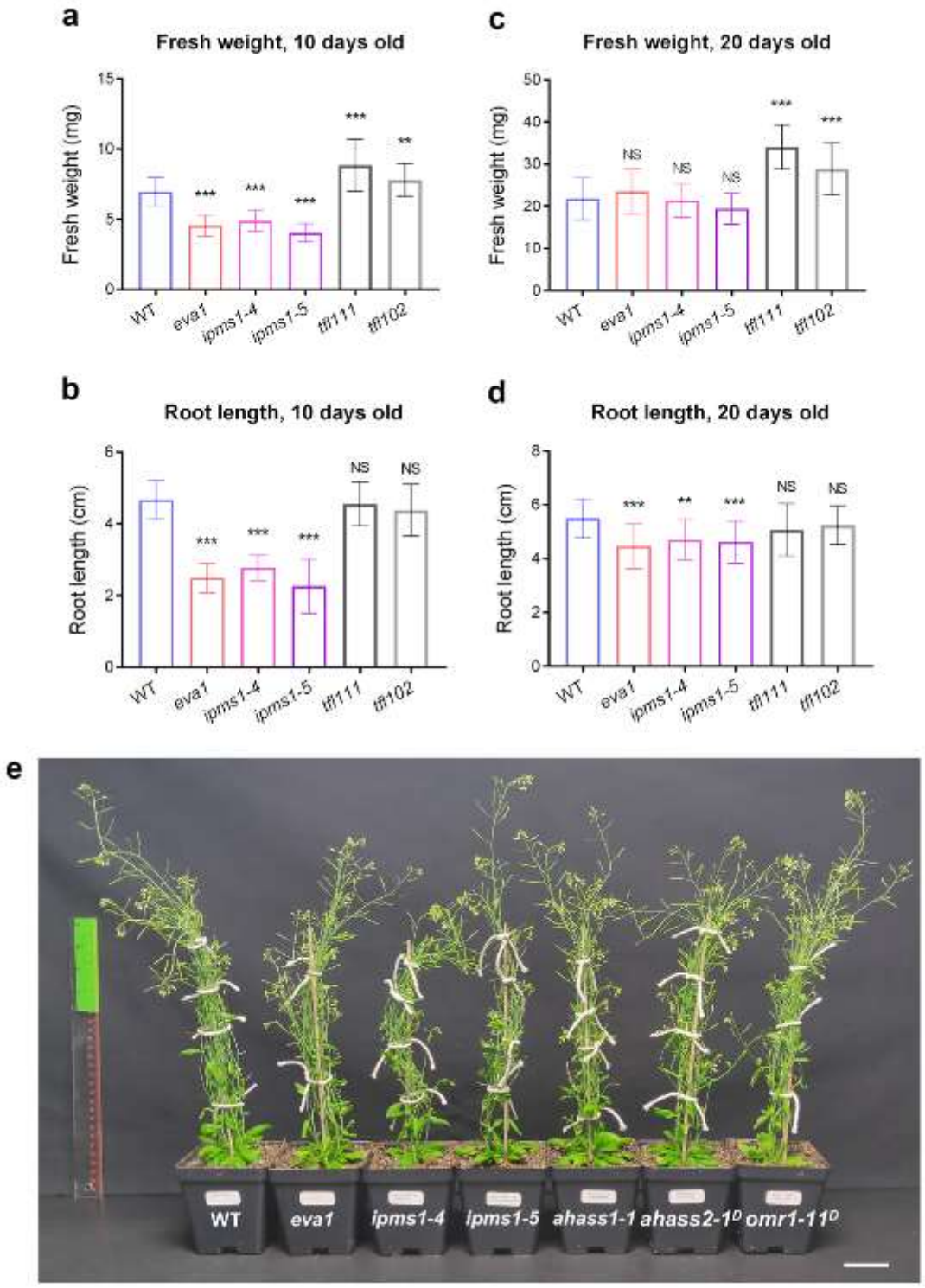

Figure 3.6 Mutations of *IPMS1* affect plant growth at early stage.

Figure 3.6 (cont'd) a - d, Wild type (WT) and five mutants of *IPMS1* were measured for fresh weight and length of primary root at 10 days old stage (**a** and **b**) and 20 days old stage (**c** and **d**). *tfl111* and *tfl102* are two independent EMS lines of *ipms1-1*^{D}, bearing a SNP mutation that abolishes the allosteric domain of IPMS1. Values are mean ± SD. The asterisks indicate significant differences compared to wild type (n = 30 for each genotype at 10 days old stage, n = 20 for each genotype at 20 days old stage; ***$p < 0.001$, **$p < 0.01$, NS, $p > 0.05$ and not significant, unpaired *t* test).
e, A photograph of six weeks old plants of wild type (WT) and mutants of three key enzymes for BCAA biosynthesis. Scale bar, 5 cm.

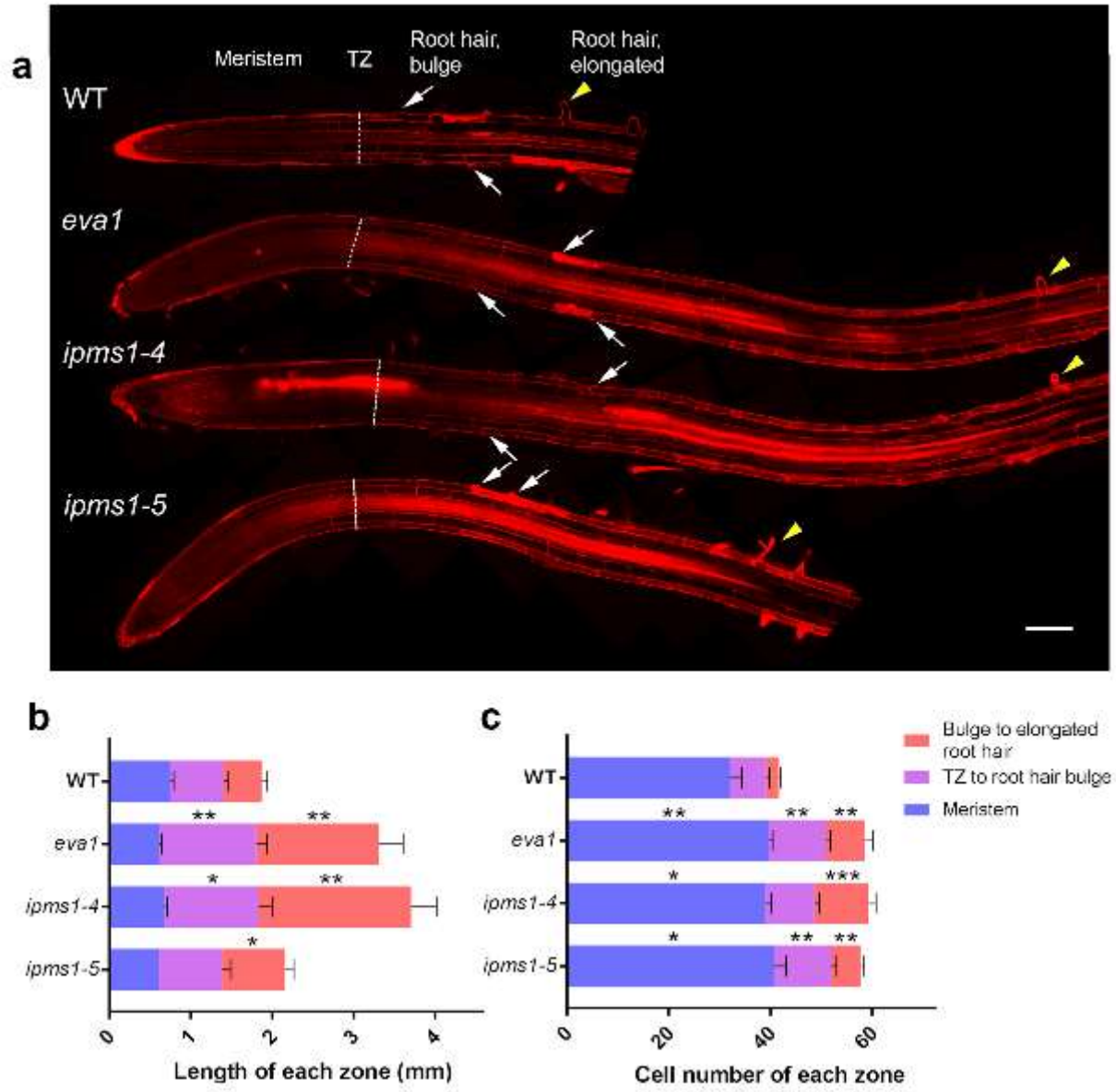

Figure 3.7 Root tip staining and analyses.

a, Propidium iodide staining of the root tips of 10 days old wild type (WT), *eva1*, *ipms1-4* and *ipms1-5* seedlings. Meristem is the region between the quiescent center and the transition zone (TZ; defined as the position of first elongating cortical cell). Dashed lines indicate the location of TZ, white arrows point to root hair bulges, yellow arrowheads point to the first elongated root hair that is at least 50 μm long. Scale bar, 200 μm.
b and **c**, Analyses of length (**b**) and cell number (**c**) of three zones in the root tip. Values are mean ± SEM. The asterisks indicate significant differences compared to the same zone of wild type (n = 9 for each genotype; ***p < 0.001, **p < 0.01, *p < 0.05, unpaired *t* test).

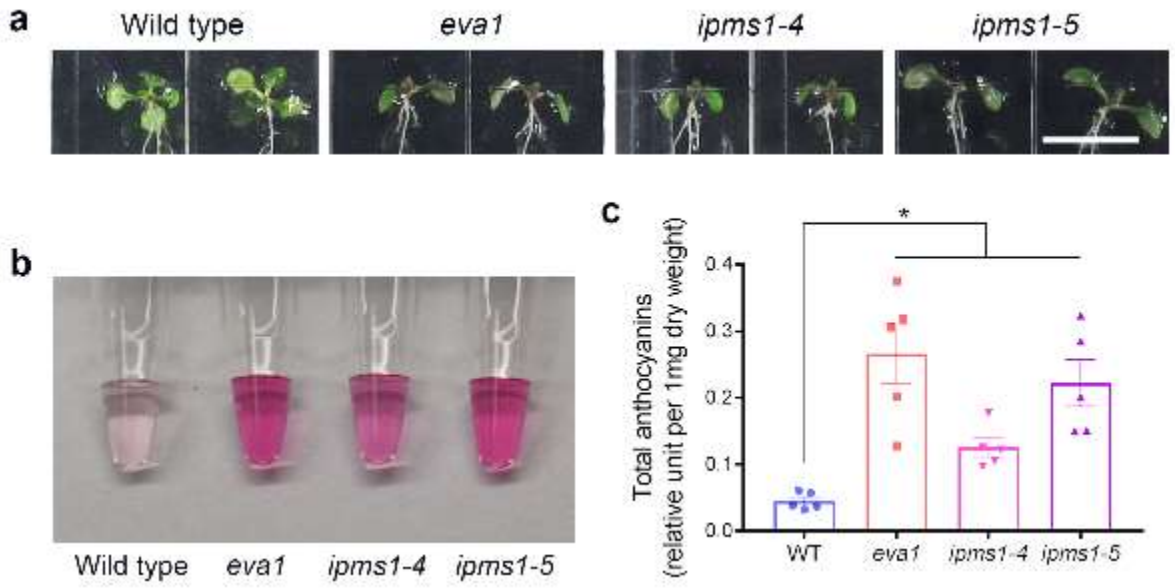

Figure 3.8 Accumulation of anthocyanins in *eva1* and *IPMS1* loss-of-function mutants.

a, Visible accumulation of anthocyanins in 10 days old seedlings, particularly in cotyledon petioles and emerging true leaves. Scale bar, 1 cm.
b, Extracts of total anthocyanins from aerial tissues of 10 days old seedlings.
c, Measurement of total anthocyanins. Samples that contain 50 µL extraction buffer per 1 mg dry weight were measured for 532 nm absorbance. Values are mean ± SEM. The asterisk indicates significant differences between each mutant line and the wild type (n = 5 for each genotype; *p < 0.05, unpaired *t* test).

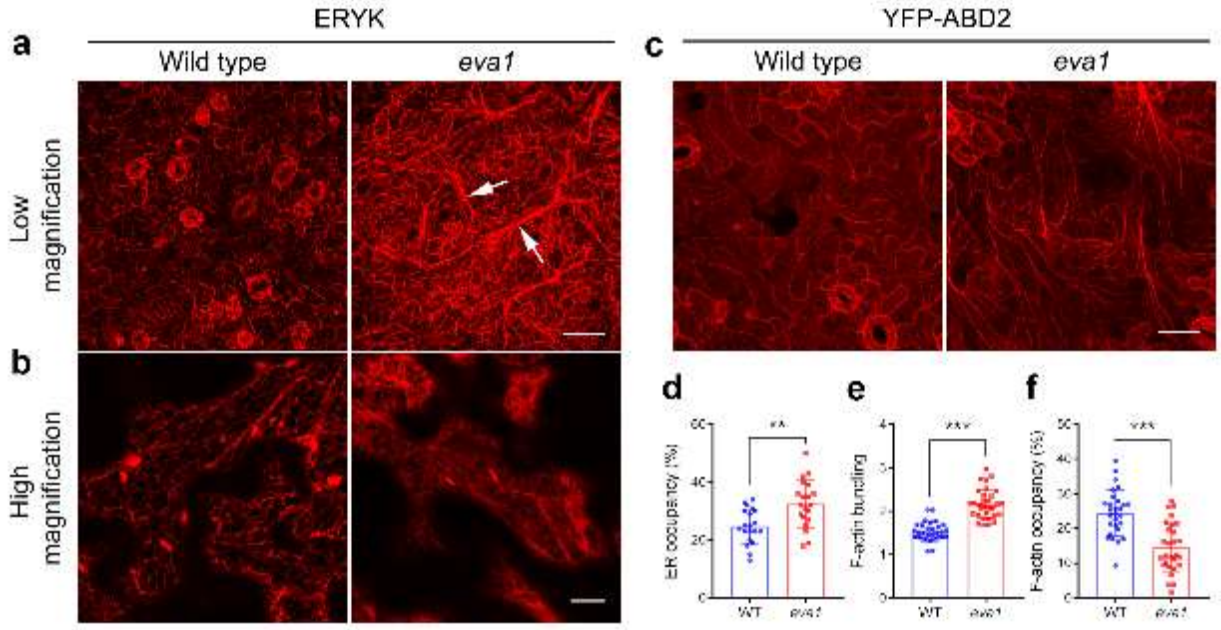

Figure 3.9 Mutation of *IPMS1* affects the ER morphology and the F-actin organization.

a and **b,** Confocal images of the wild type and *eva1* cotyledon epidermal cells expressing ER marker ERYK. (**a**) Low-magnification Z-stack projection images show the ER morphology in *eva1* is altered, featuring longer and more thickened ER strands, as the arrows indicate. Scale bar, 50 μm. (**b**) High-magnification single-plane images show enlarged ER sheets in *eva1* mutant. Scale bar, 10 μm.

c, Confocal images of the wild type and *eva1* cotyledon epidermal cells expressing F-actin marker YFP-ABD2. Scale bar, 50 μm.

d, Quantification of ER occupancy, which measures the percentage of the area occupied by ER in the total field of view (n = 28 for each genotype). Single-plane images were used for the quantification. Columns show mean ± SD. The asterisks indicate significant differences compared to the wild type (**p < 0.01, unpaired *t* test).

e and **f**, Quantitative evaluation of the F-actin organization using two parameters. Quantification of skewness (**e**) indicates higher level of F-actin bundling in eva1 compared to wild type (n = 32 for each genotype); measurement of density (**f**) percentage suggests lower occupancy of F-actin in eva1 compared to wild type (n = 28 for each genotype). Z-stack projection images were used for the quantification. Columns show mean ± SD. The asterisks indicate significant differences compared to the wild type (***p < 0.001, unpaired *t* test).

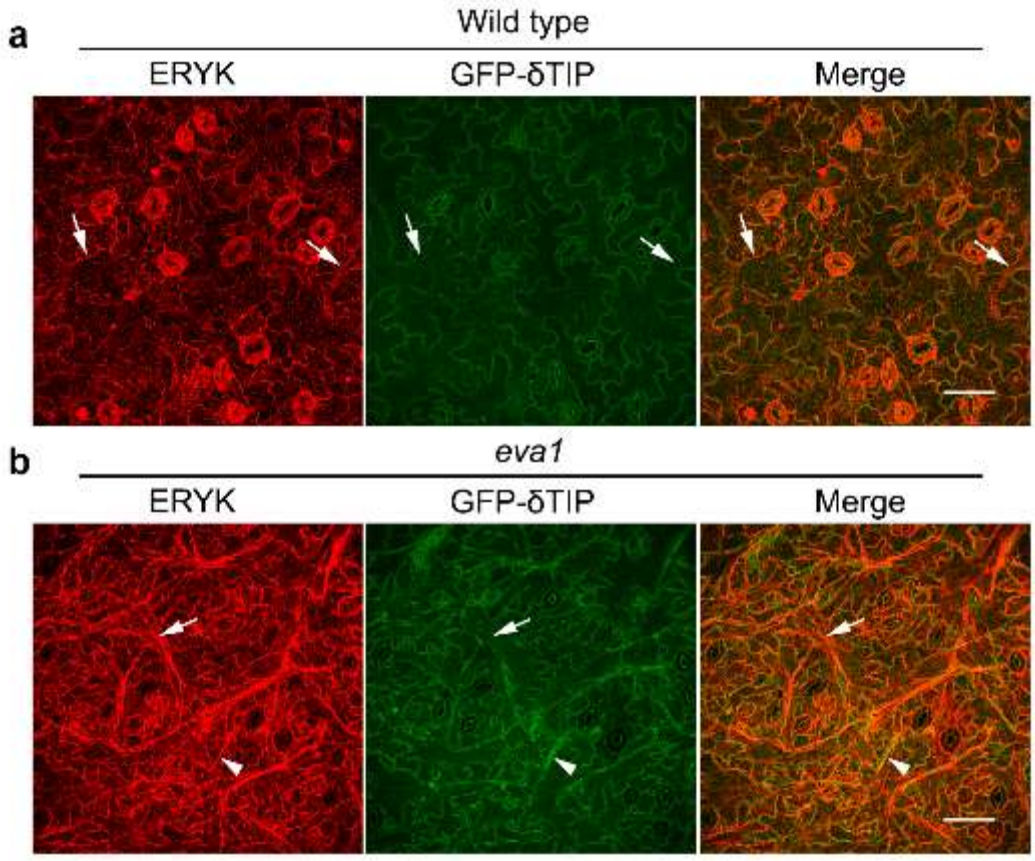

Figure 3.10 The ER strands and transvacuolar strands are partially overlapping structures.

Confocal images of the wild type (**a**) and *eva1* (**b**) mutant cotyledon epidermal cells expressing ER marker (ERYK) and tonoplast marker (GFP-δTIP). Arrows point to exclusive formation of ER strands without transvacuolar strands. Arrowheads indicate where vacuole membranes aggregate without thick ER strands. Scale bars, 50 μm. All images are maximal Z-stack projection images.

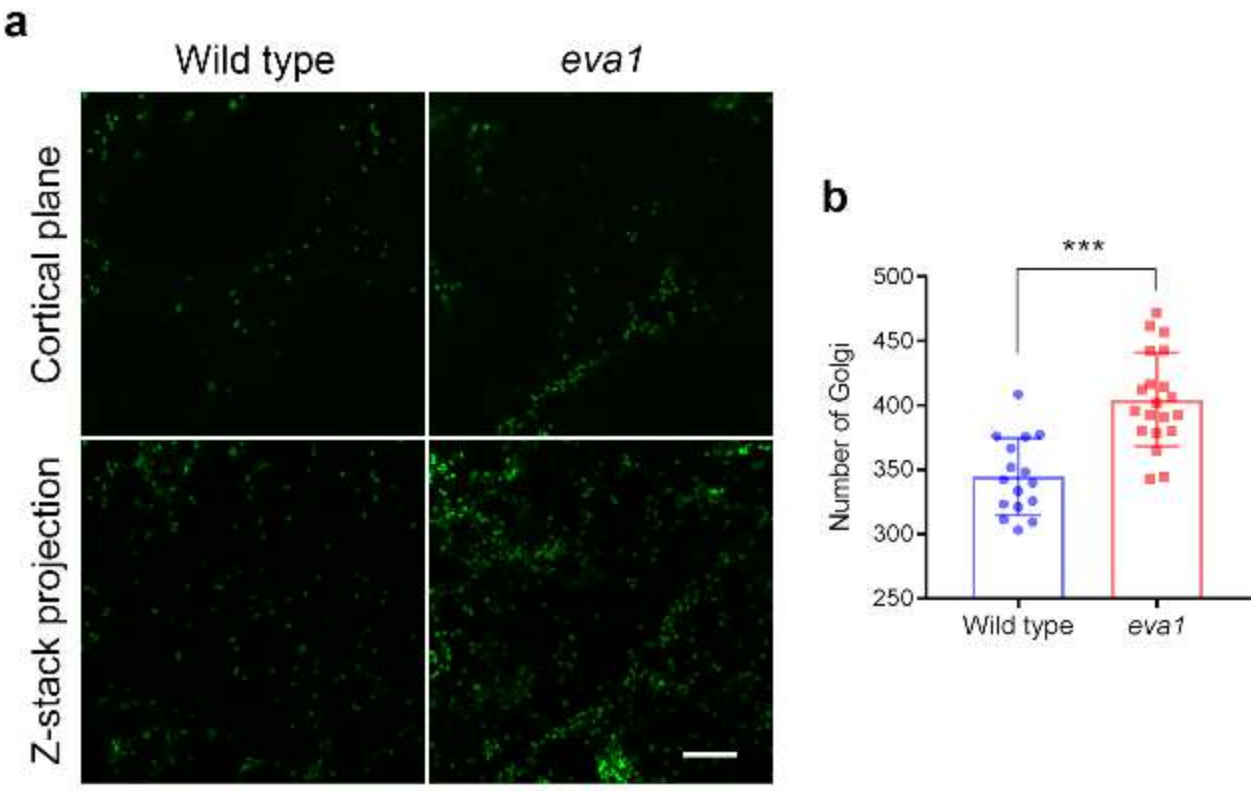

Figure 3.11 The number and distribution of Golgi are altered in *eva1* mutant.

a, Confocal images of the wild type and *eva1* mutant cotyledon epidermal cells expressing a Golgi marker GFP-CASP. Single images (top panel) show Golgi in the cortical focal plane. Maximal Z-stack projection images (bottom panel) show Golgi in a single cell. Scale bar, 10 μm.
b, The numbers of Golgi in each genotype were measured in independent field of view squares (100 μm x 100 μm; wild type, n = 16, *eva1*, n = 20). Columns show mean ± SD. The asterisks indicate significant differences compared to the wild type (***$p < 0.001$, unpaired *t* test).

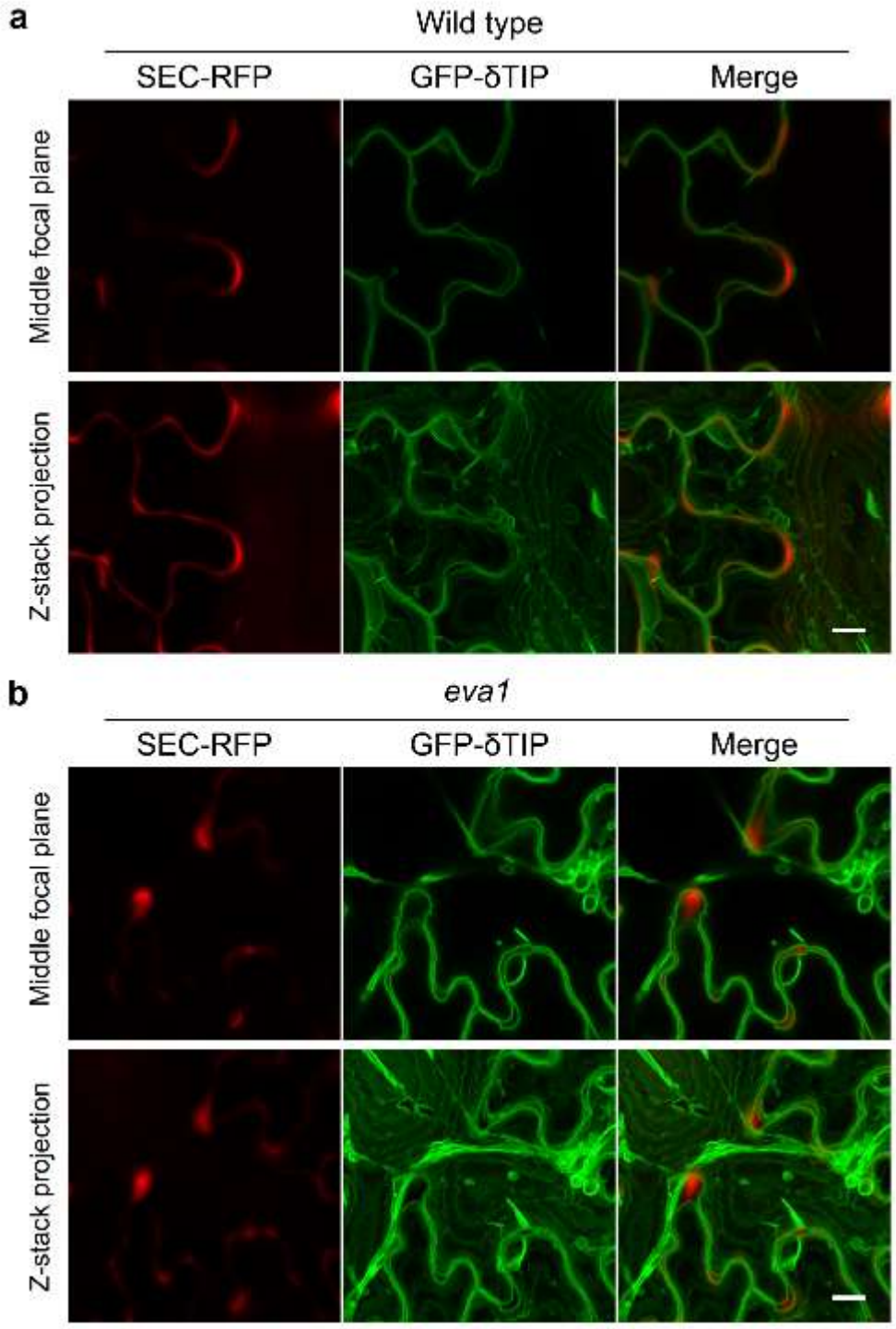

Figure 3.12 The eva1 mutation does not affect secretion of a bulk flow marker to the apoplast.

Confocal images of the wild type (**a**) and *eva1* mutant (**b**) cotyledon epidermal cells expressing SEC-RFP and GFP-δTIP. Scale bars, 10 μm.

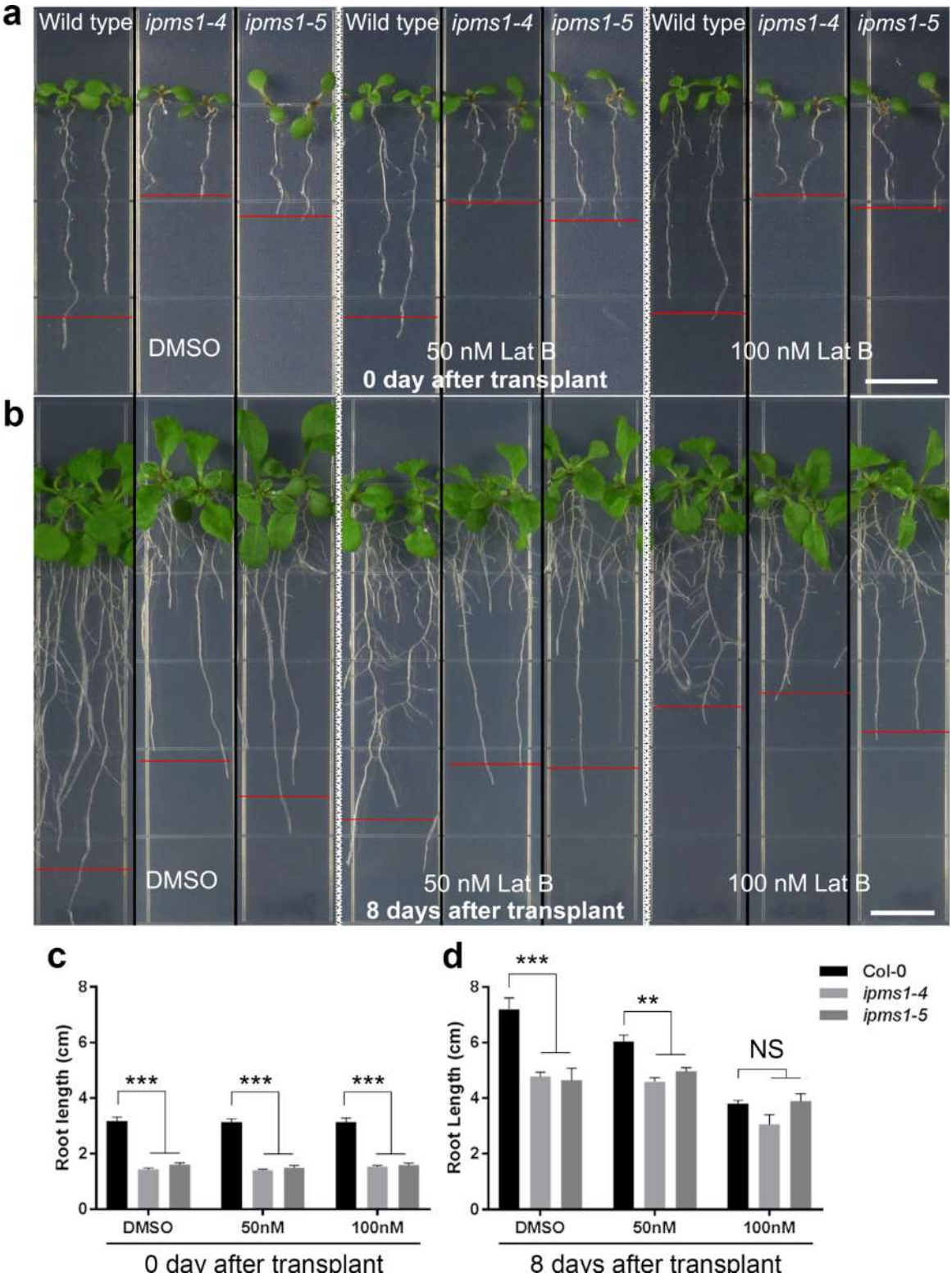

Figure 3.13 Compared to wild type, *IPMS1* loss-of-function mutants are less sensitive to Lat B.

Figure 3.13 (cont'd) a and **b**, 10 days old wild type (Col-0), *ipms1-4* and *ipms1-5* seedlings germinated and grew on ½ LS and 1% sucrose medium was transplanted to ½ LS and 1% sucrose medium containing DMSO, 50 nM Lat B or 100 nM Lat B. Photographs were taken immediately after transplant (**a**) and 8 days after transplant (**b**). Scale bars, 1 cm.
c and **d**, Quantification of primary root length of the wild type, *ipms1-4* and *ipms1-5* seedlings when 0 day (**c**) and 8 days (**d**) after transplant. Values are mean ± SEM. The asterisks indicate significant differences compared to the wild type (n = 8 for each genotype on a specific medium; ***$p \leq 0.001$, **$p \leq 0.01$, NS, $p > 0.05$ and not significant, unpaired *t* test).

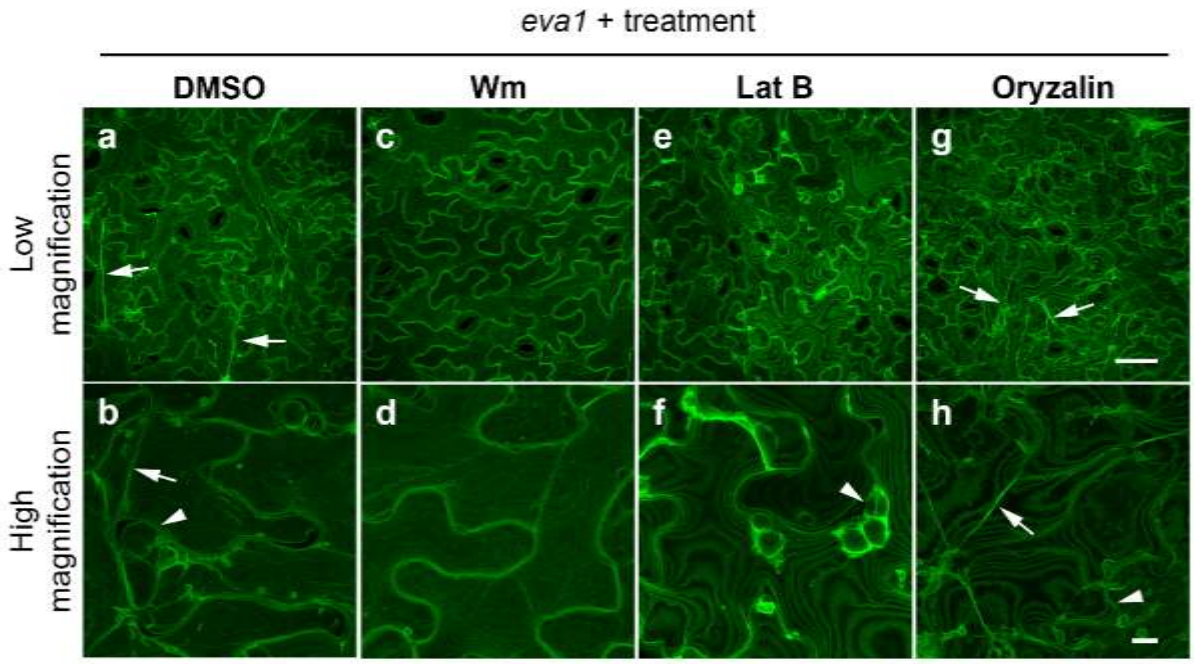

Figure 3.14 Chemical interventions can fully or partially rescue the vacuolar mutant phenotypes of *eva1*.

a - **h**, Confocal images of cotyledon epidermal cells expressing GFP-δTIP from 10 days old *eva1* plants. Images were acquired after 2 hours treatment of DMSO (**a** and **b**), wortmannin (Wm, **c** and **d**), latrunculin B (Lat B; **e** and **f**), or oryzalin (**g** and **h**). The top panel (**a**, **c**, **e**, and **g**) presents images of lower magnification with a scale bar of 50 μm. The bottom panel (**b**, **d**, **f**, and **h**) presents images of higher magnification with a scale bar of 10 μm. Arrowheads suggest unfused vacuolar structures and arrows pinpoint enhanced transvacuolar strands. All the images are Z-stack maximal projections.

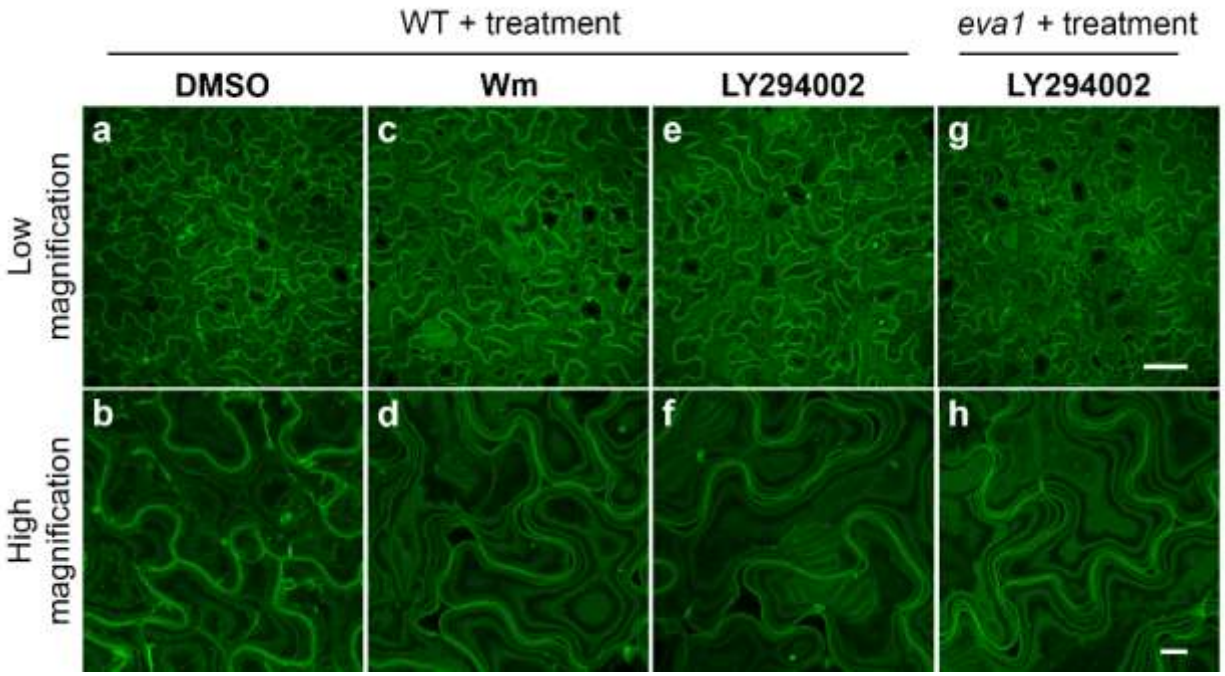

Figure 3.15 Chemical treatment with PI3K/TOR dual inhibitors wortmannin and LY294002.

Confocal images of cotyledon epidermal cells expressing tonoplast marker GFP-δTIP from 10 days old wild type (WT) and *eva1* plants. Images were acquired after 3 hours treatment of DMSO (**a** and **b**), wortmannin (Wm; **c** and **d**) or LY294002 (**e** - **h**). Scale bar in the top panel, 50 μm. Scale bar in the bottom panel, 10 μm. All the images are Z-stack maximal projections.

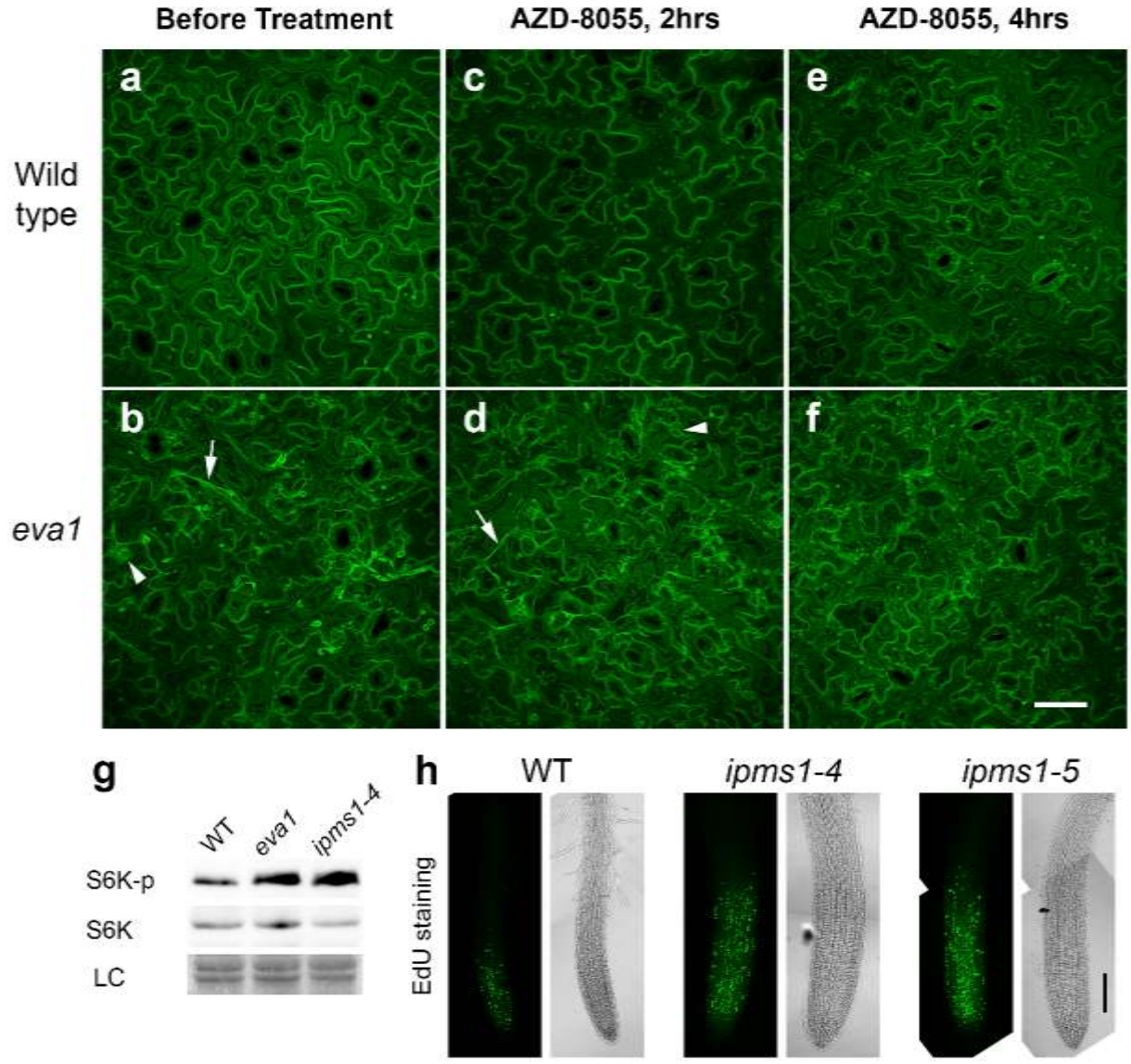

Figure 3.16 Vacuolar mutant phenotypes of eva1 is correlated with up-regulated TOR activity.

a - **f**, TOR inhibitor AZD-8088 treatment rescues vacuolar mutant phenotypes of *eva1*. Confocal images were acquired before (**a** and **b**), after 2 hours (**c** and **d**), and after 4 hours (**e** and **f**) 5 μM AZD-8055 treatment of wild type and *eva1* mutant. Arrowheads indicate unfused vacuolar structures and arrows point to enhanced transvacuolar strands. All the images are Z-stack maximal projections. Scale bar, 50 μm.
g, Immunoblotting detected phosphorylation of S6K by TOR, using specific antisera against S6K-phosphorylated and S6K. LC, loading control with Ponceau S staining.
h, EdU staining detected root meristem activity of 10 days old seedlings. For each genotype, an image of green pseud-ocolor shows EdU-stained newly synthesized DNA and a bright-field image shows structure of root tip. Scale bar, 100 μm.

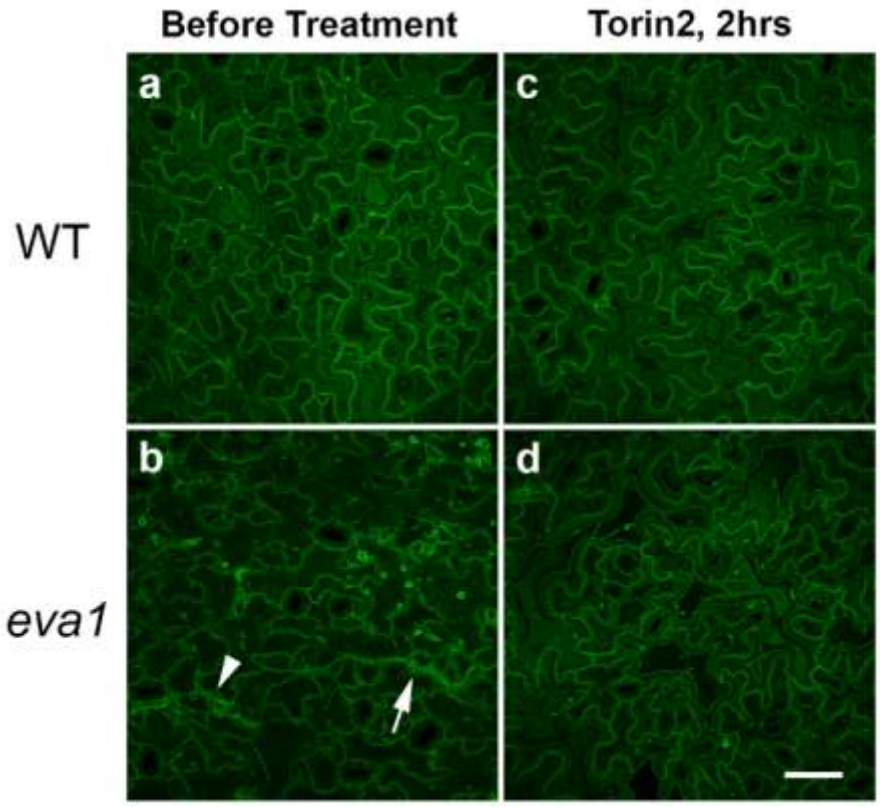

Figure 3.17 Another TOR inhibitor Torin2 exerts more potent effects on the vacuolar phenotypes of eva1.

Confocal images of cotyledon epidermal cells expressing tonoplast marker (GFP-δTIP) from 10 days old wild type (WT) or *eva1* mutant. The images were acquired before (**a** and **b**) and after (**c** and **d**) 2 hours 1 μM Torin2 treatment of wild type (WT) and *eva1* mutant. Arrowhead indicates unfused vacuolar structures. Arrow suggests enhanced transvacuolar strands. Scale bar, 50 μm. All the images are Z-stack maximal projections.

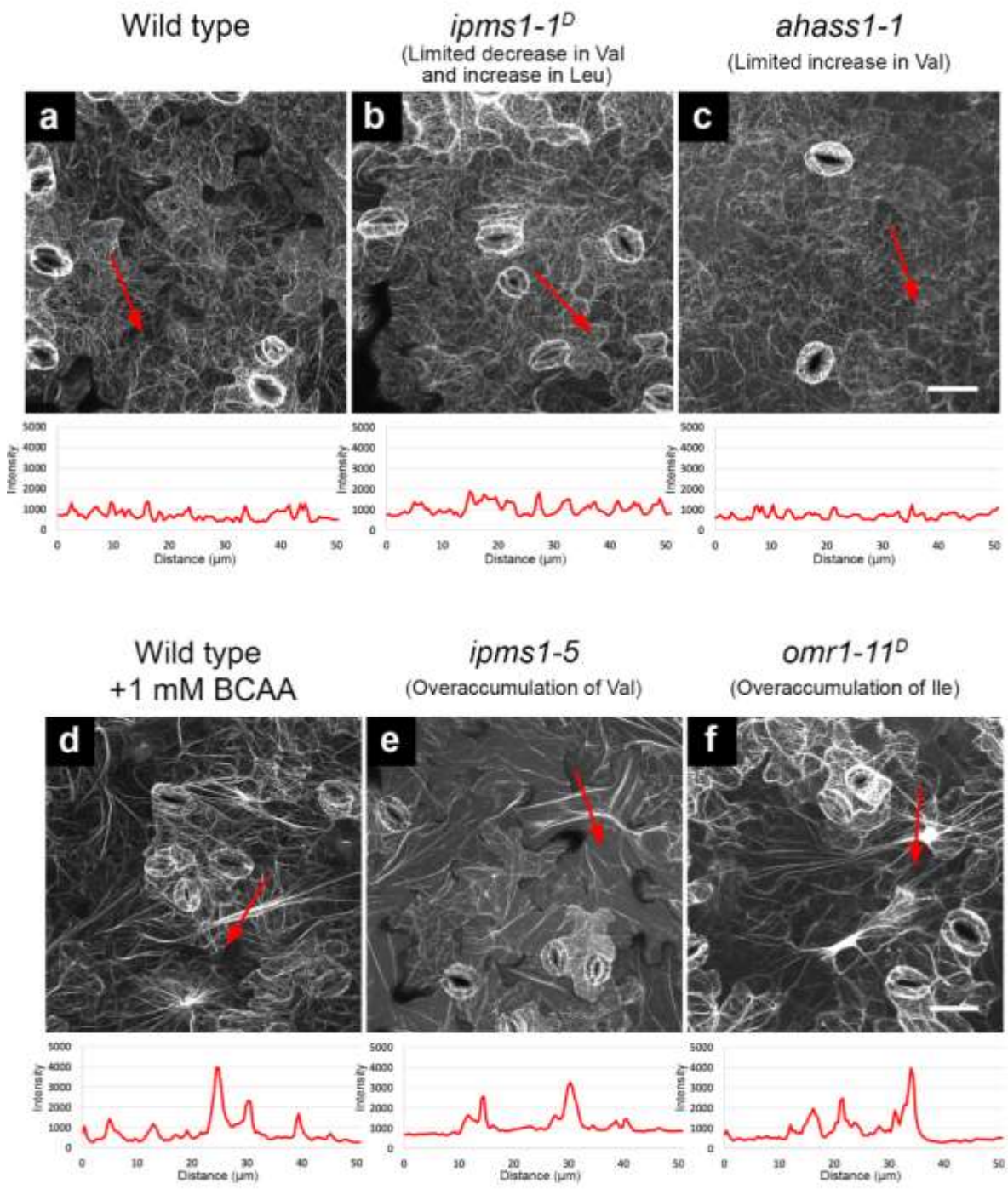

Figure 3.18 Exogeneous feeding of BCAAs or overaccumulation of BCAAs due to mutations of committed enzymes of the BCAA biosynthetic pathway affects actin organization, which is dependent on functional TOR but not RAPTOR1B.

Figure 3.18 (cont'd)

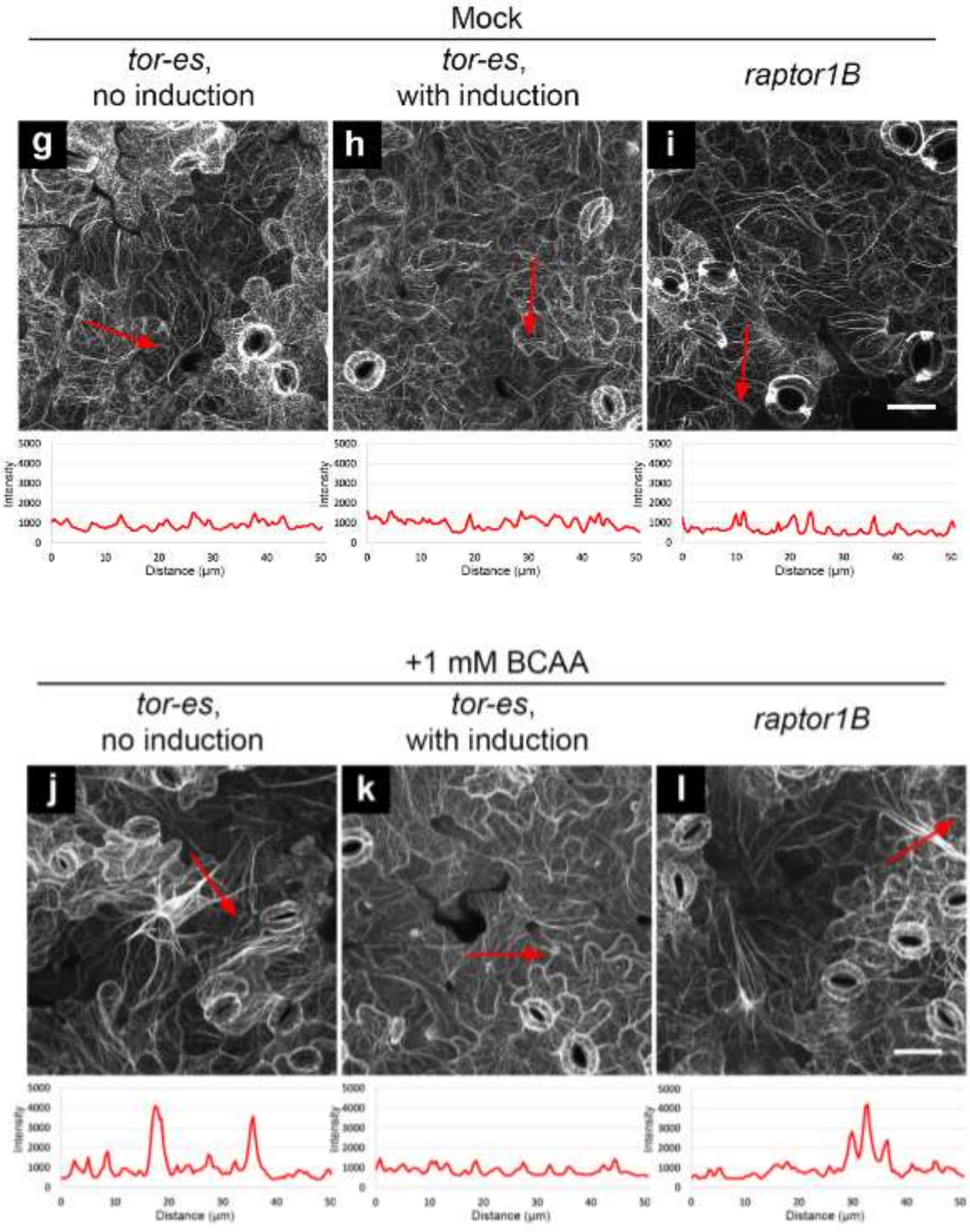

Figure 3.18 (cont'd) Organization of actin cytoskeleton presented by confocal images of cotyledon epidermal cells expressing F-actin marker YFP-ABD2. All the images are Z-stack maximal projections. For each image, a red line with an arrow in the end was drawn; and a chart beneath the image presents plotted intensity of fluorescence (gray value) against distance from the start point of the red line.

a - f, Images acquired from wild type (Col-0, **a**) and mutants of BCAA biosynthetic enzymes with limited alteration of BCAA levels (**b** and **c**) or overaccumulation of BCAAs (**e** and **f**) that were growing on normal Arabidopsis growth medium; and wild type that were growing on medium supplemented with 1 mM BCAA (**d**).

The alteration of BCAA levels in the mutants of BCAA biosynthetic enzymes (**b**, **c**, **e**, and **f**) were characterized in Xing and Last, 2017, Plant Cell. Scale bars, 50 μm.

g - l, Images acquired from wild type, *tor-es* mutants without or with induction using estradiol, and *raptor1B* mutants that were growing on normal Arabidopsis growth medium (Mock, **g - i**) and medium supplemented with 1 mM BCAA (**j - l**). Scale bars, 50 μm

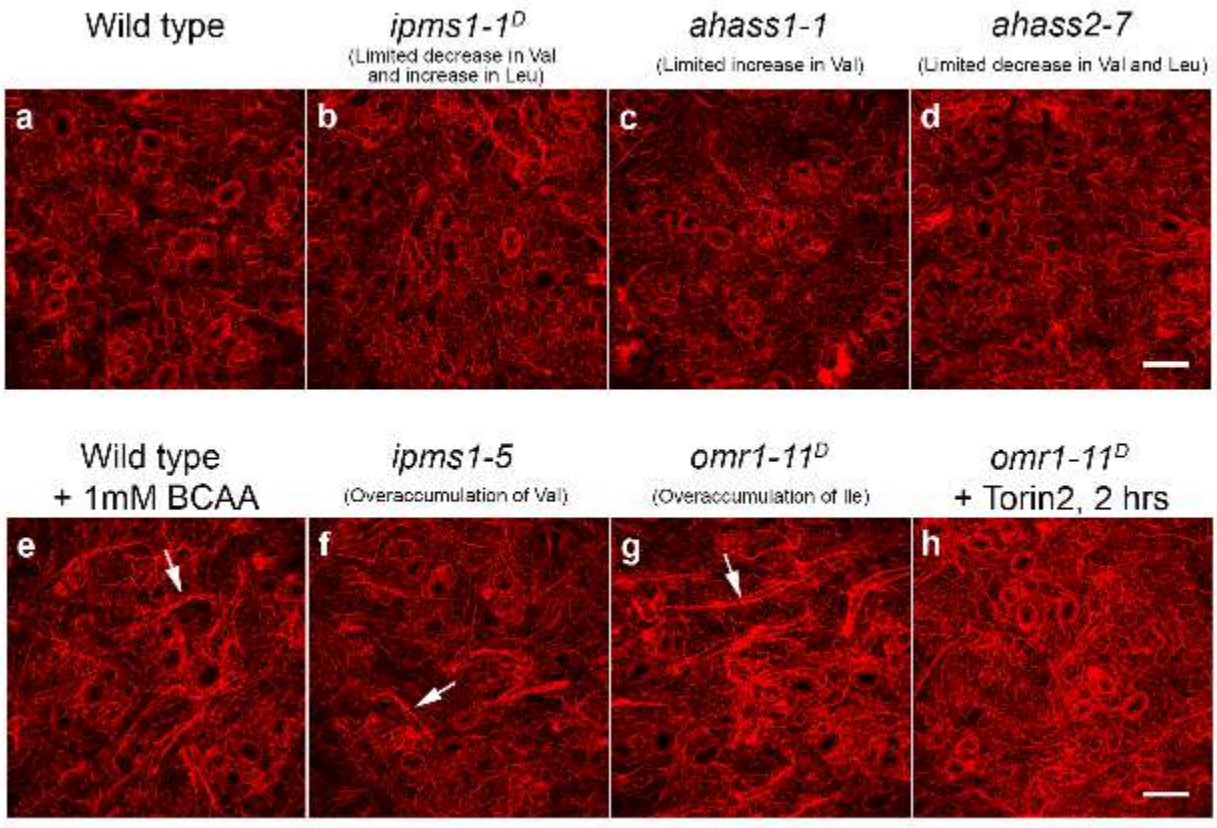

Figure 3.19 Exogeneous feeding of BCAAs or overaccumulation of BCAAs due to mutations of the BCAA biosynthetic pathway alters morphology of the ER network to form enhanced ER strands.

Architecture of the ER network presented by confocal images of cotyledon epidermal cells expressing ER marker ERYK in 10 days old wild type (Col-0) and mutants with distinct BCAA profiles, which were characterized by Xing and Last, 2017, Plant Cell. All the images are Z-stack maximal projections.

a - **d**, The ER morphology is not significantly altered in wild type (**a**) and mutants with limited alteration of BCAA levels (**b** - **d**) that were growing on normal Arabidopsis growth medium. Scale bar, 50 μm.

e - **h**, Disrupted ER morphology in wild type that was growing on medium supplemented with 1 mM BCAAs (**e**), and mutants that overaccumulate BCAAs (**f** and **g**). Arrows point to the enhanced ER strands. Enhancement of ER strands in *omr1-11*^{D} mutant (**g**) was recovered by 2 hours treatment of 1 μM Torin2 (**h**). Scale bar, 50 μm.

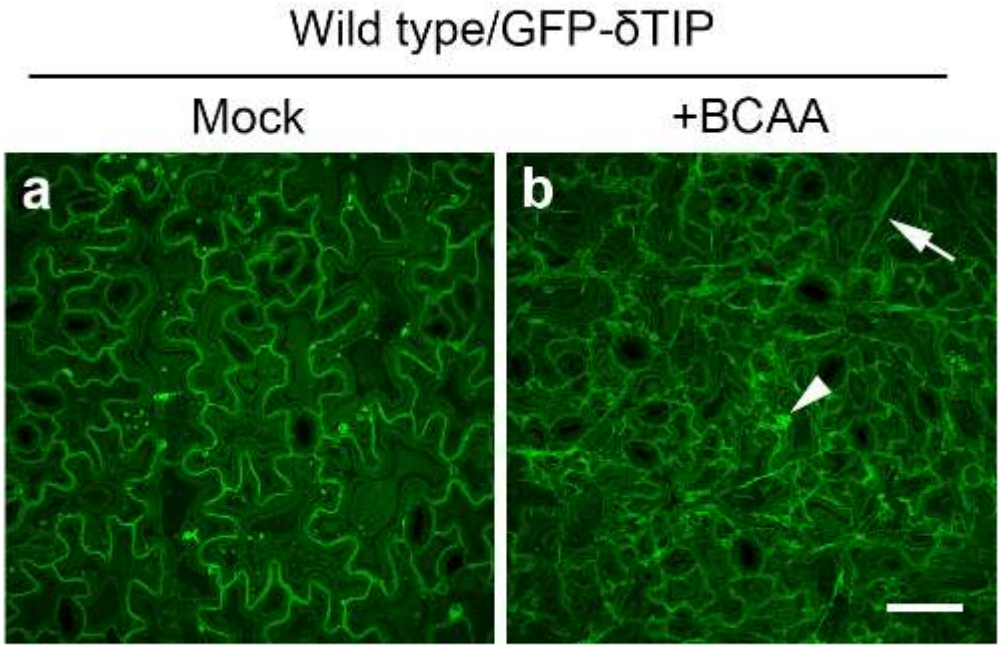

Figure 3.20 Exogeneous feeding of BCAAs affects morphology of the lytic vacuole.

Confocal images of cotyledon epidermal cells expressing tonoplast marker GFP-δTIP in 10 days old wild type that were growing on Arabidopsis growth medium without (**a**) or with (**b**) 1 mM BCAA supplementation. Arrowhead indicates unfused vacuolar structures and arrow points to enhanced transvacuolar strands. Scale bar, 50 μm. Images are Z-stack maximal projections.

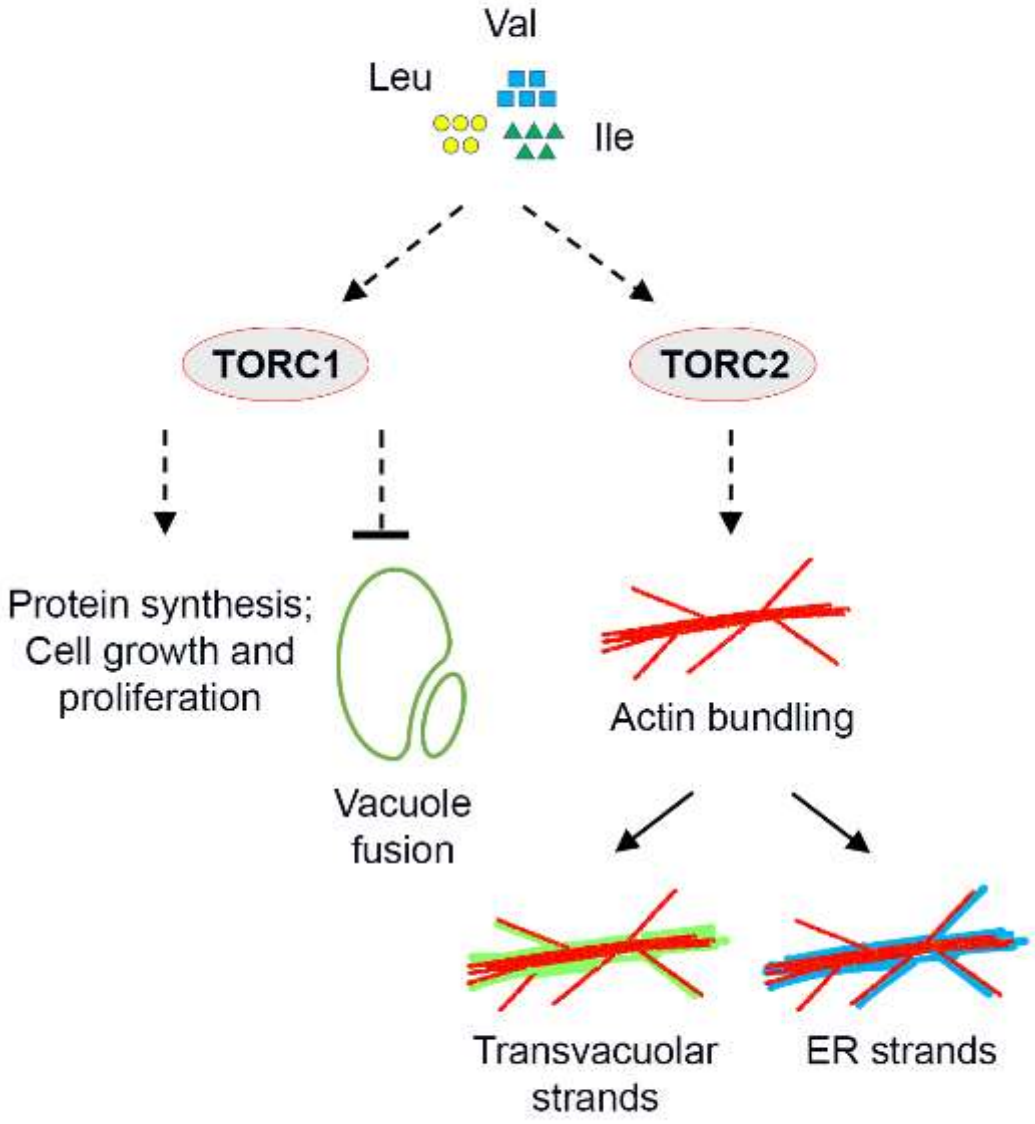

Figure 3.21 Working model of TOR-regulated subcellular processes.

Overaccumulation of BCAA Val, Leu and Ile stimulates TOR signaling. Except for the well-established downstream processes such as protein synthesis and cell proliferation, vacuole fusion and actin reorganization are likely also regulated by TOR signaling. Reorganization of the actin cytoskeleton is independent of TORC1, and prominent transvacuolar strands and ER strands are subsequently formed due to the strong interactions between the endomembranes and the F-actin.

REFERENCES

REFERENCES

1. Saxton, R.A. & Sabatini, D.M. mTOR signaling in growth, metabolism, and disease. *Cell* **168**, 960-976 (2017).

2. Kim, J. & Guan, K.L. mTOR as a central hub of nutrient signalling and cell growth. *Nat. Cell Biol.* **21**, 63-71 (2019).

3. Shi, L., Wu, Y. & Sheen, J. TOR signaling in plants: conservation and innovation. *Development* **145** (2018).

4. Xie, J., Wang, X. & Proud, C.G. Who does TORC2 talk to? *Biochem. J.* **475**, 1721-1738 (2018).

5. Li, X. *et al.* Differential TOR activation and cell proliferation in Arabidopsis root and shoot apexes. *Proc. Natl. Acad. Sci. USA* **114**, 2765-2770 (2017).

6. Chen, G.-H., Liu, M.-J., Xiong, Y., Sheen, J. & Wu, S.-H. TOR and RPS6 transmit light signals to enhance protein translation in deetiolating Arabidopsis seedlings. *Proc. Natl. Acad. Sci. USA* **115**, 12823-12828 (2018).

7. Schepetilnikov, M. *et al.* GTPase ROP2 binds and promotes activation of target of rapamycin, TOR, in response to auxin. *EMBO J.* **36**, 886-903 (2017).

8. Pfeiffer, A. *et al.* Integration of light and metabolic signals for stem cell activation at the shoot apical meristem. *eLife* **5**, e17023 (2016).

9. Zhang, Z. *et al.* TOR signaling promotes accumulation of BZR1 to balance growth with carbon availability in Arabidopsis. *Curr. Biol.* **26**, 1854-1860 (2016).

10. Xiong, F.J. *et al.* Brassinosteriod Insensitive 2 (BIN2) acts as a downstream effector of the Target of Rapamycin (TOR) signaling pathway to regulate photoautotrophic growth in Arabidopsis. *New Phytol.* **213**, 233-249 (2017).

11. Wang, P. *et al.* Reciprocal regulation of the TOR kinase and ABA receptor balances plant growth and stress response. *Mol. Cell* **69**, 100-112 e106 (2018).

12. Malinovsky, F.G. *et al.* An evolutionarily young defense metabolite influences the root growth of plants via the ancient TOR signaling pathway. *eLife* **6**, e29353 (2017).

13. Dong, Y. *et al.* Sulfur availability regulates plant growth via glucose-TOR signaling. *Nat. Commun.* **8** (2017).

14. Xiong, Y. *et al.* Glucose-TOR signalling reprograms the transcriptome and activates meristems. *Nature* **496**, 181–186 (2013).

15. Xing, A. & Last, R.L. A regulatory hierarchy of the Arabidopsis branched-chain amino acid metabolic network. *Plant Cell* **29**, 1480-1499 (2017).

16. Sarbassov, D.D. *et al.* Rictor, a novel binding partner of mTOR, defines a rapamycin-insensitive and raptor-independent pathway that regulates the cytoskeleton. *Curr. Biol.* **14**, 1296-1302 (2004).

17. Jacinto, E. *et al.* Mammalian TOR complex 2 controls the actin cytoskeleton and is rapamycin insensitive. *Nat. Cell Biol.* **6**, 1122-U1130 (2004).

18. Galili, G., Amir, R. & Fernie, A.R. The Regulation of Essential Amino Acid Synthesis and Accumulation in Plants. *Annu. Rev. Plant Biol.* **67**, 153-178 (2016).

19. Maliga, P. Isolation and Characterization of Mutants in Plant-Cell Culture. *Annu. Rev. Plant Physiol. Plant Mol. Biol.* **35**, 519-542 (1984).

20. Ren, M. *et al.* Target of rapamycin signaling regulates metabolism, growth, and life span in Arabidopsis. *Plant Cell* **24**, 4850-4874 (2012).

21. Zhao, L. *et al.* Autophagy contributes to sulfonylurea herbicide tolerance via GCN2-independent regulation of amino acid homeostasis. *Autophagy* **14**, 702-714 (2018).

22. Mubeen, U., Juppner, J., Alpers, J., Hincha, D.K. & Giavalisco, P. Target of rapamycin inhibition in Chlamydomonas reinhardtii triggers de novo amino acid synthesis by enhancing nitrogen assimilation. *Plant Cell* **30**, 2240-2254 (2018).

23. Garcia, A.V., Al-Yousif, M. & Hirt, H. Role of AGC kinases in plant growth and stress responses. *Cell. Mol. Life Sci.* **69**, 3259-3267 (2012).

24. Feiguelman, G., Fu, Y. & Yalovsky, S. ROP GTPases structure-function and signaling pathways. *Plant Physiol.* **176**, 57-79 (2018).

25. Deprost, D. *et al.* The Arabidopsis TOR kinase links plant growth, yield, stress resistance and mRNA translation. *EMBO Rep.* **8**, 864-870 (2007).

26. Moreau, M. *et al.* Mutations in the Arabidopsis homolog of LST8/GβL, a partner of the target of Rapamycin kinase, impair plant growth, flowering, and metabolic adaptation to long days. *Plant Cell* **24**, 463-481 (2012).

27. Salem, M.A. *et al.* RAPTOR controls developmental growth transitions by altering the hormonal and metabolic balance. *Plant Physiol.* **177**, 565-593 (2018).

28. Salem, M.A., Li, Y., Wiszniewski, A. & Giavalisco, P. Regulatory-associated protein of TOR (RAPTOR) alters the hormonal and metabolic composition of Arabidopsis seeds, controlling seed morphology, viability and germination potential. *Plant J.* **92**, 525-545 (2017).

29. Anderson, G.H., Veit, B. & Hanson, M.R. The Arabidopsis AtRaptor genes are essential for post-embryonic plant growth. *BMC Biol.* **3**, 12 (2005).

30. Deprost, D., Truong, H.N., Robaglia, C. & Meyer, C. An Arabidopsis homolog of RAPTOR/KOG1 is essential for early embryo development. *Biochem. Biophys. Res. Commun.* **326**, 844-850 (2005).

31. Xiong, Y. & Sheen, J. Rapamycin and glucose-target of rapamycin (TOR) protein signaling in plants. *J. Biol. Chem.* **287**, 2836-2842 (2012).

32. Ueda, H. *et al.* Myosin-dependent endoplasmic reticulum motility and F-actin organization in plant cells. *Proc. Natl. Acad. Sci. USA* **107**, 6894-6899 (2010).

33. Avila, E.L. *et al.* Tools to study plant organelle biogenesis. Point mutation lines with disrupted vacuoles and high-speed confocal screening of green fluorescent protein-tagged organelles. *Plant Physiol.* **133**, 1673-1676 (2003).

34. Cutler, S.R., Ehrhardt, D.W., Griffitts, J.S. & Somerville, C.R. Random GFP::cDNA fusions enable visualization of subcellular structures in cells of Arabidopsis at a high frequency. *Proc. Natl. Acad. Sci. USA* **97**, 3718-3723 (2000).

35. Zhang, C.H., Hicks, G.R. & Raikhel, N.V. Plant vacuole morphology and vacuolar trafficking. *Front. Plant Sci.* **5** (2014).

36. Nelson, B.K., Cai, X. & Nebenfuhr, A. A multicolored set of in vivo organelle markers for co-localization studies in Arabidopsis and other plants. *Plant J.* **51**, 1126-1136 (2007).

37. Gattolin, S., Sorieul, M. & Frigerio, L. Tonoplast intrinsic proteins and vacuolar identity. *Biochem. Soc. Trans.* **38**, 769-773 (2010).

38. de Kraker, J.W., Luck, K., Textor, S., Tokuhisa, J.G. & Gershenzon, J. Two Arabidopsis genes (IPMS1 and IPMS2) encode isopropylmalate synthase, the branchpoint step in the biosynthesis of leucine. *Plant Physiol.* **143**, 970-986 (2007).

39. Brandizzi, F. & Barlowe, C. Organization of the ER-Golgi interface for membrane traffic control. *Nat. Rev. Mol. Cell Biol.* **14**, 382-392 (2013).

40. Renna, L. *et al.* Identification and characterization of AtCASP, a plant transmembrane Golgi matrix protein. *Plant Mol. Biol.* **58**, 109-122 (2005).

41. Faso, C. *et al.* A missense mutation in the Arabidopsis COPII coat protein Sec24A induces the formation of clusters of the endoplasmic reticulum and Golgi apparatus. *Plant Cell* **21**, 3655-3671 (2009).

42. Renna, L. *et al.* Golgi Traffic and Integrity Depend on N-Myristoyl Transferase-1 in Arabidopsis. *Plant Cell* **25**, 1756-1773 (2013).

43. Renna, L. *et al.* TGNap1 is required for microtubule-dependent homeostasis of a subpopulation of the plant trans-Golgi network. *Nat. Commun.* **9**, 5313 (2018).

44. Ketelaar, T. *et al.* The actin-interacting protein AIP1 is essential for actin organization and plant development. *Curr. Biol.* **14**, 145-149 (2004).

45. Deeks, M.J. *et al.* Arabidopsis group Ie formins localize to specific cell membrane domains, interact with actin-binding proteins and cause defects in cell expansion upon aberrant expression. *New Phytol.* **168**, 529-540 (2005).

46. Sheahan, M.B., Rose, R.J. & McCurdy, D.W. Organelle inheritance in plant cell division: the actin cytoskeleton is required for unbiased inheritance of chloroplasts, mitochondria and endoplasmic reticulum in dividing protoplasts. *Plant J.* **37**, 379-390 (2004).

47. Cao, P., Renna, L., Stefano, G. & Brandizzi, F. SYP73 anchors the ER to the actin cytoskeleton for maintenance of ER integrity and streaming in Arabidopsis. *Curr. Biol.* **26**, 3245-3254 (2016).

48. Zheng, J., Han, S.W., Rodriguez-Welsh, M.F. & Rojas-Pierce, M. Homotypic vacuole fusion requires VTI11 and is regulated by phosphoinositides. *Mol. Plant* **7**, 1026-1040 (2014).

49. Wang, J., Cai, Y., Miao, Y., Lam, S.K. & Jiang, L. Wortmannin induces homotypic fusion of plant prevacuolar compartments. *J. Exp. Bot.* **60**, 3075-3083 (2009).

50. Mayer, A. *et al.* Phosphatidylinositol 4,5-bisphosphate regulates two steps of homotypic vacuole fusion. *Mol. Biol. Cell* **11**, 807-817 (2000).

51. Marshall, R.S. & Vierstra, R.D. Autophagy: the master of bulk and selective recycling. *Annu. Rev. Plant Biol.* **69**, 173-208 (2018).

52. Cui, Y. *et al.* A whole-cell electron tomography model of vacuole biogenesis in Arabidopsis root cells. *Nat. Plants* **5**, 95-105 (2019).

53. Brunn, G.J. *et al.* Direct inhibition of the signaling functions of the mammalian target of rapamycin by the phosphoinositide 3-kinase inhibitors, wortmannin and LY294002. *EMBO J.* **15**, 5256-5267 (1996).

54. Andrs, M. *et al.* Phosphatidylinositol 3-Kinase (PI3K) and phosphatidylinositol 3-kinase-related kinase (PIKK) inhibitors: importance of the morpholine ring. *J. Med. Chem.* **58**, 41-71 (2015).

55. Benjamin, D., Colombi, M., Moroni, C. & Hall, M.N. Rapamycin passes the torch: a new generation of mTOR inhibitors. *Nat. Rev. Drug Discov.* **10**, 868-880 (2011).

56. Liu, Q. *et al.* Discovery of 9-(6-aminopyridin-3-yl)-1-(3-(trifluoromethyl)phenyl)benzo[h][1,6]naphthyridin-2(1H)-one (Torin2) as a potent,

selective, and orally available mammalian target of rapamycin (mTOR) inhibitor for treatment of cancer. *J. Med. Chem.* **54**, 1473-1480 (2011).

57. Chresta, C.M. *et al.* AZD8055 is a potent, selective, and orally bioavailable ATP-competitive mammalian target of rapamycin kinase inhibitor with in vitro and in vivo antitumor activity. *Cancer Res.* **70**, 288-298 (2010).

58. Pu, Y., Luo, X. & Bassham, D.C. TOR-dependent and-independent pathways regulate autophagy in Arabidopsis thaliana. *Front. Plant Sci.* **8** (2017).

59. Schmidt, A., Kunz, J. & Hall, M.N. TOR2 is required for organization of the actin cytoskeleton in yeast. *Proc. Natl. Acad. Sci. USA* **93**, 13780-13785 (1996).

60. Roelants, F.M., Leskoske, K.L., Marshall, M.N.M., Locke, M.N. & Thorner, J. The TORC2-Dependent Signaling Network in the Yeast Saccharomyces cerevisiae. *Biomolecules* **7** (2017).

61. Stefano, G., Hawes, C. & Brandizzi, F. ER - the key to the highway. *Curr. Opin. Plant Biol.* **22**, 30-38 (2014).

62. Wu, H., Carvalho, P. & Voeltz, G.K. Here, there, and everywhere: The importance of ER membrane contact sites. *Science* **361**, eaan5835 (2018).

63. Stefano, G., Renna, L., Moss, T., Mcnew, J.A. & Brandizzi, F. In Arabidopsis, the spatial and dynamic organization of the endoplasmic reticulum and Golgi apparatus is influenced by the integrity of the C-terminal domain of RHD3, a non-essential GTPase. *Plant J.* **69**, 957-966 (2012).

64. Westrate, L.M., Lee, J.E., Prinz, W.A. & Voeltz, G.K. Form follows function: the importance of endoplasmic reticulum shape. *Annu. Rev. Biochem.* **84**, 791-811 (2015).

65. Stefano, G. & Brandizzi, F. Advances in plant ER architecture and dynamics. *Plant Physiol.* **176**, 178-186 (2018).

66. Yu, L. *et al.* Termination of autophagy and reformation of lysosomes regulated by mTOR. *Nature* **465**, 942-946 (2010).

67. Michaillat, L., Baars, T.L. & Mayer, A. Cell-free reconstitution of vacuole membrane fragmentation reveals regulation of vacuole size and number by TORC1. *Mol. Biol. Cell* **23**, 881-895 (2012).

68. Löfke, C., Dünser, K., Scheuring, D. & Kleine-Vehn, J. Auxin regulates SNARE-dependent vacuolar morphology restricting cell size. *eLife* **4**, e05868 (2015).

69. Scheuring, D. *et al.* Actin-dependent vacuolar occupancy of the cell determines auxin-induced growth repression. *Proc. Natl. Acad. Sci. USA* **113**, 452-457 (2016).

70. Boisen, S., Hvelplund, T. & Weisbjerg, M.R. Ideal amino acid profiles as a basis for feed protein evaluation. *Livestock Production Science* **64**, 239-251 (2000).

71. Shimomura, Y., Murakami, T., Nakai, N., Nagasaki, M. & Harris, R.A. Exercise promotes BCAA catabolism: Effects of BCAA supplementation on skeletal muscle during exercise. *J. Nutr.* **134**, 1583s-1587s (2004).

72. Peng, C., Uygun, S., Shiu, S.H. & Last, R.L. The impact of the branched-chain ketoacid dehydrogenase complex on amino acid homeostasis in Arabidopsis. *Plant Physiol.* **169**, 1807-1820 (2015).

73. Field, B., Furniss, C., Wilkinson, A. & Mithen, R. Expression of a Brassica isopropylmalate synthase gene in Arabidopsis perturbs both glucosinolate and amino acid metabolism. *Plant Mol. Biol.* **60**, 717-727 (2006).

74. Imhof, J. *et al.* The Small Subunit 1 of the Arabidopsis Isopropylmalate Isomerase Is Required for Normal Growth and Development and the Early Stages of Glucosinolate Formation. *PLoS ONE* **9**, e91071 (2014).

75. Schindelin, J. *et al.* Fiji: an open-source platform for biological-image analysis. *Nat. Methods* **9**, 676-682 (2012).

76. Clough, S.J. & Bent, A.F. Floral dip: a simplified method for Agrobacterium-mediated transformation of Arabidopsis thaliana. *Plant J.* **16**, 735-743 (1998).

77. Lu, Y.-J. & Day, B. Quantitative evaluation of plant actin cytoskeletal organization during immune signaling, in *Plant Pattern Recognition Receptors: Methods and Protocols*. (eds. L. Shan & P. He) 207-221 (Springer New York, New York, NY; 2017).

78. Angelovici, R. *et al.* Genome-wide analysis of branched-chain amino acid levels in Arabidopsis seeds. *Plant Cell* **25**, 4827-4843 (2013).

79. Kotogany, E., Dudits, D., Horvath, G.V. & Ayaydin, F. A rapid and robust assay for detection of S-phase cell cycle progression in plant cells and tissues by using ethynyl deoxyuridine. *Plant Methods* **6** (2010).

80. French, A.P. *et al.* Identifying biological landmarks using a novel cell measuring image analysis tool: Cell-o-Tape. *Plant Methods* **8**, 7 (2012).

81. Kim, S.J. *et al.* In the grass species Brachypodium distachyon, the production of mixed-linkage (1,3;1,4)-beta-glucan (MLG) occurs in the Golgi apparatus. *Plant J.* **93**, 1062-1075 (2018).

82. Weraduwage, S.M. *et al.* Pectin methylesterification impacts the relationship between photosynthesis and plant growth. *Plant Physiol.* **171**, 833-848 (2016).

CHAPTER 4. FUTURE PERSPECTIVES[1]

[1]Certain figures and data in this chapter include significant contribution by: a collaborator Yuxing Xu (Figure 4.5), Department of Economic Plants and Biotechnology, Yunnan Key Laboratory for Wild Plant Resources, Kunming Institute of Botany, Chinese Academy of Sciences, Kunming, China; undergraduate research assistants Nicole Szeluga (Figure 4.1 and 4.2) and Lu Liu (Section 4.3.2), MSU-DOE Plant Research Lab, Michigan State University, East Lansing, USA

4.1 FUNCTIONAL CHARACTERIZATION OF SYP73 AS A VERSATILE ACTIN ORGANIZER

4.1.1 Reasoning unappreciated functions and potential regulatory mechanisms of SYP73

Recently we characterized SYP73 as an ER-actin anchor protein in plant cells: over-expression of SYP73 remodels ER network to overlay actin cables; consistent with its molecular role of connecting ER to F-actin, the functional SYP73 is required for maintaining ER integrity as well as normal plant growth[1]. Interestingly, SYP73 belongs to SYP7, a plant-specific subfamily of SNARE proteins that form the SNARE complex, an ancient machinery that mediates membrane-membrane fusion between different endomembrane compartments in eukaryotic cells[2]. The plant genomes encode extended SNARE superfamilies, hypothetically because of the complexity of intracellular trafficking cargos and destinations in plant cells[2, 3]. Nevertheless, little is known about the rise of a novel actin binding domain from the redundant and variety of plant SNAREs, and furthermore how SYP73 influence the organization of the actin cytoskeleton.

So far, a handful of plant proteins have been identified with F-actin binding ability without bearing any conventional actin-binding domain[4-10]. Among these novel plant actin-binding proteins, SCAB1, GhCFE1A, VABs, THRUMIN1 and CROLIN1 were further characterized to cross-link actin filaments[4-6, 8, 10], presumably because of co-existence of more than one actin-binding domain in the same polypeptide or self-interaction between monomeric proteins[11]. Indeed, structural analysis of SCAB1 showed that its actin binding ability depends on a few key residues in an α-helix and SCAB1 self-interacts via an adjacent α-helical coiled-coil region[12]. The revealed structural basis for SCAB1-actin interaction provides an example of establishing a plant-specific actin binding domain upon simple α-helical structures and a few key hydrophobic residues[12], which is similar to several other conserved actin-binding domains[13, 14].

Phosphorylation is arguably the most common and versatile modification of proteins, and it has been identified as the regulatory mechanisms of many executor proteins that directly mediate ER remodeling and actin reorganization. In mammalian cells, mitotic phosphorylation modulates functions of the ER-shaping proteins to reduce the rigidity of ER network and more importantly to exclude ER membranes from the microtubule-assembled mitotic spindle. Specifically, two ER membrane-microtubule anchoring mechanisms[15], STIM1-EB1 and CLIMP-63, are subjected to mitotic phosphorylation, resulting in inhibited microtubule association[16, 17], and potentially reduced ER rigidity and destabilized ER sheets[18]. During mitosis, another ER-shaping protein Lunapark that is localized to and stabilizes the three-way junctions of ER network is also phosphorylated, leading to destabilization of three-way junctions and tubules[19]. Characterization of mitotic phosphorylation of these essential ER-shaping proteins proposes a wholistic regulation of ER remodeling in response to developmental clues. Despite the mammalian ER-microtubule anchoring proteins (i.e., STIM1-EB1 and CLIMP-63) are not functionally conserved in plants and the phosphorylation of plant Lunapark homologs has not been characterized yet[20, 21], a recent study identified phosphorylation regulation of RHD3, a plant homolog of mammalian Atlastin that mediates ER membrane fusion[22]. Compared to the mammalian Atlastin, RHD3 contains an extra Serine-enriched C-terminal stretch, which can be phosphorylated to enhance RHD3 oligomerization, and thereby to promote RHD3 mediated ER membrane fusion[22]. Similar to RHD3, other conserved or plant-specific ER-shaping proteins may arise as subjects to phosphorylation regulatory mechanisms.

In this work, we scanned the SYP73 protein sequence based on the predicted secondary structure and narrowed down its novel actin-binding domain to the first alpha helix at SYP73 N-terminus. In seeking potential regulatory mechanism of SYP73 functions, we identified *in vivo*

phosphorylation of SYP73. Furthermore, we applied point mutations of three amino acid residues of SYP73 to mimic the inactive and active status of phosphorylation and found evident alterations of SYP73 self-interaction and actin-binding abilities. Preliminary evolutionary analysis found SYP73 only exists in a group of higher plants. Taken together, these results suggest evolutionary innovation of SYP73 from the ancient membrane fusion machinery to a regulated versatile organizer of the actin cytoskeleton.

4.1.2 Identification of a novel actin-binding domain in SYP73

Previously, we searched for conserved domain or motif for actin binding in SYP73, and detected two WH2 motifs using the Eukaryotic Linear Motif (ELM) program[1, 23]. However, we did not experimentally consolidate whether the WH2 motifs, which is originally defined as binding to the actin monomer[24], are required and sufficient for SYP73 binding to F-actin. To identify the actin binding domain in SYP73, we first predicted its secondary structure using JPred4 program4. Except for two α-helical regions at the C-terminus that are corresponding to a SNARE domain and a transmembrane domain, tandem α-helices were also identified at the N-terminus of SYP73 (Figure 4.1A). We designated four α-helices as NT1 – 4 and designed SYP73-truncated proteins to scan for any region that is potentially required and sufficient for actin binding (Figure 4.1B). We expressed SYP73-truncated proteins that were tagged with YFP in tobacco leaf epidermal cells, and we found the first α-helix (NT1, 1 – 30) is required for the recombinant protein binding to F-actin (Figure 4.1C - F).

4.1.3 SYP73 binding to actin is regulated by *in vivo* phosphorylation

To identify potential phospho-regulation of SYP73 functions, we searched published phosphorylation proteomics analyses and found documented phosphorylated peptides of SYP73, suggesting three phosphorylation sites S12, T189 and T225[26-28] (Figure 4.2A). We used Phos-tag

SDS-PAGE to test whether SYP73 is phosphorylated *in vivo*. YFP tagged SYP73 and RHD3, which is reported to be phosphorylated in plants, were expressed in tobacco leaves. Following extraction of the total fraction of cytosolic and membrane-associated protein, the protein samples were incubated in buffers supplemented with or without alkaline phosphatase, and subsequently subjected to Phos-tag SDS-PAGE, which delays the migration of phospho-modified proteins. Without dephosphorylation treatment, immunoblot of SYP73-YFP using anti-GFP/YFP antiserum detected at least two signals representing proteins with different migration distances; by contrast, after overnight dephosphorylation, most proteins showed further migration (Figure 4.2B). Meanwhile, a correlation between dephosphorylation treatment and further migration distance was also displayed on the blot of YFP-RHD3 proteins (Figure 4.2B), suggesting SYP73 was phosphorylated *in vivo*.

Considering the *in vivo* phosphorylation of SYP73 possibly occurs on the three residues S12, T189 and T225, next we constructed a SYP73 phosphorylation inactive triple mutant (Phos-Inactive TM, S12A/T189A/T225A) and a SYP73 phosphorylation mimicking triple mutant (Phos-Mimicking TM, S12D/T189D/T225D), and tested whether these mutations influence protein functions. First, by expressing the SYP73 mutants fused with YFP in tobacco leaf epidermal cells, we observed changes of SYP73 function on remodeling the ER network *in vivo*. The wild-type SYP73 changed ER morphology as we previously reported[1], the Phos-Inactive mutant displayed normal ER network with ER sheets and polygonal networks, while the Phos-Mimicking mutant rearranged ER to actin cables to a seemingly larger extent (Figure 4.2C - E). Besides, we conducted a high-speed co-sedimentation assay to determine if simulated phosphorylation status affects SYP73's actin binding ability *in vitro*. The result of F-actin co-sedimentation assay (Figure 4.3)

clearly showed that Phos-Inactive mutant has lower while the Phos-Mimicking mutant has higher binding affinity to F-actin compared with the wild-type SYP73.

4.1.4 Phosphorylation regulates SYP73 self-interaction

Self-interaction is a significant mechanism for many protein functions of shaping ER membrane and regulating actin dynamics. First, self-interaction and oligomerization may enhance certain protein functions. Secondly, self-interaction may confer new functions that cannot be performed by a monomeric protein. One of the significant functions of ABPs is actin bundling. An ABP with two actin-binding domains can crosslink two actin filaments. Figure 4.4A shows that in previous research, we noticed that SDS-PAGE and coomassie blue staining of purified His-SYP73ΔTM showed a second band, the size of which corresponds to that of His-SYP73ΔTM dimer. Subsequently, we treated the purified protein with high concentration of urea, which leads to denature of proteins and disruption of self-interactions, and then observed dissolution of His-SYP73ΔTM dimer and accumulation of monomers. Yeast two-hybrid assay also suggested SYP73ΔTM can directly self-interact. Furthermore, protein prokaryotic expression and purification suggested that SYP73 dimerization is less in the Phos-Inactive mutant, more in the Phos-Mimicking mutant compared with the wild-type SYP73 (Figure 4.4B).

4.1.5 The regulated actin organizer SYP73 is specific to core eudicots

Identification of an actin-binding domain in SYP73, a member of the ancient membrane fusion machinery, also prompted an intriguing question about its emergence in the plant linage. To provide preliminary clues for answering this question, we conducted search and phylogenetic analysis of all SYP7 subfamily homologs among 51 evolutionarily representative plant species (Figure 4.5). From this topology, it can be inferred that SYP7 may obtain 3 copies by a gene triplication in the core eudicots ancestor, which may be due to genomic doubling events in the

same period. Compared with the branch where SYP71 and SYP73 are located, the branch of SYP72 is farther away from the genes of basal angiosperm. From the sequence alignment, SYP72 also has greater differences than SYP71 and 73, so it can be speculated that SYP71 and 73 are more likely to retain the function of ancestors, while 72 may acquire newer functions. Monocots do not acquire gene doubling as in core eudicots during their ancestral period, however the average length of the branch is longer, especially in grass, which may suggest that monocots, although not doubling multiple members in ancestor, gain new functions in the later stages through faster evolution. Taken together, the phylogenetic analysis indicates that SYP73 as an ER-actin anchor is an evolutionary innovation of higher plants for endomembrane-actin interactions that are specifically essential for plant cells. Further investigation is expected to examine the conservancy of SYP73 actin binding domain and its evolutionary routes in the plant linage.

4.2 IDENTIFY POTENTIAL REGULATORY MECHANISMS OF PLANT VACUOLE MORPHOGENESIS

4.2.1 Formation of the large central vacuole is a plant-specific process

Considering the essential roles and conspicuous existence of the large central vacuole in plant cells, it is surprising that so far little is known about morphogenesis of the large central vacuole. As Chapter 1 of introduction and Chapter 3 of TOR-regulated vacuole morphogenesis discussed, the large central vacuole is a plant-unique structure, and it is essential for plant cell development. In yeast cells, the vacuole morphology is sensitive to growth conditions and vacuoles constantly undergo fusion and fission processes to change their volume and number[29]. Specifically, yeast cells growing in normal conditions contain two to three medium-sized vacuoles; hypotonic, or hypo-osmotic, media induces vacuole-vacuole fusion to form a large vacuole; hypertonic, or hyper-osmotic, condition with a greater concentration of salts induces vacuole fission that forms a

large number of smaller vesicles[29]. In Arabidopsis cotyledon epidermal cells and most other plant cell types, approximately from three to eight days after seed germination, numerous small vacuoles fuse to form a large central vacuole (Figure 4.6)[30]. During the process of embryo development and seed maturation, a preexisting large vacuole in the embryonic cell divides to form numerous small protein storage vacuoles[31]. The recent time-course TEM analyses[30, 31] contributed landscapes of large central vacuole formation and deformation with in-depth description, but the regulatory mechanisms are yet to be revealed.

Because a fused large vacuole is not essential for yeast, forward genetic screens for yeast cells with defects in the secretory pathway identified mutants having numerous small vesicular structures, instead of a notable large vacuole [32]. Investigations into these mutants of vacuole morphogenesis led to characterization of most components of the vacuole membrane-membrane fusion machinery[33] and the autophagy pathway[34], and directly contributed to discoveries awarded by the Nobel Prize in Physiology or Medicine in 2013 and 2016.

However, forward genetic study of plant vacuole has been hindered by the fact that the large central vacuole is essential for the plant cell4. The absence of vacuoles in a mutant led to embryo lethality[36]. Therefore, in the past two decades a simple approach of EMS mutagenesis upon a tonoplast marker δTIP-GFP[37] was adopted to identify any single-base mutation that affects vacuole morphology[38]. However, this screen strategy only yielded mutants with minor vacuolar phenotypes, including unfused vacuoles[39], small aggregates of vacuolar membranes[40], and increased number of bulbs[41, 42]. Additionally, I followed this screening strategy and encountered several potential mutants bearing such weak vacuolar phenotypes that cannot be distinguished among F2 generation after crossing with wild type (data not shown), presumably because the plant vacuole morphology is very sensitive to environmental clues and cellular nutritional status4. More

importantly, further investigations into these mutants led to essential cell functions, including Pol II transcription and auxin signaling[42, 43], or proteins with unknown functions[39-41], suggesting that in these scenarios the impaired large central vacuole is a collateral damage caused by defective essential cellular activities.

The incompetence of forward genetic screen urged plant cell biologist to appreciate chemical genomics, which utilizes chemical inhibitors to probe the plant secretory pathway and vacuole morphogenesis mildly and transiently[44]. Meanwhile, it is not surprising that a large number of reverse genetic studies, including most recently by Takemoto et al. and Brillada et al.[45, 46], based on sequence identity between plant and yeast homologs further characterized the essential roles of the membrane-membrane fusion machinery components in forming the large central vacuole in plant cell, and thereby in plant development. Taken together, the previous efforts to study the plant vacuole demonstrated the significance of elucidating plant-specific mechanisms and the potential values of identifying mutants with severe and specific vacuolar phenotypes.

4.2.2 Newly identified mutants with defects in vacuole morphogenesis

Except for the further characterized *vac-1/eva1,* three lines were identified as recessive mutants with stably inherited vacuolar phenotypes (Figure 4.7). Compared to wild type, three mutants, *vac-1/eva1*, *vac-2* and *vac-3*, have similar unfused small vacuoles (Figure 4.7) and invaginations that were revealed z-axis sliced images (data not shown) in 10-days old cotyledon epidermal cells. The phenotype of enhanced *trans*-vacuolar strands was observed in *eva1*/*vac-1* and *vac-2*, but not *vac-3*. Compared to *vac-1/eva1,* the uncharacterized *vac-2* and *vac-3* exhibited more frequent occurrence of unfused small vacuoles and invaginations and additional aggregates of vacuolar membranes, which are possibly miniscule vesicles existing between the large central vacuole and unfused small vacuoles (Figure 4.7). Additionally, *vac-2* and *vac-3* are also different from *vac-*

1/eva1 because they showed persistent vacuolar phenotypes and severe plant growth phenotypes, rather than transient phenotypes that only appear in the early stage of plant growth (data not shown). These observations imply that the underlying mechanism is possibly related to certain essential cellular activities that constantly regulates vacuole morphology and plant growth, instead of the functions of signaling pathway that depends on particular signaling inputs.

vac-4 was identified with increased number and size of "bulbs", which are named because of spherical structures and bright fluorescence. The bulbs were observed in multiple plant cell types by expressing the most frequently used vacuole markers, such as fluorescent protein tagged TIP aquaporins and vacuolar SNARE proteins[41, 47-50]. TEM imaging suggested that bulbs are double-layer vacuolar structures formed by invagination of the single-layer tonoplast[48], explaining why bulbs glow at least doubled intensity of fluorescence[48-50]. However, the biogenesis and the function of bulbs are still unclear[49].

Previously, *vti11* and *sgr2-1* mutants were characterized with reduced occurrence of bulbs, suggesting the SNARE membrane fusion machinery is involved in formation of bulbs[49]. *iyo-1*, *keg-1* and *rbb1-1* mutants displayed increased number of bulbs, but the functional connections between the causal mutations and bulb morphogenesis were undetermined[41, 42, 51]. Compared with the previously identified mutants with bulb-related phenotypes[41, 49], *vac-4* exhibits three unique features: expect for increased number of bulbs, the mutant shows wild type-like vacuole morphology without additional complex vacuolar structures; not only the number but also the size of bulbs are increased in the mutant; in wild type bulbs appear and last for approximately three days, but in mutants bulbs exist for approximately another 3 days and then disapprear[41]. Therefore, investigation of *vac-4* may lead to mechanisms of bulb morphogenesis, especially in terms of its formation, size control and absorption by the tonoplast.

4.3 AN EMERGING FIELD OF PLANT TOR SIGNALING: PLANT-SPECIFIC QUESTIONS STAND OUT

Identification of genetic materials and conditions in which plant TOR signaling is substantially up-regulated allowed us to characterize the functional consequences TOR activation at both cellular and plant-growth levels. Besides, previous studies using transient TOR inhibitor treatment and mutants of TOR signaling components revealed the influences of acute and enduring inhibition of TOR signaling. Taken together, these reports suggest that TOR signaling impacts various aspects of plant growth and development, including most prominently the activities of root and shoot apical meristems, nitrogen assimilation and specialized metabolism. Reasoning of the functional connection between BCAA homeostasis, TOR activity and plant growth prompted us to hypothesize that an inconsistency between nutritional status and metabolic signaling activity is detrimental to plant growth and development. Furthermore, this hypothesis highlights the practical significance of investigating TOR in a context of plant-specific metabolic and developmental mechanisms for optimized plant TOR signaling and improved plant growth and nutritional values. In this emerging field of studying plant TOR signaling, I found how plant cells sense nutrients, coordinate the unique metabolic pathways for plant growth are the most pressing questions.

4.3.1 Amino acid sensing in plant cells

Amino acids are the building blocks for proteins and several types of amino acids are markers of cellular nutritional levels that regulates the activity of TOR signaling. Meanwhile, the amino acid sensing mechanisms in eukaryotic cells are reasonably corresponding to these two roles of amino acids. On the one hand, depletion of any one type of amino acid leads to accumulation of unloaded tRNAs that bind to GCN2 kinase, which halts the translation initiation[52]. On the other hand, several types of amino acids are specifically sensed as inputs of the TOR signaling. Recent studies in

mammalian cells identified cytosolic sensors of arginine[53], leucine[54] and methionine-derived S-adenosylmethionine[55] and a lysosomal membrane-localized amino acid transporter that senses multiple amino acids in the lysosome lumen[56]. The yeast genome encodes several proteins that are closely related to certain mammalian amino acid sensors, but whether they similarly sense amino acids and regulate TOR requires further investigation[57]. In Arabidopsis, the amino acid permease (AAP) family of conserved amino acid transporters are among the first identified plant homologs based on sequence identity[58, 59], but these plasma membrane-localized transporters are responsible for amino acid uptake from the apoplast and they have not been indicated to sense the environmental amino acid concentration[60].

Based on the recently identified human amino acid sensors and key components of the amino acid sensing pathways, a recent BLAST analysis yielded potential homologs in invertebrates and fungi, but not in plant species[61]. In fact, so far studies of plant TOR signaling have only identified TOR, LST8 and Raptor through BLAST of the mammalian homologs[62], leaving an open question whether the amino acid sensing mechanism and TOR complex configuration are conserved cross kingdoms. But nevertheless, our research in Chapter 3 contributed to answering this question by revealing the conservancy of TOR activation by BCAAs in Arabidopsis. Additionally, it is also noteworthy that homologs may diverge across kingdoms and functional homologs may rise as evolutionary innovations. One example is the long haul from discovery of yeast AVO3, the defining TOR-interactor of TORC2, to identification of its mammalian homolog Rictor, which shared merely 25% sequence identity4. Therefore, the amino acid sensing mechanism in plant cells is still expected to be unveiled by combined approaches of multi-sequence alignment, biochemistry and genetics.

4.3.2 Dissect TOR downstream processes that are pertinent to plant growth phenotypes

Accumulating evidence suggest a general correlation between TOR signaling activity and plant growth and development. On the one hand, a dossier of reports on gene silencing or chemical inhibition of TOR signaling found inhibited plant growth[66-71]. On the other hand, etiolation and sugar starvation followed by exposure to light and glucose stimulate TOR signaling, causing increased activities of shoot and root apical meristems[72-74]. In terms of constitutive over-expression of TOR, a characterization of four T-DNA insertion lines with higher levels TOR transcripts reported similarly promoted growth of aerial tissue and roots and reduced sensitivity to osmotic stress[66]. A later study utilized one of the four T-DNA insertion lines also reported increased fresh weight, albeit to a minor extent4. In another study, transgenic rice lines with high-level expression of Arabidopsis TOR exhibited promoted growth, as well as improved efficiencies of photosynthesis and water utilization[76]. Interestingly, tradeoffs of TOR-promoted plant growth were not detected in the conditions of these studies, and it is yet unknown how a potential nutritional deficit is compensated to sustain the promoted growth.

Our phenotypic analyses of *ipms1* mutants of up-regulated TOR signaling (see Chapter 3) identified increased activity of root apical meristem and plant growth phenotypes that are related to distortion of subcellular structures. In the *ipms1* loss-of-function mutants, despite the cell number and DNA synthesis were increased in the root apical meristem, the primary root is much shorter than wild type and the formation of lateral roots and root hairs were inhibited (Figure 3.7; Figure 3.13). These prominent dual phenotypes that correlated with meristem activation and actin re-organization provide an invaluable opportunity to decouple the TOR-regulated plant growth promotion and inhibition. Furthermore, I have EMS mutagenized the *ipms1* loss-of-function lines and initiated a screen for mutants with recovered root development.

4.4 TOWARDS A SYSTEMATIC UNDERSTANDING OF ENDOMEMBRANE-CYTOSKELETON INTERACTIONS

4.4.1 Potential membrane-cytoskeleton interactions

Although several proteins are emerging as motors and connectors of the plant endomembranes with the cytoskeleton, several questions remain open. First, the mechanisms underlying the interactions between cytoskeleton and major endomembrane compartments are still largely unknown. For example, numerous studies suggest that abolishment of myosin XI motors significantly impairs ER dynamics; however, it is still unclear whether myosins directly connect with nuclear envelope, ER membrane or vacuoles. Meanwhile, the exact localizations of more than a dozen identified myosin adaptors remain mysterious[77]. Moreover, it is yet unclear whether any anchoring mechanisms, other than the already identified proteins, may connect ER network, vacuoles and other vesicular structures to actin filaments or microtubules. Several questions also remain unanswered about the interactions between cytoskeleton system and the plant cell's unique membrane structures. For example, chloroplast movement to avoid intense light is achieved by membrane-actin interactions. The chloroplast outer envelope is bound to dynamically polymerizing short chloroplast-actin filaments by CHUP1 and other anchoring proteins[78]. It is still unclear whether myosin motors also contribute to chloroplast movement, and how the light signal coordinates dynamic actin polymerization and membrane-actin filament anchoring mechanisms. Stromules are tubular structures that protrude from plastids and function during immunity[79]. The role of actin cytoskeleton in stromule formation is not understood. Stromules are long and branched tubular structures that frequently overlay actin filaments and the ER network[80, 81]. Stromule movement depends on actin filaments and myosin XI[82, 83]. Besides, CHUP1, the anchor between chloroplast envelope and actin filament, is involved in stromule

formation[84]. However, isolated chloroplasts without actin filaments or ATP for myosin also spontaneously form stromules[85], raising the question on the identity of the underlying mechanism.

Little is also known about the role of the cytoskeleton in mediating organelle-organelle interactions in plant cells. Organelle-organelle interactions are widely observed and are required for organelle dynamics, collaborated metabolic processes, and signal transductions[86-90]. Imaging cultured mammalian cells with higher resolution further illustrated that these interactions are frequent and dynamic as expected, while they can also be intense and simultaneously occur between multiple organelles[91]. Studies also illustrated mechanisms of cytoskeleton system components mediated organelle-organelle interactions, such as ER-associated mitochondrial and endosomal division[92-94]. Studies in plant cells have reported similar organelle-organelle interactions and their participation in organelle dynamics and metabolic processes[95-101]. Among these topics, a convergence of the actin and microtubules at EPCS has been investigated in plant cells [102] but further research is required to reveal the function of such an organization.

4.4.2 What are the upstream inputs of cytoskeletal signaling?

Studies of the plant actin cytoskeleton that combined biochemical, genetic and imaging approaches have been instrumental to appreciate the actin dynamics that are directly regulated by various actin-binding proteins [103, 104]. Several actin-binding proteins are directly regulated by ROP GTPases in plant cells, in manners that are conserved to Rac and Rho GTPases in yeast and mammalian cells [105, 106]. Besides, membrane phosphoinositides such as $PI(4,5)P_2$ and $PI(3,4,5)P_3$ might be involved in signaling to various actin-binding proteins in the cytosol, but the detailed mechanisms are not clear [107]. A third major regulatory mechanism for actin-binding proteins is direct phosphorylation. However, many yeast and mammalian kinases involved in this process, such as certain members of the AGC family of protein kinases, seem not existing or have adapted functions in plants[108]. In

addition to conventional actin-binding proteins, it would be also intriguing to explore potential regulatory mechanisms for the more recently identified plant membrane-associated actin-binding proteins, such as NETs, VAPs and SYP73. Beyond the level of direct regulation of actin-binding proteins, certain types of receptors on the mammalian cell plasma membrane transduce extracellular signals to activate cytoplasmic actin cytoskeleton components[109-111]. To conclude, further analysis of the regulatory mechanisms of the conserved and novel actin-binding proteins has the potential to illustrate a landscape of endomembrane compartment morphogenesis and dynamics integrated by membrane-cytoskeleton interactions.

4.4.3 From subcellular structures to cell functions

One rule of thumb whereby biologists view this world is that structures determine functions and functions are fulfilled by specific structures. As our knowledge of establishment and maintenance of individual organelles is increasing in depth, intriguing questions arise as how organelles and cellular structures such as cytoskeleton interact and collaborate to realize specific cellular functions in response to extracellular stimuli.

Several plant cell models have been adopted to study this question. Polar growth of pollen tube and root hair cells requires acto-myosin system-propelled vesicular trafficking in the cell apex and actin filament-facilitated organelle extension in the elongating cell. Stomatal opening and closure are triggered by various signals and directly achieved through dynamic fusion of vacuoles, rearrangement of microtubule arrays and actin filaments, as well as call wall modification[116, 117]. Actin-dependent vacuole fusion is a general mechanism that also applies to vacuoles in guard cells[118]. Recent work showed that stomatal movement also requires microtubule-directed cellulose synthase complex movement on the plasma membrane [119].

Numerous studies revealed the reorganization of actin cytoskeleton as an important cellular response for plant defense, during both effector triggered immunity (ETI) that is initiated from the cytoplasm, and pattern-triggered immunity (PTI) that is perceived by receptors on the plasma membrane[120, 121]. Actin-binding capping proteins reside on the cytosolic side of ER membrane and mediate actin remodeling during PTI[122, 123]. Another actin-binding protein profilin is also involved in PTI[124]. Meanwhile, little is known about the signal transduction from receptors on the plasma membrane to actin-binding proteins in the cytosol, or how this process is potentially affected by the association between of actin-binding proteins and endomembranes. Interestingly, recent work reported that the membrane-actin anchoring protein CHUP1 facilitates chloroplast movement towards pathogen interface[125], suggesting that plant defense can directly employ membrane-cytoskeleton interactions to mobilize organelles to battle pathogenesis. To conclude, further studies on these topics would illustrate how the plant cell endomembrane and cytoskeleton collaborate in response to developmental and environmental clues.

APPENDIX

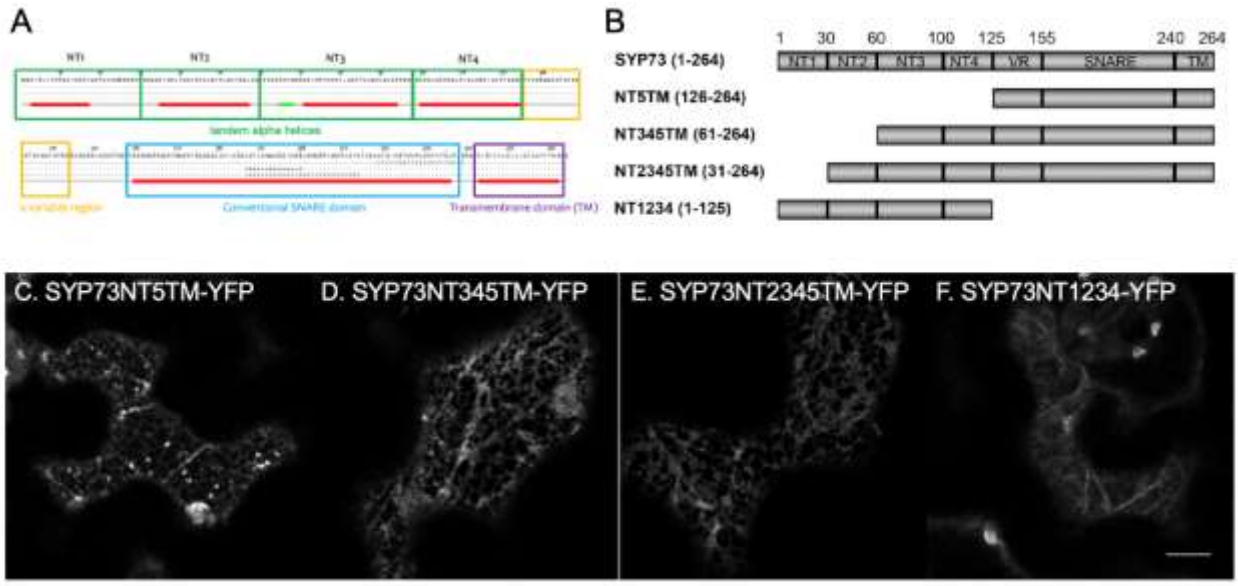

Figure 4.1 Identification of a novel actin-binding domain in SYP73.

(A) Diagram of predicted secondary structures of SYP73. Red bars indicate α-helical regions predicted by Jpred.
(B) Design of SYP73-truncated proteins to test actin binding ability. Predicted secondary structures were labeled. NT, N-terminal α-helix; VR, variable region; TM, transmembrane domain.
(C - F) Confocal images of tobacco leaf epidermal cells expressing the SYP73-truncated proteins that were tagged with YFP. Scale bar, 10 μm.

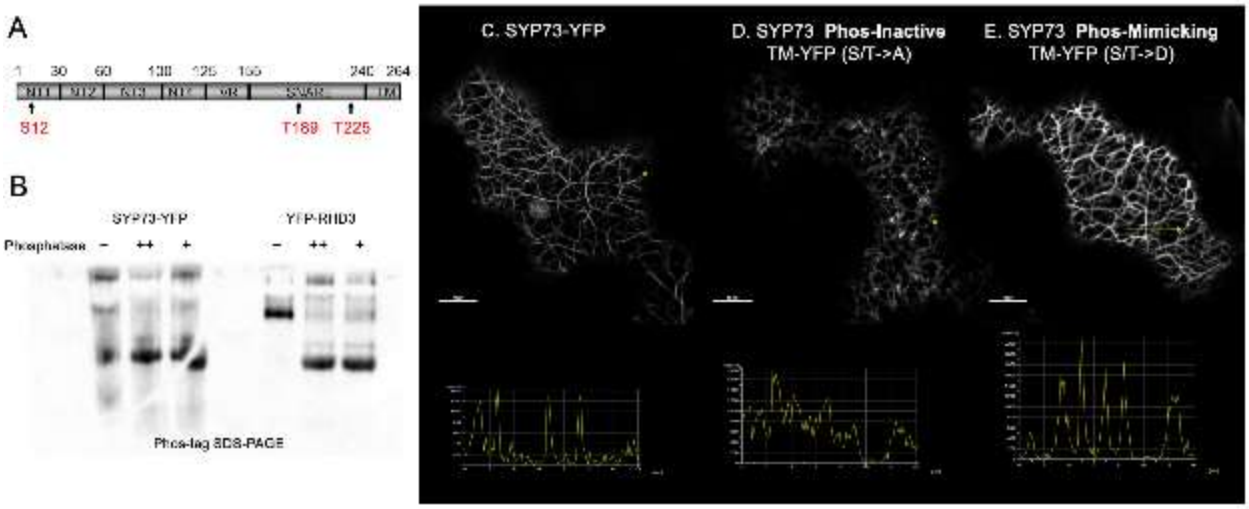

Figure 4.2 SYP73 is phosphorylated *in vivo*.

(A) Diagram of SYP73 protein with predicted secondary structures and potential phosphorylation sites.
(B) Detection of SYP73 *in vivo* phosphorylation using Phos-tag SDS-PAGE. SYP73-YFP proteins expressed in tobacco leaves were extracted and incubated in mock for two hours (−), or incubated with alkaline phosphatase for two hours (+) or overnight (++). After the dephosphorylation treatment, protein samples were subjected to Phos-tag SDS-PAGE and detected by anti-GFP/YFP antiserum. YFP-RHD3 was used as a positive control because of its known phosphorylation modification.
(C - E) Confocal images of tobacco leaf epidermal cells expressing the YFP-tagged wild-type (C) and mutant (D and E) SYP proteins. In each image, a yellow arrow was drawn to measure the intensity of fluorescent signals, which is plotted against distance and shown in the bottom panel. Scale bars, 10 μm.

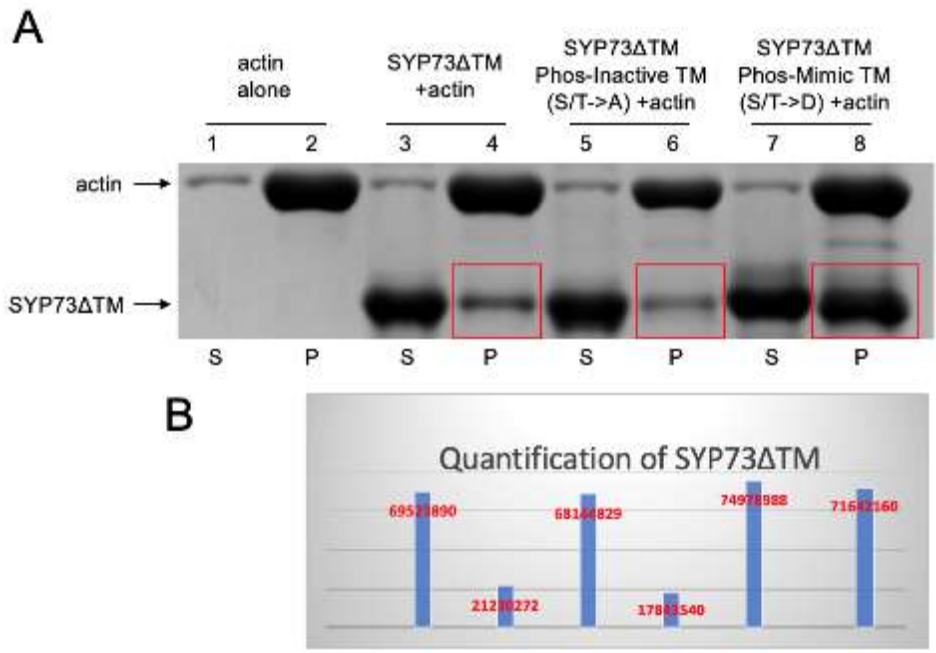

Figure 4.3 Simulated phosphorylation status affects SYP73 actin binding ability *in vitro*.

(A) High-speed co-sedimentation assay compared actin binding abilities of wild-type and mutants of SYP73ΔTM. Red boxes indicate the amount of SYP73ΔTM co-sedimented with actin in the pellet (P) fraction.
(B) Densitometric quantification of SYP73ΔTM in supernatant (S) and pellet (P) fractions (A, lanes 3 - 8).

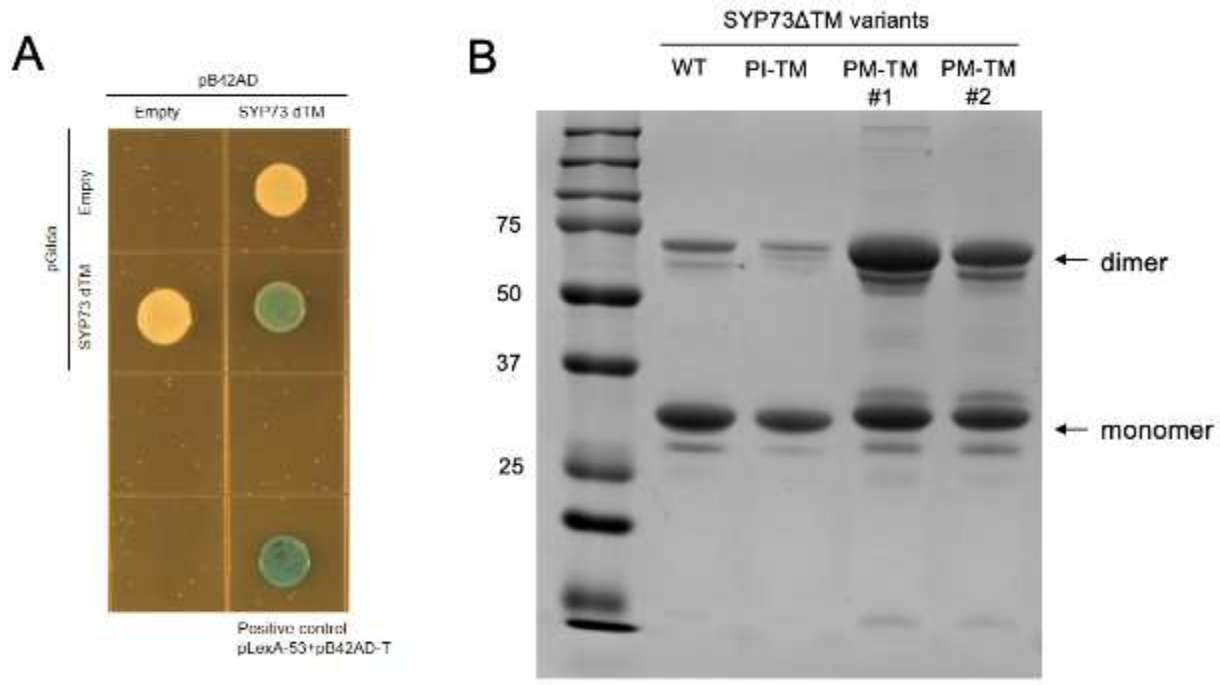

Figure 4.4 Phosphorylation status affects SYP73 self-interaction.

(A) Yeast two-hybrid detection of SYP73 self-interaction.
(B) Dimerization of purified wild-type SYP73ΔTM and mutants with simulated phosphorylation status. WT, wild type; PI-TM, phospho-inactive triple mutant; PM-TM, phospho-mimicking triple mutant.

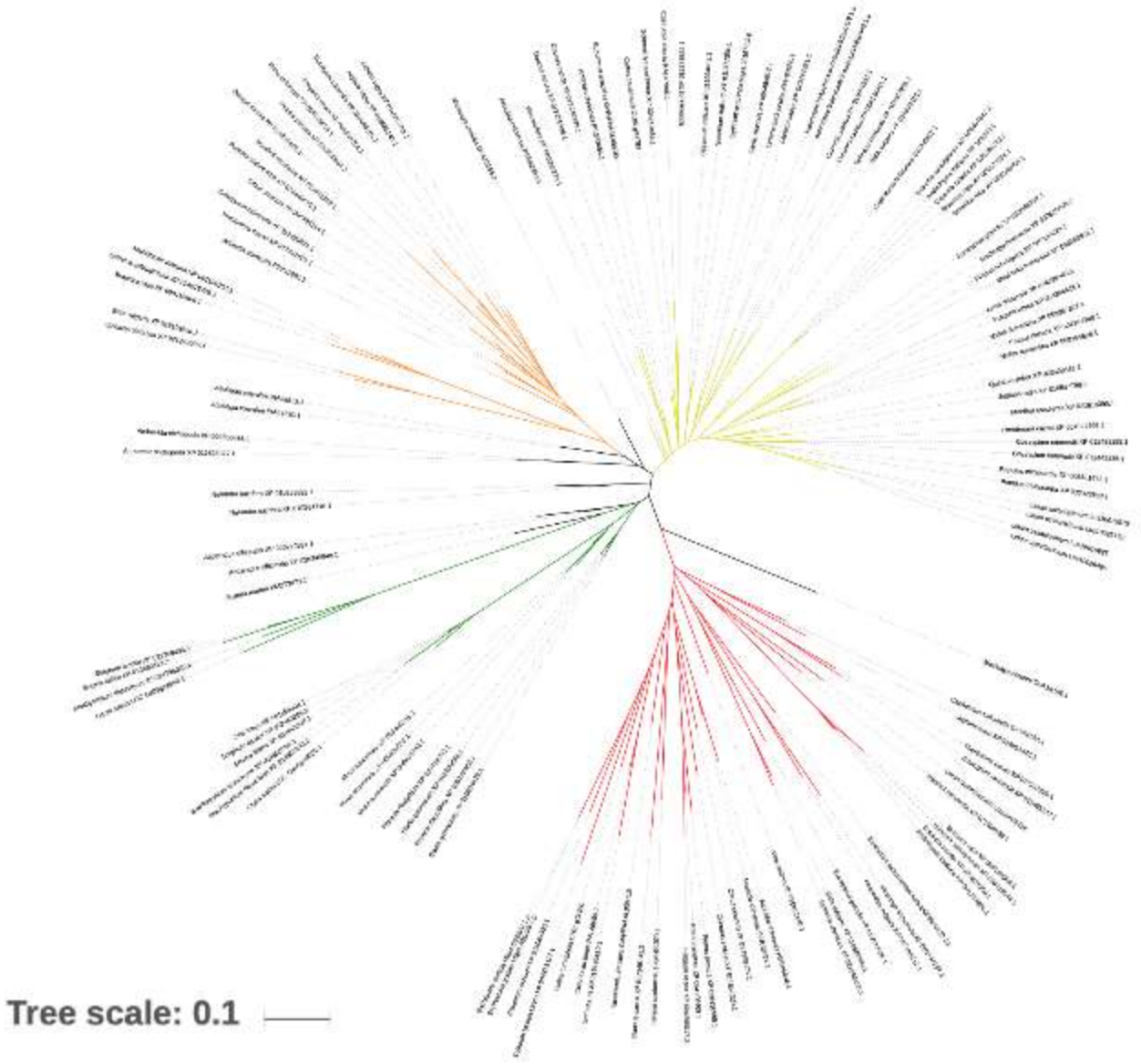

Figure 4.5 Phylogenetic analysis of the SYP7 subfamily in angiosperms suggests the existence of SYP73 in core eudicots.

A phylogenetic analysis of the SYP7 subfamily in angiosperms is shown by unrooted trees because the highly similar SYP7 family genes were not identified in plant genomes older than *Amborella*. Genes from the core eudicots can be clustered into three branches that contain either Arabidopsis thaliana SYP71 (yellow branch), SYP72 (red branch) or SYP73 (orange branch). Genes from monocots are clustered into a single branch (green branch), and other basal angiosperm (black branches) are scattered at the center of the unrooted tree with a low bootstraps rate.
The 50 species involved in phylogenetic analysis were from 28 orders, covering the major angiosperms that have been sequenced so far, with *Amborella* as the most basic group. SYP71, 72 and 73 of *Arabidopsis thaliana* were used as query sequences to search for homologous sequences in the representative gene model sequences of the genomes of various species by BLASTP.

Figure 4.5 (cont'd) Multiple sequence alignments were finished by clustalW2, a phylogenetic tree was reconstructed by RAxML.

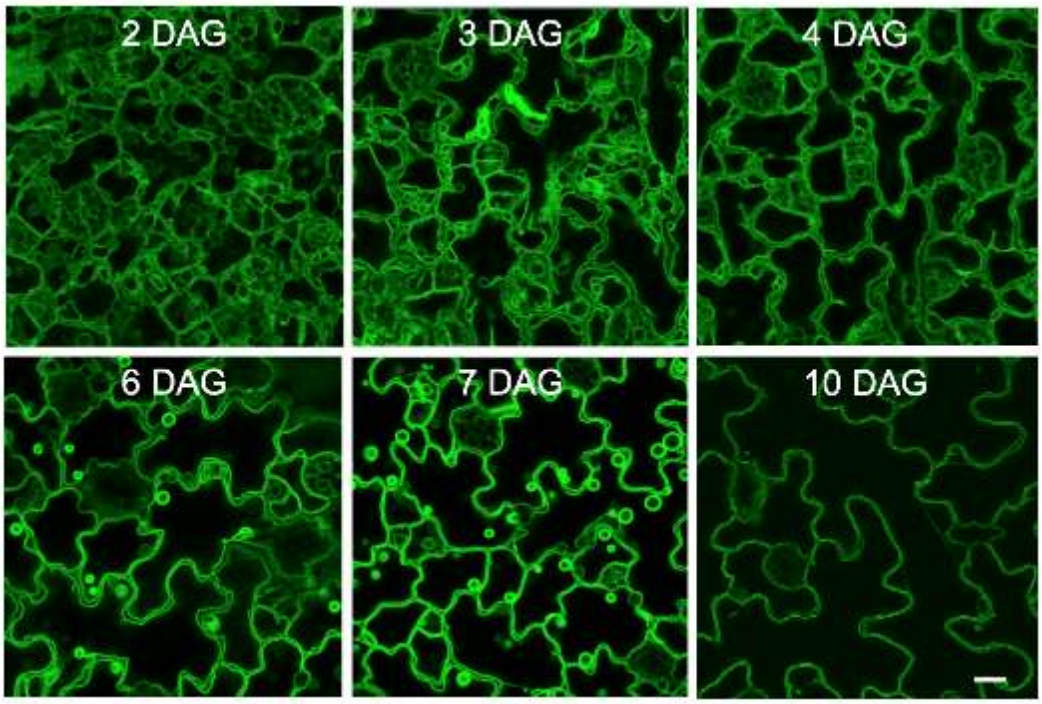

Figure 4.6 Vacuole morphogenesis in wild-type cotyledon epidermal cells.

Confocal images show wild-type cotyledon epidermal cells expressing the tonoplast marker GFP-δTIP in seedlings of 2, 3, 4, 6, 7 and 10 days after germination (DAG). Scale bar = 10 μm.

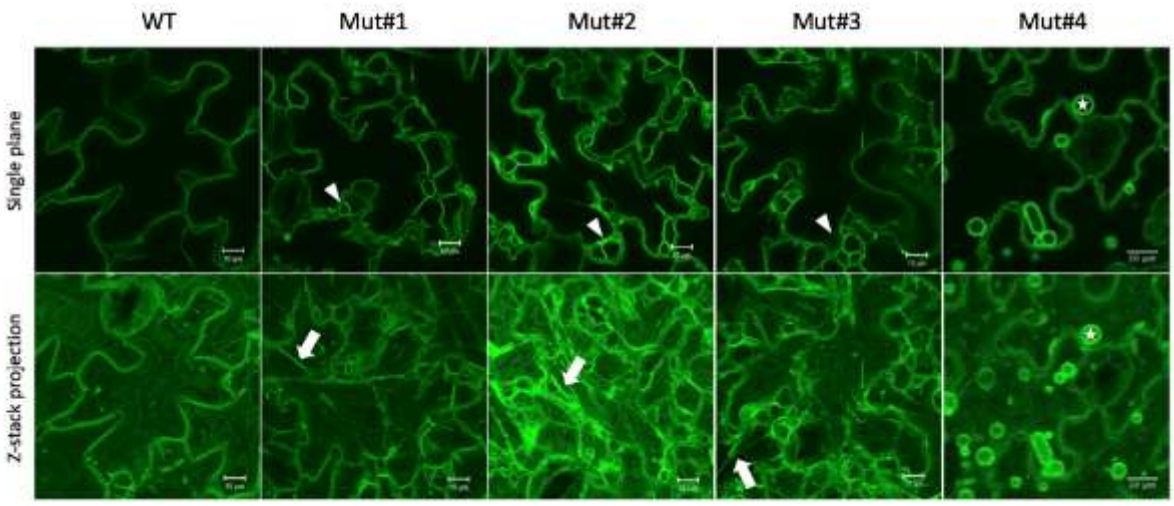

Figure 4.7 Vacuolar phenotypes of four vacuolar mutant lines.

Confocal images show cotyledon epidermal cells expressing the tonoplast marker GFP-δTIP in 7 days old seedlings. Inserted shapes indicate structures of enhanced transvacuolar strands (arrow), unfused small vacuoles (arrowhead) and "bulbs" (star). Scale bars = 10 μm.

REFERENCES

REFERENCES

1. Cao, P., Renna, L., Stefano, G. & Brandizzi, F. SYP73 Anchors the ER to the Actin Cytoskeleton for Maintenance of ER Integrity and Streaming in Arabidopsis. *Current Biology* **26**, 3245-3254 (2016).

2. Lipka, V., Kwon, C. & Panstruga, R. SNARE-Ware: The role of SNARE-Domain proteins in plant biology. *Annual Review of Cell and Developmental Biology* **23**, 147-174 (2007).

3. Kim, S.J. & Brandizzi, F. News and views into the SNARE complexity in Arabidopsis. *Frontiers in Plant Science* **3** (2012).

4. Zhao, Y. *et al.* The Plant-Specific Actin Binding Protein SCAB1 Stabilizes Actin Filaments and Regulates Stomatal Movement in Arabidopsis. *Plant Cell* **23**, 2314-2330 (2011).

4. Lv, F.N. *et al.* GhCFE1A, a dynamic linker between the ER network and actin cytoskeleton, plays an important role in cotton fibre cell initiation and elongation. *Journal of Experimental Botany* **66**, 1877-1889 (2015).

6. Ma, B. *et al.* Arabidopsis vacuolar H+-ATPase (V-ATPase) B subunits are involved in actin cytoskeleton remodeling via binding to, bundling, and stabilizing F-actin. *Journal of Biological Chemistry* **287**, 19008-19017 (2012).

7. Oikawa, K. *et al.* CHLOROPLAST UNUSUAL POSITIONING1 is essential for proper chloroplast positioning. *Plant Cell* **15**, 2805-2815 (2003).

8. Whippo, C.W. *et al.* THRUMIN1 Is a Light-Regulated Actin-Bundling Protein Involved in Chloroplast Motility. *Current Biology* **21**, 59-64 (2011).

9. Deeks, M.J. *et al.* A superfamily of actin-binding proteins at the actin-membrane nexus of higher plants. *Current Biology* **22**, 1595-1600 (2012).

10. Jia, H.L. *et al.* Arabidopsis CROLIN1, a Novel Plant Actin-binding Protein, Functions in Cross-linking and Stabilizing Actin Filaments. *Journal of Biological Chemistry* **288**, 32277-32288 (2013).

11. Pollard, T.D. Actin and Actin-Binding Proteins. *Cold Spring Harbor Perspectives in Biology* **8** (2016).

12. Zhang, W., Zhao, Y., Guo, Y. & Ye, K.Q. Plant Actin-binding Protein SCAB1 Is Dimeric Actin Cross-linker with Atypical Pleckstrin Homology Domain. *Journal of Biological Chemistry* **287**, 11981-11990 (2012).

13. Galkin, V.E., Orlova, A., Cherepanova, O., Lebart, M.C. & Egelman, E.H. High-resolution cryo-EM structure of the F-actin-fimbrin/plastin ABD2 complex. *Proceedings of the National Academy of Sciences of the United States of America* **105**, 1494-1498 (2008).

14. Klein, M.G. *et al.* Structure of the actin crosslinking core of fimbrin. *Structure* **12**, 999-1013 (2004).

14. Westrate, L., Lee, J., Prinz, W. & Voeltz, G. Form follows function: the importance of endoplasmic reticulum shape. *Annual review of biochemistry* **84**, 791-811 (2015).

16. Vedrenne, C., Klopfenstein, D.R. & Hauri, H.P. Phosphorylation controls CLIMP-63-mediated anchoring of the endoplasmic reticulum to microtubules. *Molecular Biology of the Cell* **16**, 1928-1937 (2005).

17. Smyth, J.T., Beg, A.M., Wu, S.L., Putney, J.W. & Rusan, N.M. Phosphoregulation of STIM1 Leads to Exclusion of the Endoplasmic Reticulum from the Mitotic Spindle. *Current Biology* **22**, 1487-1493 (2012).

18. Sandoz, P.A. & Van der Goot, F.G. (Portland Press Limited, 2015).

19. Wang, S., Tukachinsky, H., Romano, F.B. & Rapoport, T.A. Cooperation of the ER-shaping proteins atlastin, lunapark, and reticulons to generate a tubular membrane network. *Elife* **5**, e18605 (2016).

20. Ueda, H. *et al.* Endoplasmic Reticulum (ER) Membrane Proteins (LUNAPARKs) are Required for Proper Configuration of the Cortical ER Network in Plant Cells (vol 59, pg 1931, 2018). *Plant and Cell Physiology* **59**, 2166-2166 (2018).

21. Kriechbaumer, V. *et al.* Arabidopsis Lunapark proteins are involved in ER cisternae formation. *New Phytologist* **219**, 990-1004 (2018).

22. Ueda, H. *et al.* Phosphorylation of the C Terminus of RHD3 Has a Critical Role in Homotypic ER Membrane Fusion in Arabidopsis. *Plant physiology* **170**, 867-880 (2016).

23. Dinkel, H. *et al.* ELM 2016-data update and new functionality of the eukaryotic linear motif resource. *Nucleic Acids Research* **44**, D294-D300 (2016).

24. Chereau, D. *et al.* Actin-bound structures of Wiskott-Aldrich syndrome protein (WASP)-homology domain 2 and the implications for filament assembly. *Proceedings of the National Academy of Sciences of the United States of America* **102**, 16644-16649 (2005).

24. Drozdetskiy, A., Cole, C., Procter, J. & Barton, G.J. JPred4: a protein secondary structure prediction server. *Nucleic Acids Research* **43**, W389-W394 (2015).

26. Kim, D.Y., Scalf, M., Smith, L.M. & Vierstra, R.D. Advanced Proteomic Analyses Yield a Deep Catalog of Ubiquitylation Targets in Arabidopsis. *Plant Cell* **25**, 1523-1540 (2013).

27. Menz, J., Li, Z., Schulze, W.X. & Ludewig, U. Early nitrogen-deprivation responses in Arabidopsis roots reveal distinct differences on transcriptome and (phospho-) proteome levels between nitrate and ammonium nutrition. *Plant Journal* **88**, 717-734 (2016).

28. Zulawski, M., Braginets, R. & Schulze, W.X. PhosPhAt goes kinases-searchable protein kinase target information in the plant phosphorylation site database PhosPhAt. *Nucleic Acids Research* **41**, D1176-D1184 (2013).

29. Li, S.C. & Kane, P.M. The yeast lysosome-like vacuole: Endpoint and crossroads. *BBA-Mol. Cell Res.* **1793**, 650-663 (2009).

30. Cui, Y. *et al.* A whole-cell electron tomography model of vacuole biogenesis in Arabidopsis root cells. *Nat. Plants* **5**, 95-105 (2019).

31. Feeney, M., Kittelmann, M., Menassa, R., Hawes, C. & Frigerio, L. Protein Storage Vacuoles Originate from Remodeled Preexisting Vacuoles in Arabidopsis thaliana. *Plant Physiol.* **177**, 241-254 (2018).

32. Novick, P., Field, C. & Schekman, R. Identification of 23 Complementation Groups Required for Post-Translational Events in the Yeast Secretory Pathway. *Cell* **21**, 205-215 (1980).

33. Wickner, W. Membrane Fusion: Five Lipids, Four SNAREs, Three Chaperones, Two Nucleotides, and a Rab, All Dancing in a Ring on Yeast Vacuoles. *Annu Rev Cell Dev Bi* **26**, 115-136 (2010).

34. He, C.C. & Klionsky, D.J. Regulation Mechanisms and Signaling Pathways of Autophagy. *Annu Rev Genet* **43**, 67-93 (2009).

34. Zhang, C.H., Hicks, G.R. & Raikhel, N.V. Plant vacuole morphology and vacuolar trafficking. *Front. Plant Sci.* **5** (2014).

36. Rojo, E., Gillmor, C.S., Kovaleva, V., Somerville, C.R. & Raikhel, N.V. VACUOLELESS1 is an essential gene required for vacuole formation and morphogenesis in Arabidopsis. *Dev. Cell* **1**, 303-310 (2001).

37. Cutler, S.R., Ehrhardt, D.W., Griffitts, J.S. & Somerville, C.R. Random GFP::cDNA fusions enable visualization of subcellular structures in cells of Arabidopsis at a high frequency. *Proc. Natl. Acad. Sci. USA* **97**, 3718-3723 (2000).

38. Avila, E.L. *et al.* Tools to Study Plant Organelle Biogenesis. Point Mutation Lines with Disrupted Vacuoles and High-Speed Confocal Screening of Green Fluorescent Protein-Tagged Organelles. *Plant Physiol.* **133**, 1673-1676 (2003).

39. Zheng, J., Han, S.W., Rodriguez-Welsh, M.F. & Rojas-Pierce, M. Homotypic vacuole fusion requires VTI11 and is regulated by phosphoinositides. *Mol. Plant* **7**, 1026-1040 (2014).

40. Agee, A.E. *et al.* MODIFIED VACUOLE PHENOTYPE1 Is an Arabidopsis Myrosinase-Associated Protein Involved in Endomembrane Protein Trafficking. *Plant Physiol.* **152**, 120-132 (2010).

41. Han, S.W., Alonso, J.M. & Rojas-Pierce, M. REGULATOR OF BULB BIOGENESIS1 (RBB1) Is Involved in Vacuole Bulb Formation in Arabidopsis. *Plos One* **10** (2015).

42. Sanmartin, M. *et al.* A Molecular Switch for Initiating Cell Differentiation in Arabidopsis. *Curr. Biol.* **21**, 999-1008 (2011).

43. Munoz, A. *et al.* RIMA-Dependent Nuclear Accumulation of IYO Triggers Auxin-Irreversible Cell Differentiation in Arabidopsis. *Plant Cell* **29**, 575-588 (2017).

44. Hicks, G.R. & Raikhel, N.V. Opportunities and challenges in plant chemical biology. *Nat. Chem. Biol.* **5**, 268-272 (2009).

44. Takemoto, K. *et al.* Distinct sets of tethering complexes, SNARE complexes, and Rab GTPases mediate membrane fusion at the vacuole in Arabidopsis. *Proc. Natl. Acad. Sci. USA* **115**, E2457-E2466 (2018).

46. Brillada, C. *et al.* Phosphoinositides control the localization of HOPS subunit VPS41, which together with VPS33 mediates vacuole fusion in plants. *Proc. Natl. Acad. Sci. USA* **115**, Eb305-Eb314 (2018).

47. Gu, Y.N. & Innes, R.W. The KEEP ON GOING Protein of Arabidopsis Recruits the ENHANCED DISEASE RESISTANCE1 Protein to Trans-Golgi Network/Early Endosome Vesicles. *Plant Physiol.* **155**, 1827-1838 (2011).

48. Saito, C. *et al.* A complex and mobile structure forms a distinct subregion within the continuous vacuolar membrane in young cotyledons of Arabidopsis. *Plant J.* **29**, 245-255 (2002).

49. Saito, C. *et al.* The occurrence of 'bulbs', a complex configuration of the vacuolar membrane, is affected by mutations of vacuolar SNARE and phospholipase in Arabidopsis. *Plant J.* **68**, 64-73 (2011).

50. Saito, C. *et al.* Qualitative difference between "bulb" membranes and other vacuolar membranes. *Plant Signaling & Behavior* **6**, 1914-1917 (2011).

51. Gu, Y.N. & Innes, R.W. The KEEP ON GOING Protein of Arabidopsis Regulates Intracellular Protein Trafficking and Is Degraded during Fungal Infection. *Plant Cell* **24**, 4717-4730 (2012).

52. Efeyan, A., Comb, W.C. & Sabatini, D.M. Nutrient-sensing mechanisms and pathways. *Nature* **517**, 302-310 (2015).

53. Chantranupong, L. *et al.* The CASTOR Proteins Are Arginine Sensors for the mTORC1 Pathway. *Cell* **165**, 153-164 (2016).

54. Wolfson, R.L. *et al.* METABOLISM Sestrin2 is a leucine sensor for the mTORC1 pathway. *Science* **351**, 43-48 (2016).

54. Gu, X. *et al.* SAMTOR is an S-adenosylmethionine sensor for the mTORC1 pathway. *Science* **358**, 813-818 (2017).

56. Wyant, G.A. *et al.* mTORC1 Activator SLC38A9 Is Required to Efflux Essential Amino Acids from Lysosomes and Use Protein as a Nutrient. *Cell* **171**, 642-+ (2017).

57. Gonzalez, A. & Hall, M.N. Nutrient sensing and TOR signaling in yeast and mammals. *EMBO J.* **36**, 397-408 (2017).

58. Frommer, W.B., Hummel, S. & Riesmeier, J.W. Expression Cloning in Yeast of a Cdna-Encoding a Broad-Specificity Amino-Acid Permease from Arabidopsis-Thaliana. *Proc. Natl. Acad. Sci. USA* **90**, 5944-5948 (1993).

59. Hsu, L.C., Chiou, T.J., Chen, L.S. & Bush, D.R. Cloning a Plant Amino-Acid Transporter by Functional Complementation of a Yeast Amino-Acid-Transport Mutant. *Proc. Natl. Acad. Sci. USA* **90**, 7441-7445 (1993).

60. Tegeder, M. Transporters involved in source to sink partitioning of amino acids and ureides: opportunities for crop improvement. *J. Exp. Bot.* **65**, 1865-1878 (2014).

61. Wolfson, R.L. & Sabatini, D.M. The Dawn of the Age of Amino Acid Sensors for the mTORC1 Pathway. *Cell Metabolism* **26**, 301-309 (2017).

62. Shi, L., Wu, Y. & Sheen, J. TOR signaling in plants: conservation and innovation. *Development* **145** (2018).

63. Schmidt, A., Kunz, J. & Hall, M.N. TOR2 is required for organization of the actin cytoskeleton in yeast. *Proc. Natl. Acad. Sci. USA* **93**, 13780-13785 (1996).

64. Jacinto, E. *et al.* Mammalian TOR complex 2 controls the actin cytoskeleton and is rapamycin insensitive. *Nat. Cell Biol.* **6**, 1122-U1130 (2004).

64. Sarbassov, D.D. *et al.* Rictor, a novel binding partner of mTOR, defines a rapamycin-insensitive and raptor-independent pathway that regulates the cytoskeleton. *Curr. Biol.* **14**, 1296-1302 (2004).

66. Deprost, D. *et al.* The Arabidopsis TOR kinase links plant growth, yield, stress resistance and mRNA translation. *EMBO Rep.* **8**, 864-870 (2007).

67. Moreau, M. *et al.* Mutations in the Arabidopsis Homolog of LST8/G beta L, a Partner of the Target of Rapamycin Kinase, Impair Plant Growth, Flowering, and Metabolic Adaptation to Long Days. *Plant Cell* **24**, 463-481 (2012).

68. Caldana, C. *et al.* Systemic analysis of inducible target of rapamycin mutants reveal a general metabolic switch controlling growth in Arabidopsis thaliana. *Plant J.* **73**, 897-909 (2013).

69. Juppner, J. *et al.* The target of rapamycin kinase affects biomass accumulation and cell cycle progression by altering carbon/nitrogen balance in synchronized Chlamydomonas reinhardtii cells. *Plant J.* **93**, 355-376 (2018).

70. Salem, M.A. *et al.* RAPTOR Controls Developmental Growth Transitions by Altering the Hormonal and Metabolic Balance. *Plant Physiol.* **177**, 565-593 (2018).

71. Ren, M.Z. *et al.* Target of Rapamycin Signaling Regulates Metabolism, Growth, and Life Span in Arabidopsis. *Plant Cell* **24**, 4850-4874 (2012).

72. Xiong, Y. *et al.* Glucose-TOR signalling reprograms the transcriptome and activates meristems. *Nature* **496**, 181–186 (2013).

73. Chen, G.-H., Liu, M.-J., Xiong, Y., Sheen, J. & Wu, S.-H. TOR and RPS6 transmit light signals to enhance protein translation in deetiolating Arabidopsis seedlings. *Proc. Natl. Acad. Sci. USA* **115**, 12823-12828 (2018).

74. Li, X. *et al.* Differential TOR activation and cell proliferation in Arabidopsis root and shoot apexes. *Proceedings of the National Academy of Sciences* **114**, 2765-2770 (2017).

74. Dong, Y., Teleman, A.A., Jedmowski, C., Wirtz, M. & Hell, R. The Arabidopsis THADA homologue modulates TOR activity and cold acclimation. *Plant Biol.* **21**, 77-83 (2019).

76. Bakshi, A. *et al.* Ectopic expression of Arabidopsis Target of Rapamycin (AtTOR) improves water-use efficiency and yield potential in rice (vol 7, 42835, 2017). *Scientific Reports* **7** (2017).

77. Kurth, E.G. *et al.* Myosin-driven transport network in plants. *Proc. Natl. Acad. Sci. U.S.A.* **114**, E1385-E1394 (2017).

78. Wada, M. & Kong, S.-G. Actin-mediated movement of chloroplasts. *J. Cell Sci.* **131**, jcs210310 (2018).

79. Hanson, M.R. & Hines, K.M. Stromules: Probing formation and function. *Plant Physiol.* **176**, 128-137 (2018).

80. Schattat, M., Barton, K., Baudisch, B., Klosgen, R.B. & Mathur, J. Plastid stromule branching coincides with contiguous endoplasmic reticulum dynamics. *Plant Physiol.* **155**, 1667-1677 (2011).

81. Hanson, M.R. & Sattarzadeh, A. Stromules: Recent insights into a long neglected feature of plastid morphology and function. *Plant Physiol.* **155**, 1486-1492 (2011).

82. Kwok, E.Y. & Hanson, M.R. Microfilaments and microtubules control the morphology and movement of non-green plastids and stromules in Nicotiana tabacum. *Plant J.* **35**, 16-26 (2003).

83. Natesan, S.K.A., Sullivan, J.A. & Gray, J.C. Myosin XI is pequired for actin-associated movement of plastid stromules. *Molecular Plant* **2**, 1262-1272 (2009).

84. Caplan, J.L. *et al.* Chloroplast stromules function during innate immunity. *Dev. Cell* **34**, 45-57 (2015).

84. Ho, J. & Theg, S.M. The formation of stromules in vitro from chloroplasts isolated from Nicotiana benthamiana. *PLoS One* **11**, 1-14 (2016).

86. Phillips, M.J. & Voeltz, G.K. Structure and function of ER membrane contact sites with other organelles. *Nature Reviews Molecular Cell Biology* **17**, 69-82 (2016).

87. Settembre, C., Fraldi, A., Medina, D.L. & Ballabio, A. Signals from the lysosome: a control centre for cellular clearance and energy metabolism. *Nature Reviews Molecular Cell Biology* **14**, 283-296 (2013).

88. Tatsuta, T., Scharwey, M. & Langer, T. Mitochondrial lipid trafficking. *Trends Cell Biol.* **24**, 44-52 (2014).

89. Barbosa, A.D., Savage, D.B. & Siniossoglou, S. Lipid droplet-organelle interactions: emerging roles in lipid metabolism. *Curr. Opin. Cell Biol.* **35**, 91-97 (2015).

90. Hurlock, A.K., Roston, R.L., Wang, K. & Benning, C. Lipid trafficking in plant cells. *Traffic* **15**, 915-932 (2014).

91. Valm, A.M. *et al.* Applying systems-level spectral imaging and analysis to reveal the organelle interactome. *Nature* **546**, 162–167 (2017).

92. Hoyer, M.J. *et al.* A novel class of ER membrane proteins regulates ER-associated endosome fission. *Cell* **175**, 254-265 (2018).

93. Lee, J.E., Westrate, L.M., Wu, H.X., Page, C. & Voeltz, G.K. Multiple dynamin family members collaborate to drive mitochondrial division. *Nature* **540**, 139–143 (2016).

94. Rowland, A.A., Chitwood, P.J., Phillips, M.J. & Voeltz, G.K. ER contact sites define the position and timing of endosome fission. *Cell* **159**, 1027-1041 (2014).

94. Staehelin, L.A. The plant ER: a dynamic organelle composed of a large number of discrete functional domains. *Plant J.* **11**, 1151-1165 (1997).

96. Boevink, P. *et al.* Stacks on tracks: the plant Golgi apparatus traffics on an actin/ER network. *Plant J.* **15**, 441-447 (1998).

97. Boevink, P., SantaCruz, S., Hawes, C., Harris, N. & Oparka, K.J. Virus-mediated delivery of the green fluorescent protein to the endoplasmic reticulum of plant cells. *Plant J.* **10**, 935-941 (1996).

98. Stefano, G. *et al.* ER network homeostasis is critical for plant endosome streaming and endocytosis. *Cell Discovery* **1**, 15033 (2015).

99. Gao, H.B. *et al.* In vivo quantification of peroxisome tethering to chloroplasts in tobacco epidermal cells using optical tweezers. *Plant Physiol.* **170**, 263-272 (2016).

100. Sparkes, I.A. *et al.* Bleach it, switch it, bounce it, pull it: using lasers to reveal plant cell dynamics. *J. Exp. Bot.* **62**, 1-7 (2011).

101. Mehrshahi, P. *et al.* Transorganellar complementation redefines the biochemical continuity of endoplasmic reticulum and chloroplasts. *Proc. Natl. Acad. Sci. U.S.A.* **110**, 12126-12131 (2013).

102. Wang, P.W., Hawes, C. & Hussey, P.J. Plant endoplasmic reticulum-plasma membrane contact sites. *Trends Plant Sci.* **22**, 289-297 (2017).

103. Li, J.J., Blanchoin, L. & Staiger, C.J. Signaling to actin stochastic dynamics. *Annu. Rev. Plant Biol.* **66**, 415-440 (2015).

104. Staiger, C.J. Signaling to the actin cytoskeleton in plants. *Annu. Rev. Plant Physiol. Plant Mol. Biol.* **51**, 257-288 (2000).

104. Feiguelman, G., Fu, Y. & Yalovsky, S. ROP GTPases structure-function and signaling pathways. *Plant Physiol.* **176**, 57-79 (2018).

106. Hall, A. & Nobes, C.D. Rho GTPases: molecular switches that control the organization and dynamics of the actin cytoskeleton. *Philos. Trans. R. Soc. Lond. B Biol. Sci.* **355**, 965-970 (2000).

107. Bezanilla, M., Gladfelter, A.S., Kovar, D.R. & Lee, W.L. Cytoskeletal dynamics: A view from the membrane. *J. Cell Biol.* **209**, 329-337 (2015).

108. Rademacher, E.H. & Offringa, R. Evolutionary adaptations of plant AGC kinases: from light signaling to cell polarity regulation. *Front Plant Sci* **3** (2012).

109. Vicente-Manzanares, M., Choi, C.K. & Horwitz, A.R. Integrins in cell migration – the actin connection. *J. Cell Sci.* **122**, 199-206 (2009).

110. Vazquez-Victorio, G., Gonzalez-Espinosa, C., Espinosa-Riquer, Z.P. & Macias-Silva, M. GPCRs and actin–cytoskeleton dynamics, in *G Protein-Coupled Receptors*, Vol. 132. (ed. A.K. Shukla) 165-188 (Academic Press, 2016).

111. Brunton, V.G., MacPherson, I.R.J. & Frame, M.C. Cell adhesion receptors, tyrosine kinases and actin modulators: a complex three-way circuitry. *Biochimica Et Biophysica Acta-Molecular Cell Research* **1692**, 121-144 (2004).

112. Fu, Y. The cytoskeleton in the pollen tube. *Curr. Opin. Plant Biol.* **28**, 111-119 (2015).

113. Cai, G., Parrotta, L. & Cresti, M. Organelle trafficking, the cytoskeleton, and pollen tube growth. *J. Integr. Plant Biol.* **57**, 63-78 (2015).

114. Qi, X.Y., Sun, J.Q. & Zheng, H.Q. A GTPase-dependent fine ER is required for localized secretion in polarized growth of root hairs. *Plant Physiol.* **171**, 1996-2007 (2016).

114. Griffing, L.R., Lin, C., Perico, C., White, R.R. & Sparkes, I. Plant ER geometry and dynamics: biophysical and cytoskeletal control during growth and biotic response. *Protoplasma* **254**, 43-56 (2017).

116. Eisinger, W., Ehrhardt, D. & Briggs, W. Microtubules are essential for guard-cell function in Vicia and Arabidopsis. *Molecular Plant* **5**, 601-610 (2012).

117. Lucas, J.R., Nadeau, J.A. & Sack, F.D. Microtubule arrays and Arabidopsis stomatal development. *J. Exp. Bot.* **57**, 71-79 (2006).

118. Li, L.J., Ren, F., Gao, X.Q., Wei, P.C. & Wang, X.C. The reorganization of actin filaments is required for vacuolar fusion of guard cells during stomatal opening in Arabidopsis. *Plant Cell and Environment* **36**, 484-497 (2013).

119. Rui, Y. & Anderson, C.T. Functional analysis of cellulose and xyloglucan in the walls of stomatal guard cells of Arabidopsis. *Plant Physiol.* **170**, 1398-1419 (2016).

120. Day, B., Henty, J.L., Porter, K.J. & Staiger, C.J. The pathogen-actin connection: A platform for defense signaling in plants. *Annu. Rev. Phytopathol.* **49**, 483-506 (2011).

121. Li, P. & Day, B. Battlefield cytoskeleton: Turning the tide on plant immunity. *Mol. Plant-Microbe Interact.* **32**, 25-34 (2019).

122. Li, J.J., Henty-Ridilla, J.L., Staiger, B.H., Day, B. & Staiger, C.J. Capping protein integrates multiple MAMP signalling pathways to modulate actin dynamics during plant innate immunity. *Nature Communications* **6**, 7206 (2015).

123. Jimenez-Lopez, J.C. *et al.* Heterodimeric capping protein from Arabidopsis is a membrane-associated, actin-binding protein. *Plant Physiol.* **166**, 1312-1328 (2014).

124. Sun, H. *et al.* Profilin negatively regulates formin-mediated actin assembly to modulate PAMP-triggered plant Immunity. *Curr. Biol.* **28**, 1882-1895 (2018).

124. Toufexi, A. *et al.* Chloroplasts navigate towards the pathogen interface to counteract infection by the Irish potato famine pathogen. *bioRxiv*, 516443 (2019).